# Modelling extinction and reignition in turbulent flames

By
Markus Kostka

Thesis Submitted for the Degree of
Doctor of Philosophy
in the Faculty of Engineering of the University of London
and
Diploma of Imperial College

Department of Mechanical Engineering
Imperial College London
February 2008

# Abstract

The presented work attempts to extend the conditional moment closure method for non-premixed, turbulent combustion to predict extinction and reignition phenomena in turbulent flames.

The conditional moment closure method is one of a class of conserved scalar modelling approaches in turbulent non-premixed combustion, where chemistry is treated as mainly dependent on the mixing of oxidizer and fuel. However, as designers of combustion devices aim for higher turbulence rates to enhance mixing and promote combustion, chemical conversion is not solely determined by the rate at which fuel and oxidizer are mixed, but kinetic effects become important.

Therefore it is necessary in these cases, to consider a second variable to govern the evolution of the chemical system. This variable will parameterise the chemical conversion process from cold, mixed reactants at fixed equivalence ratio to an equilibrium state.

Equations describing the chemical system as a function of these two variables, the conserved scalar, commonly referred to as mixture fraction and the progress variable, can be derived and constitute the doubly conditioned moment closure equations. However, solution of this set of equations is computationally expensive and key parameters describing the rate of dissipation of the progress variable, which is a reactive scalar, are not yet fully understood.

By considering conditional fluctuations of the progress variable, applying simple relationships for scalar dissipation and using a pre-computed functional dependence of conditional moments on the progress variable, the effect of double conditioning on the chemical source term and on the overall chemistry predictions can be examined.

The methodology is tested for its capability to predict the turbulent, piloted flames of the Sandia D-F series. These laboratory flames show an increasing degree of local extinction and reignition due to varying turbulence levels. Hence they provide an ideal benchmark for the study of models trying to predict these phenomena.

# Acknowledgements

First and foremost I would like to thank my supervisor, Dr Andreas Kronenburg, for his guidance, the opportunity to study at Imperial, pursue research in his group and learn invaluable lessons about science and life. I would also like to express my gratitude towards the Department of Mechanical Engineering as well as the Engineering and Physical Science Research Council for financial support of my studies.

Furthermore, I thank my colleagues and friends - Magrino Bini, John Campbell, Dr Marie Godart, Dr Malte Jaensch, Anthony Jefferies, Dr Amir Kadiric, Dr Sabine Munch, Dr Salvador Navarro-Martinez, Dr Pemra Ozbek, Dr Vassia Paloumbi, Dr Andreas Papoutsakis, Dr Tamer Zaki; all of which have contributed to a stimulating and pleasant atmosphere in the office and at Imperial College in general. Also I want to thank my friends at home, Bastian and Tim, for they have never let the distance erode our friendship. Thank you Stacey, for being a true friend and many things more.

Special thanks goes to Drs John Keays and Markus Hartinger, who have become and will hopefully stay good friends for all the years to come. You have put things in perspective for me more than once and I will always remember the good times we had.

I was carried through this endeavour by the love and support of my family, my brother Stefan, and my parents, Helena and Manfred. I will always be grateful to you for believing in me.

*Für Helena und Manfred*

# Contents

# List of Figures

# List of Tables

# Nomenclature

## Greek Symbols

| | | |
|---|---|---|
| $\alpha$ | Thermal diffusivity | $m^2/s$ |
| $\alpha_i^*$ | Ratio of flamelet and premixed flame solution | - |
| $\chi$,$\chi_\xi$ | Scalar dissipation rate of conserved scalar | $1/s$ |
| $\chi_{h_s}$ | Scalar dissipation rate of reactive scalar | $1/s$ |
| $\chi_{sgs}$ | Subgrid scale scalar dissipation rate | $1/s$ |
| $\Delta$ | Filter width | $m$ |
| $\eta$ | Sample space variable of conserved scalar | - |
| $\gamma_t$ | Proportionality factor | - |
| $\tau_{sgs}$ | Subgrid stress tensor | $kg/(s^2\,m)$ |
| $\tau$ | Stress tensor | $kg/(s^2\,m)$ |
| $\mu$ | Dynamic viscosity | $kg/(m\,s)$ |
| $\mu_t$ | Turbulent dynamic viscosity | $kg/(m\,s)$ |
| $\nu$ | Kinematic viscosity | $m^2\,s$ |
| $\nu_i$ | Stoichiometric coefficient of species $i$ | - |
| $\phi$ | Scalar quantity | - |
| $\rho$ | Density | $kg/m^3$ |

| | | |
|---|---|---|
| $\sigma_i$ | Lennard-Jones collision diameter | $m$ |
| $\widetilde{\xi''^2}$ | Conserved scalar subgrid variance | - |
| $\xi$ | Conserved scalar, mixture fraction | - |
| $\zeta$ | Sample space variable of progress variable | - |

**Roman Symbols**

| | | |
|---|---|---|
| $\ell$ | Integral length scale | $m$ |
| $\ell$ | Length | $m$ |
| $\ell_\eta$ | Kolmogorov length scale | $m$ |
| $\boldsymbol{f}$ | Body force | $m/s^2$ |
| $\boldsymbol{I}$ | Identity matrix | - |
| $\boldsymbol{S}$ | Strain rate tensor | $1/s$ |
| $\boldsymbol{u}$ | Velocity vector | $m/s$ |
| $\mathcal{L}$ | Leonard term | $m^2/s^2$ |
| $\mathcal{M}_i$ | Chemical symbol of species $i$ | - |
| $A$ | Frequency factor | $1/s$ |
| $c$ | Progress variable | $J/kg$ |
| $C_\xi$ | Variance model parameter | - |
| $C_i$ | Concentration of species $i$ | $kmol/m^3$ |
| $c_p$ | Specific heat capacity at constant pressure | $J/(kg\ K)$ |
| $C_S$ | Smagorinsky parameter | - |
| $D_i$ | Binary diffusion coefficient | $J/(m\ s\ K)$ |
| $E$ | Activation energy | $kJ/mol$ |

| | | |
|---|---|---|
| $e_y$ | Fluctuation term | $1/s$ |
| $G$ | Filter kernel | - |
| $g_i$ | Scaling factor | - |
| $h$ | Total specific enthalpy | $J/kg$ |
| $h^\circ_{f,i}$ | Standard enthalpy of formation of species $i$ | $J/kg$ |
| $h_s$ | Sensible enthalpy | $J/kg$ |
| $J$ | Diffusive flux | - |
| $k$ | Reaction rate constant | $kmol/m^3/s$ |
| $k_B$ | Boltzmann constant | $J/K$ |
| $k_T$ | Thermal conductivity | $J/(m\ s\ K)$ |
| $Le_i$ | Lewis number for species $i$ | - |
| $M_i$ | Atomic weight of element $i$ | $kg$ |
| $N$ | Number of species | - |
| $P$ | Probability density | - |
| $p$ | Pressure | $Pa$ |
| $Pr$ | Prandtl number | - |
| $Q^s$ | Singly conditioned mean | - |
| $Q^{d,0}$ | Doubly conditioned reference field | - |
| $Q^{d,ref}$ | Scaled doubly conditioned reference field | - |
| $Q_i$ | Conditional mean of species $i$ | - |
| $q_R$ | Radiative heat source | $kg/(m^3\ s)$ |
| $R$ | Universal gas constant | $kJ/(kmol\ K)$ |

| | | |
|---|---|---|
| $Re$ | Reynolds number | - |
| $Sc_i$ | Schmidt number for species $i$ | - |
| $T$ | Temperature | $K$ |
| $t$ | Time | $s$ |
| $t_\xi$ | Conserved scalar time scale | $s$ |
| $t_{h_s}$ | Reactive scalar time scale | $s$ |
| $V$ | Volume | $kg/m^3$ |
| $W$ | Mean molecular weight of mixture $i$ | $kg/kmol$ |
| $W_i$ | Molecular weight of species $i$ | $kg/kmol$ |
| $w_i$ | Chemical source of species $i$ | $1/s$ |
| $X_i$ | Mole fraction of species $i$ | - |
| $Y''$ | Fluctuations about the conditional mean | - |
| $Y_i$ | Mass fraction of species $i$ | - |
| $Z_i$ | Element mass fraction of element $i$ | - |

Chapter 1

# Introduction and Outline

## 1.1 Introduction

Modern civilisation relies on the availability of vast amounts of energy to operate industrial and domestic appliances. Although a lot of effort is being made to provide alternative energy sources like solar, wind, water or ocean current technologies, the combustion of fossil fuels is unlikely to be replaced as the main primary energy source in the near future.

Therefore, the issues associated with hydrocarbon combustion need to be addressed. The rising cost of oil and related fossil fuels make the quest for more efficient combustion technologies worthwhile. On the other hand, controlling emissions is necessary, since environmental concerns have led governments to impose restrictions on the amount of pollutants that can be released into the atmosphere.

To aid the design process of such novel technologies computational tools have become invaluable. Many parametric studies necessary for optimisation and assertion of design features are now carried out computationally rather than having to build physical models of the device and conduct experiments. This saves money

and time and gives a more detailed view of the various physical phenomena and their individual importance. However, for these computational tools to be of any value, the models of the underlying physics have to be sound and their results trustworthy.

In many fields of engineering interest such models are already very mature. For example the finite element method and their application to solid mechanics problems. This has been introduced into engineering practise decades ago and is nowadays a part of many commercial design softwares, where stress analysis of virtual components can be performed quite accurately.

In the field of fluid dynamics and related disciplines such as combustion modelling a lot of progress has been made as well. Commercial software is available to model the aerodynamic behaviour of aeroplanes, trucks or even pollutant dispersion in entire city blocks. Meteorology heavily relies on computational fluid dynamics methods to provide reasonable weather forecasts. But even though these techniques are available, many problems remain unsolved for a lot of industrially relevant conditions. Unfortunately, turbulent combustion combines two of the most challenging of these problems.

The turbulence closure problem has been the focus of many scientists for almost a century. Some turbulence modelling approaches have been proposed with varying success. But so far no unified model, let alone theory, exists which gives reasonably accurate predictions for the range of possible turbulence levels.

With combustion taking place in a turbulent flow field, the coupling between heat release through chemical reaction and fluid properties introduces additional modelling problems.

Traditionally two distinct cases have been identified and approached separately in combustion science - premixed and non-premixed combustion. Premixed combustion is primarily viewed as a fluid dynamic discontinuity and the combustion closures seek to find appropriate quantifications of the mean speed of flame propagation, taking into account wrinkling of the flame front which cannot be resolved.

As for non-premixed combustion, conserved scalar approaches have a long tradition and have proved to be both effective and accurate in many instances. Burke and Schumann identified diffusion to be the factor determining chemical conversion rates [8], hence they coined the term '*diffusion flame*'. In subsequent years the fast chemistry assumption and a conserved scalar formalism have been introduced. Reactive quantities can then be uniquely related to this conserved scalar. This makes it possible to decouple chemistry from the fluid dynamics. From a fluid dynamics perspective the problem of diffusion flames is therefore reduced merely to a problem of the mixing described by the conserved scalar. Therefore, the conserved scalar is widely referred to as mixture fraction. An early review of the topic is given by Bilger [3].

Although this approach introduces interesting ideas, the assumption of fast chemistry is easily refuted for many combustion scenarios. It is only valid when representative chemical time scales are smaller than all other timescales of physical phenomena present in the system, which is certainly not the case for slow, pollutant forming reactions or high Reynolds number flows that induce high strain rates and cause local extinction.

One step away from the fast chemistry assumption was the flamelet model introduced in the early 1980s; an early review of this approach is given by Peters

[56]. By means of a coordinate transformation from physical space to a coordinate base attached to the isosurface of stoichiometric mixture fraction and the main coordinate direction normal to it, an equation is derived for chemical species and enthalpy with mixture fraction as independent variable. Additionally, the scalar dissipation rate serves as a parameter describing the intensity of the mixing of fuel and oxidizer. This method has found widespread use in its steady and unsteady form, as well as in Eulerian and Lagrangian interpretations. The field of flamelet modelling and a thorough overview of relevant studies can be found in Peters [57].

The early 1990s brought about an new approach to turbulent non-premixed combustion modelling exploiting the conserved scalar formalism. Kilmenko [43] and Bilger [4] independently proposed the conditional moment closure method, commonly abbreviated CMC. An extensive synthesis of the method is given by Klimenko and Bilger [44]. Although arriving at the same set of equations, Klimenko and Bilger took different routes for the derivation. Bilger's starting point is the notion that fluctuations in species concentration or temperature largely coincide with the fluctuations of the conserved scalar. Therefore, he proposed a decomposition of reactive quantities into their conditional mean and their deviation. Together with the reactive scalar transport equation and some mathematical manipulations, the CMC equations follow. In his approach, Klimenko considers the joint probability density function (p.d.f.) of a conserved scalar and a reactive scalar. Since a transport equation for this p.d.f. can easily be derived he applies the mathematical definition of a conditional mean and derives a partial differential equation for the conditional mean of a reactive scalar, the CMC equations.

Although similar in their mathematical form, the flamelet model and the conditional moment closure method differ in some subtle ways. Firstly, the derivation

of the flamelet equation assumes scale separation, which means some characteristic measure of the flame thickness has to be smaller than the smallest turbulent scales. This assumption is refuted by Bilger [2] for many cases of non-premixed combustion. Nevertheless, the flamelet model usually yields good predictions for cases where flames are well established. The assumption of a particular scale of the flame is not needed for the derivation of the CMC equations. Moreover, the CMC method provides a consistent way of incorporating convective effects, since they appear naturally from the reactive species or the joint p.d.f. transport equation. However, since both approaches contain the usually most significant contributions, namely the source and diffusion in scalar space, arguments about fundamental difference and superiority of one or the other model seem to be of a more theoretical nature.

Despite their success in many applications, conserved scalar approaches fail to give satisfactory results in cases with a large degree of local extinction and re-ignition. This is due to the fact that mixture fraction does not suffice to describe a flame in the case of transient phenomena like extinction and reignition where several physical processes other than molecular diffusion are competing at comparable time and length scales. The flame cannot be described as a diffusion flame anymore. There is no more balance between reaction and diffusion for which mixture fraction serves well as a parameterisation, as molecular transport does not happen in one main direction anymore. The diffusion flame structure is perturbed by turbulence and processes like flame propagation or autoignition might become important. To address these issues, a straightforward remedy comes to mind, namely the introduction of a second parameter. This is usually taken to be some sort of progress variable, taking into account the local reaction progress, hence,

allowing for one additional degree of freedom.

This was done by Pierce & Moin in their flamelet/progress variable approach [60] and its capability to predict extinction and reignition was assessed by Ihme et al. [32]. As progress variable they chose nondimensional temperature, normalised by the maximum and minimum values at stoichiometric composition.

Another rigorous way to introduce a progress variable as second independent parameter is the double conditioning of reactive quantities (DCMC). This is an obvious extension of the CMC approach. Instead of solving transport equations for the first statistical moment of reactive quantities conditioned on mixture fraction only, it is straightforward to derive these equations conditioned on two independent variables [44]. The first variable remains mixture fraction. The other one is a suitably chosen quantity, describing the progress of reaction.

Several analyses have examined the potential of this approach and results are encouraging. Cha et al. [10] found in their a priori DNS study, that DCMC is able to capture extinction to some extent. As a progress variable scalar dissipation rate, $\chi$, was chosen.

Kronenburg et al. [45, 48] assessed the potential of DCMC with sensible enthalpy as second conditioning variable in an a priori manner. They found good agreement between DCMC predictions and DNS.

Other feasible approaches to treat deviations from a purely mixing dominated combustion mode are available, such as second-order conditional moment closure [11, 41]. However, the identification of parameters governing the combustion physics and chemistry, and trying to reduce the fluctuations about the doubly conditioned mean, rather than finding a model accounting for these fluctuations

in terms of second order statistics, seems to be the more intuitive choice.

Another branch of turbulent non-premixed combustion modelling are p.d.f.-methods. This is a stochastic approach, in which a numerical solution to the joint probability density function of all chemical quantities (species concentration, enthalpy) is sought. This approach does not suffer from the deficiencies of conserved scalar methods, since it considers all possible degrees of freedom and does not restrict the attainable region in composition space. This fact however, makes this method computationally very expensive and restrictions of the resolution of phase space have to be made due to limited computational resources. Furthermore, although the chemical source appears in closed form, the micromixing rate of subgrid inhomogeneities has to be approximated. This is still an active area of research and various approaches have been developed. Nonetheless, a lot of research with some impressive success has been done in this field [16, 26, 35, 67, 77].

Apart from the chemistry treatment, the accurate and reliable prediction of the flow and conserved scalar field is crucial to the success of combustion simulations. For many decades the Reynolds averaged Navier-Stokes (RANS) approach has been the prime choice, where ensemble averages of all quantities are solved for. The influence of fluctuations about the average is captured by turbulence models. RANS computations have a runtime of the order of a few hours or even less and are therefore very efficient to employ, but the setup of these simulations is not particularly generic. Empirical parameters for turbulence models have to be adjusted according to the specific setup or geometry under investigation, and transient, unsteady effects are not satisfactorily captured.

This led to the development of a new approach in computational fluid dynamics.

In the 1960s meteorologists realised that small scale, regional weather forecasts rely heavily upon unsteady features of the flow in the atmosphere. RANS was therefore not suited, since it is not capable of providing predictions of these small scale features. The other extreme is direct numerical simulation (DNS) where all turbulent length scales are resolved, thus requiring a high spatial resolution. DNS was and still is, computationally so expensive that it cannot be applied to atmospheric flow simulations. Even a conservative estimation yields an atmospheric Reynolds number of $Re > 10^8$ ($u \approx 1m/s, \ell \approx 1km$). The computational effort, expressed in the number of grid nodes needed, scales with $Re^{9/4}$. The basic principle of DNS is that all relevant turbulent scales down to the Kolmogorov scale, $\ell_\eta$, are captured, such there is no need to employ turbulence models. However, this requirement cannot be realised given modern computational resources.

In a pioneering work, Smagorinsky applied a new technique, nowadays known as large eddy simulation (LES) [69]. Leonard [49] then provided mathematical rigour and applied a spatial filter to the flow parameters and examined the influence of filtering on the Navier-Stokes equations. This removes fine scale, spatial fluctuations and motion such that only the large, energy containing structures remain and are directly computed. The filtering gave rise to an additional term similar to the Reynold stresses known in the RANS context, quantifying the influence of the unresolved scale on the resolved ones. Since it involved spatial rather than temporal fluctuations, this term was labelled subgrid-scale (SGS) stress. Assuming subgrid-scale energy production balancing dissipation, he proposed a simple model for this term which is still widely used.

Significant advances in the field of LES were made in the early 1990s when Germano et al. [29] proposed a methodology that determines a coefficient in

Smagorinsky's model equation dynamically rather than it being prescribed a priori. Several variations of this general idea have been developed of which Lilly [51] is one of the more significant ones and it is widely used. It improved the method's computational stability by using a slightly different derivation of the equation for the coefficient. This formulation minimises singularities, which aids numerical stability. Another method was proposed by Piomelli and Liu [61] which smooths the coefficient field in time. This makes spatial averaging unnecessary and stabilises simulations. This method was used for present work.

Large eddy simulation has become increasingly popular since it resolves large parts of the turbulent spectrum and therefore, fairly simple models for the residual, subgrid scale contributions can be employed. Especially for cases where large scale unsteady features are present, LES offers an advantage over an ensemble averaged method such as RANS.

Early studies using large eddy simulation to predict a turbulent diffusion flame were carried out by Branley and Jones [6, 7] and Pitsch and Steiner [65]. Both used a conserved scalar approach. Since then, LES has successfully been applied to reactive flows with a variety of combustion models [35, 36, 55, 67, 68, 62]. A recent overview of the field of large eddy simulation of both non-premixed and premixed combustion is given by Pitsch [63].

Recently Navarro-Martinez et al. [55] have carried out an LES incorporating CMC in a fully predictive manner. They have used classical singly conditioned moment closure, and it has proven to predict well the pollutant formation for the benchmark flame Sandia D which is characterised by a low level of local extinction.

## 1.2 Outline

The present work and the methodology described in this thesis aims to build on the conditional moment closure method for large eddy simulation (LES-CMC) framework. The objective is to extend LES-CMC, such that more challenging scenarios like local extinction and reignition can be predicted. The new method is called extended conditional moment closure, short CMCe. A way of approximating the conditional fluctuations of a suitably chosen progress variable has to be found. This is achieved by solving a conditional variance equation. Based on that, the doubly conditioned chemical source term is approximated by constructed and scaled reference fields, mimicking doubly conditioned moments. The conditional probability density of the progress variable is assumed to follow a $\beta$-function. The performance of the proposed method is assessed by simulating the Sandia piloted jet flames D-F, which exhibit various levels of local extinction and reignition and are a standard benchmark testcase for combustion models.

The thesis is structured in the following way.

Chapter 2 introduces the fundamental equations of turbulent gaseous combustion. The Navier-Stokes equations are given along with constitutive relationships, such as the ideal gas law, Fickian diffusion or Arrhenius kinetics. Furthermore, some relevant nondimensional parameters are presented. Additionally, intrinsic challenges to the solution of this closed system of equations are discussed and the need for modelling approaches is stressed.

Chapter 3 introduces fundamentals, terminology and the set of equations used for large eddy simulation. Common closure strategies for the subgrid stresses are presented, along with the basic principle behind the dynamic modelling approach.

Furthermore, the generation of artificial inflow turbulence is discussed.

Chapter 4 describes the conditional moment closure method. The conserved scalar approach to turbulent combustion modelling is introduced. Basic ideas and definitions from probability theory are given to highlight the connection of conditional moment closure to transported p.d.f. methods. The singly and doubly conditioned moment closure equations are given and common closure strategies discussed. Additionally, details of the numerical solution of the conditional moment closure equations are described.

Chapter 5 introduces the extended source term closure. Sensible enthalpy is introduced as progress variable. The choice of progress variable and the validity of the $\beta$-p.d.f. assumption for the conditional p.d.f. are discussed. Approaches for obtaining the conditional progress variable variance are presented and some fundamental issues are highlighted. Modelling of various terms of the conditional variance equation is described and the construction of doubly conditioned reference fields is explained.

Chapter 6 describes the experimental setup of the piloted jet flames of the Sandia D-F series. The setup of the simulations carried out is presented. The results are reported and the performance of the proposed methodology is assessed.

Chapter 7 closes with some conclusions about the work carried out, implications of the results and some directions and ideas for further research into this field of engineering importance.

Chapter 2

# The Governing Equations of Turbulent Reacting Flows

For a system which can be regarded a continuum, the equations governing turbulent reacting flows are the mathematical formulation of the principle of *conservation of mass* and *Newton's second law of motion* as well as some thermodynamical and otherwise constitutive relations. This chapter will briefly state the set of equations to lay the groundwork for the following chapters where derivatives of the basic equations will be presented. For a detailed derivation of these equations refer to Bird et al. [5].

## 2.1 Fundamental principles

In this section, transport equations will be presented that are a direct consequence of fundamental principles of classical physics.

### 2.1.1 Conservation of Mass

The notion that, in the absence of nuclear effects, mass can neither be created nor destroyed is represented by the continuity equation,

$$\frac{\partial \rho}{\partial t} + \nabla \cdot \rho u = 0, \tag{2.1}$$

with $\rho$ denoting density and $u$ being the velocity vector.

### 2.1.2 Transport of Momentum

Newton's second law of motion states that the rate of change of momentum of a body equals the sum of all external forces acting on that body. This notion is represented by the momentum equation,

$$\frac{\partial \rho u}{\partial t} + \nabla \cdot \rho uu = -\nabla p + \nabla \cdot \tau + \rho f, \tag{2.2}$$

where $p$ represents the pressure, $\tau$ the viscous stress tensor and $f$ the sum of all body forces.

#### The Stress Tensor

If Newtonian behaviour of the fluid can be assumed, the viscous stress tensor $\tau$ is given by

$$\tau = 2\mu S - \frac{2}{3}\mu \nabla \cdot u \, I \tag{2.3}$$

with $\mu$ denoting the dynamic viscosity, $\boldsymbol{I}$ the identity matrix and $\boldsymbol{S}$ the strain rate tensor. This relation models the shear stresses occurring within the fluid as proportional to the strain rate. A common approximation to the viscosity for multicomponent mixtures will be given in section 2.2.

**The Strain Rate Tensor**

The strain rate tensor is defined as

$$\boldsymbol{S} = \frac{1}{2}((\nabla \boldsymbol{u}) + (\nabla \boldsymbol{u})^T). \tag{2.4}$$

It is the quantification of the shear rate in the flow, which is needed for the three-dimensional form of Newtons formula, that connects the shear forces in a flow to the shear rate through the viscosity.

### 2.1.3 Transport of Enthalpy

The conservation of mass implies conservation of all extensive quantities. Therefore a transport equation for the total specific enthalpy, $h$, can be formulated.

$$\frac{\partial \rho h}{\partial t} + \nabla \cdot \rho \boldsymbol{u}\, h = \frac{Dp}{Dt} - \nabla \cdot J_h + q_R - (\boldsymbol{\tau} : \nabla \boldsymbol{u}), \tag{2.5}$$

where $J_h$ represents the diffusive flux of enthalpy, and $q_R$ is a radiative heat source.

### 2.1.4 Transport of Chemical Species

A direct consequence of the conservation of mass is the equation governing the transport of chemical species $i$. It follows directly from the conservation of element mass and accounts for chemical conversion processes. It is conveniently formulated as a transport equation for the species mass fraction $Y_i$,

$$\frac{\partial \rho Y_i}{\partial t} + \nabla \cdot \rho u Y_i = -\nabla \cdot J_{Y_i} + \rho w_i, \tag{2.6}$$

where $J_{Y_i}$ represents the diffusive flux of the species and $w_i$ the source of that species from chemical conversion.

It shall be pointed out that mass fraction $Y_i$ and mole fraction $X_i$ are easily converted via the relation

$$Y_i = \frac{W_i}{W} X_i, \tag{2.7}$$

where $W_i$ is the molecular weight of species $i$ and $W$ is the mean molecular weight, which is given by

$$W = \left( \sum_{i=1}^{N} \frac{Y_i}{W_i} \right)^{-1}. \tag{2.8}$$

Here, $N$ is the number of chemical species of the mixture.

## 2.2 Thermodynamical and constitutive relations

This section will present complimentary relations to the partial differential equation from the previous section, that are necessary to get full closure. These are the equations where distinctions have to be made regarding the fluid under con-

sideration.

### 2.2.1 The Equation of State

To close the system of equations an expression is needed to relate pressure, density and temperature, thereby specifying the thermodynamical state. If ideal gas and mixture behaviour can be assumed, the pressure is given by:

$$p = \rho \frac{RT}{W}, \tag{2.9}$$

with $R$ denoting the universal gas constant and $W$ the mean molecular weight.

### 2.2.2 Viscosity

Viscosity is the quantity which relates the strain rate tensor and the stress tensor in the momentum equation (2.2). It is a macroscopic quantity which depends on the composition of the mixture as well as the local temperature and pressure.

Kinetic theory provides an expression for the viscosity of a single component $i$ as [31]:

$$\mu_i = \frac{5}{16} \frac{\sqrt{\pi m_i k_B T}}{\pi \sigma_i^2 \Omega^{(2,2)^*}}, \tag{2.10}$$

where $m_i$ denotes molecular mass, $k_B$ the Boltzmann constant and $\sigma_i$ the Lennard-Jones collision diameter. The collision integral $\Omega^{(2,2)^*}$ is a function of temperature. This is only to point out the main parameters influencing viscosity.

The viscosity of the multicomponent mixture of gases is modelled by the semi-

empirical formula by Wilke [79], with modifications by Bird et al. [5],

$$\mu = \sum_{i=1}^{N} \frac{X_i \mu_i}{\sum_{j=1}^{N} X_j \Phi_{ij}}, \tag{2.11}$$

with

$$\Phi_{ij} = \frac{1}{\sqrt{8}} \left(1 + \frac{W_i}{W_j}\right)^{-1/2} \left(1 + \left(1 + \frac{\mu_i}{\mu_j}\right)^{1/2} + \left(1 + \frac{W_j}{W_i}\right)^{1/4}\right)^2 . \tag{2.12}$$

### 2.2.3 Heat Conduction

The diffusive flux of enthalpy in equation (2.5) is commonly approximated by *Fourier's law of heat conduction* [5]. It is a macroscopic quantification of the heat or enthalpy transported on a molecular level. It is in accordance with kinetic gas theory and states that the diffusive heat flux is proportional to and of opposite sign as the local temperature gradient. The mathematical form is

$$J_h = -k_T \nabla T, \tag{2.13}$$

with $k_T$ denoting thermal conductivity.

### 2.2.4 Mass Diffusion

The diffusive mass flux appearing in equation (2.6) can be approximated by *Fick's law of diffusion* [5]. It is a model for binary diffusion driven by a concentration gradient and states that the diffusive flux of a particular species is proportional to and of opposite sign as the concentration gradient of that species. It is expressed

mathematically as

$$J_{Y_i} = -\rho D_i \nabla Y_i, \tag{2.14}$$

where $D_i$ is the binary diffusion coefficient of species $i$. This relation is strictly valid only for binary mixtures. However, in certain circumstances it is still a reasonable approximation of diffusion in multicomponent gas mixtures. Drawing on fundamental work by Curtiss and Hirschfelder [18] and Chapman and Cowling [14] Williams concludes, that if one species is dominating the mixture it can be viewed as a *background* fluid and the remaining components as *trace* species [80]. In the case of gaseous combustion processes with air as oxygen carrier, nitrogen would be this background component with mass fractions $Y_{N_2}$ of about 0.7. In that case, the transport process of diffusion can be viewed as binary diffusion between each individual trace species with the background fluid. For this, the binary diffusion coefficient of species $i$ with the background fluid can be taken as the diffusion coefficient $D_i$.

### 2.2.5 Nondimensional Parameters

Dimensional analysis of the transport equations (2.5) and (2.6) gives nondimensional parameters describing the magnitude of the molecular diffusion terms. These parameters will be outlined below and common assumptions in combustion modelling will be discussed.

### The Prandtl Number

The thermal conductivity in equation (2.13) appears in a non dimensional parameter called the *Prandtl* number. It is defined as

$$Pr = \frac{c_P \mu}{k_T} = \frac{\nu}{\alpha} \tag{2.15}$$

with $c_P$ denoting the specific heat capacity at constant pressure, $\alpha$ the thermal diffusivity and $\nu$ the kinematic viscosity. For most common gases the Prandtl number is found to be of the order of 0.7 [80].

### The Schmidt Number

The equivalent of the Prandtl number for heat conduction is the *Schmidt* number for mass diffusion. It is defined as

$$Sc_i = \frac{\mu}{\rho D_i}. \tag{2.16}$$

Again, the Schmidt number is found to be slightly less than unity for many gases [80].

### The Lewis Number

The *Lewis* number is defined as

$$Le = \frac{k_T}{\rho D_i c_P}, \tag{2.17}$$

and can easily be shown to be the ratio of Schmidt and Prandtl number:

$$Le_i = \frac{Sc_i}{Pr}. \tag{2.18}$$

The Lewis number is a measure of the relative magnitude of heat transfer through conduction compared to mass diffusion [80] and a common assumption in gaseous combustion modelling is that of a unity Lewis number which has been adopted throughout the present work.

### Transport Coefficients

With the nondimensional parameters presented in the previous section, molecular transport coefficients for enthalpy and mass can be related to the mixture viscosity. With the approximation of equal diffusivities for all species, the molecular diffusivity is obtained as

$$D = D_i = \frac{\mu}{\rho Sc} \tag{2.19}$$

and heat conductivity as

$$k_T = \frac{c_P \mu}{Pr}. \tag{2.20}$$

## 2.2.6 The Reaction Rate

An arbitrary reversible reaction can be described as follows

$$\sum_{i=1}^{N} \nu_i' \mathcal{M}_i \rightleftharpoons \sum_{i=1}^{N} \nu_i'' \mathcal{M}_i, \tag{2.21}$$

where $\nu_i'$ is the stoichiometric coefficient for species $i$ as a reactant and $\nu_i''$ the stoichiometric coefficient for species $i$ as a product, whereas $\mathcal{M}_i$ denotes the chemical symbol of species $i$.

The rate of reaction for species $i$ in a chemical system with $r$ reactions can then be expressed as

$$w_i = \sum_{k=1}^{r} (\nu_{i,k}'' - \nu_{i,k}') \left[ k_f \prod_{j=1}^{N} C_j^{\nu_{j,k}'} - k_b \prod_{j=1}^{N} C_j^{\nu_{j,k}''} \right] \tag{2.22}$$

where $C_j$ denotes the concentration of species $j$ and is obtained as

$$C_j = \frac{\rho Y_j}{W_j}. \tag{2.23}$$

This relation is frequently called the *law of mass action* since it captures the dependence of the reaction rate on the available mass of reactants, expressed as concentration. It is simply explaining that, on a molecular level, a binary reaction between two molecules is more likely to take place the more molecules of these two species are present.

### 2.2.7 The Arrhenius Reaction Rate Constant

The influence of temperature on the reaction rate is contained in the specific reaction rate constant which is commonly approximated by the empirical Arrhenius law [80]:

$$k = A\, e^{-\frac{E}{RT}} \tag{2.24}$$

with $A$ denoting the frequency factor and $E$ the activation energy. The frequency factor $A$ exhibits a weak dependence on temperature which is given as

$$A = BT^n, \tag{2.25}$$

where $B$ and $n$ are constants, specific to the reaction of interest.

## 2.3 Multiscale Nature of Turbulent Combustion

The set of equations presented in the preceding sections is closed, provided suitable boundary conditions and models for molecular properties are at hand. These equations describe all the physical and chemical processes that determine the evolution of the system and its chemical composition at any point in space and time.

No analytical solution to the full, unsimplified system has yet been found. In fact, the *Clay Mathematics Institute* has named the solution of the Navier-Stokes equations as one of seven *'Millennium Prize Problems'* and will award 1 million dollars to anyone who is able to provide a solution [33]. Their problem description already includes the simplification of constant density and viscosity. This highlights, that an analytical solution for the original problem is unlikely to be found.

However, the numerical solution of this system is a viable option. In that case a solution to these partial differential equations is sought at discrete points in space and time. This gives rise to another problem.

The different physical and chemical processes introduce a wide range of length and time scales. For the numerical solution to capture all phenomena, all relevant scales have to be resolved.

Turbulence theory provides an estimate of the fluid dynamics' range of scales. From the integral length scale $\ell_I$, which is commonly assumed to be of the order of geometric features of the domain in which the flow is considered, to the smallest scale of turbulence, the Kolmogorov scale $\ell_\eta$, where turbulent energy is dissipated. An important way to charactrise turbulent flow is by means of the Reynolds number $Re$. It is defined as

$$Re = \frac{\rho u \ell}{\mu}, \tag{2.26}$$

where $u$ is some characteristic, mean, large scale velocity, $\ell$ a characteristic length scale, $\rho$ the density and $\mu$ the dynamic viscosity. The Reynolds number is a dimensionless quantity and describes the ratio of inertial to viscous forces in a flow. The higher the Reynolds number, the more unstable is the behaviour of the Navier-Stokes equations. If a critical range of the Reynolds number is approached, transition from laminar to turbulent flow takes place. The flow becomes random and with increasing Reynolds number turbulence intensifies.

If the Reynolds number of a particular flow is known, the ratio of Kolmogorov scale to integral length scale can be estimated. The Kolmogorov scale $\ell_\eta$, is defined as [66]:

$$\ell_\eta \equiv \left(\frac{\nu^3}{\varepsilon}\right)^{1/4}, \tag{2.27}$$

where $\varepsilon$ denotes the rate of dissipation of turbulent kinetic energy. Dimensional

analysis gives a scaling for this disspation rate, namely:

$$\varepsilon = u^3/\ell. \tag{2.28}$$

Combining these two equations leads to an estimate of the ratio of Kolmogorov and the large length scales [66]:

$$\ell_\eta/\ell \sim Re^{-\frac{3}{4}}. \tag{2.29}$$

Turbulence enhances mixing. This makes it possible to decrease residence time in technical devices and design smaller apparatuses. That is the reason why engineers designing technical devices such as furnaces, chemical reactors, or other process engineering machinery, consider it a desired mode of operation.

With Reynolds numbers easily exceeding values of the order of $10^4$ for standard applications, it is estimated that at least three orders of magnitude ($\ell_\eta/\ell \sim (10^5)^{-\frac{3}{4}} = 10^{-3}$) are covered by the relevant length scales.

If chemical reaction takes place within this turbulent flow, additional length and time scales are introduced, some of which are even smaller than the Kolmogorov scale [57].

This might give an idea why even though a mathematical description of the problem is at hand, it is unfeasible even with the most powerful of computers to resolve all time and length scales involved for a realistic engineering device.

Therefore techniques have been developed that attempt to provide means of making accurate predictions of quantities characterising the flow, without the need to resolve the full range of scales. One of these techniques is large eddy simulation

(LES) , details of which will be presented in the following chapter.

Chapter 3

# Large Eddy Simulation

In large eddy simulation (LES) a spatial filter is applied to all transport equations. This separates the large scale turbulent motion from the small scales. The small scale motion is commonly assumed to behave more isotropic, therefore, relatively simple expressions can be used to model them. This chapter will outline the mathematical foundations of large eddy simulation and present the set of equations being solved, including all modelled quantities.

## 3.1 The Spatial Filter and Favre Filtering

A spatial filter is defined as the convolution of a quantity $\phi(x,t)$ with the filter kernel $G(x,\Delta)$. The kernel $G$ is a function of space and the filter width $\Delta$. The physical interpretation of the filtering procedure is the damping of high frequency oscillations in the flow or scalar fields. It yields a local, spatial average of flow parameters according to the characteristic length scale of the filter, $\Delta$. Formally this procedure can be written as the following volume integral over the entire

domain of interest:

$$\bar{\phi}(x,t) = \int_V G((x - x', \Delta)\, \phi(x', t)\, dV, \tag{3.1}$$

with $V$ being volume and the overbar denoting a filtered quantity.

Note, that this is the mathematical basis to define the quantity that is being solved for in an implicit large eddy simulation. The filtering provides mathematical means to separate large scale from small scale motion. In this way it is possible to examine, and to quantify the effect of the small, subgrid scale motion on the resolved, mean quantities.

It is common practice in turbulence modelling to employ Favre averaging to overcome the need to model terms involving density fluctuations. This was introduced by Favre [23].

Favre averaging, or in the context of large eddy simulation, Favre filtering is defined as

$$\tilde{\phi} = \frac{\overline{\rho\phi}}{\bar{\rho}}, \tag{3.2}$$

with the tilde denoting a Favre filtered quantity.

### 3.1.1 The Subgrid Scale

The spatial filter separates the large scale, low frequency, low wavenumber part of the turbulent spectrum from the small scale, high frequency, high wavenumber part. The latter is often referred to as subgrid scale. The resolved, large scale part can alternatively be interpreted as a weighted (weighted with the filter kernel

$G$) volumetric average of the flow variables. Therefore it is necessary to define a measure for the fluctuation about this average within the volume in which the average value is defined.

This measure is the subgrid scale variance, $\widetilde{\phi''^2}$. Germano introduced the concept of generalised central moments [27] and expanded on his concept later [28] to maintain some fundamental properties such as the fact that the mean of a fluctuation should vanish. He proposes a definition for the subgrid variance as:

$$\widetilde{\phi''^2} \equiv \widetilde{\phi\phi} - \widetilde{\phi}\widetilde{\phi}. \tag{3.3}$$

Wherever this correlation apprears in a transport equation the full expression will be retained for the sake of clarity.

## 3.2 The Filtered Transport Equations

If the spatial filter is applied to the fundamental transport equations introduced in chapter 2, a new set of equations can be derived which form the basis for large eddy simulations.

### 3.2.1 The Filtered Continuity Equation

Since the continuity equation (2.1) is linear in all its variables $\rho$ and $u$, the filtered form looks just like the unfiltered

$$\frac{\partial \bar{\rho}}{\partial t} + \nabla \cdot \bar{\rho}\widetilde{u} = 0. \tag{3.4}$$

### 3.2.2 The Filtered Momentum Equation

The momentum equation is nonlinear in $u$. Therefore, the filtering procedure gives rise to terms involving correlations of so called subgrid contributions of velocity. They are often referred to as subgrid or residual stresses. The momentum equation solved in the case of large eddy simulation becomes

$$\frac{\partial \bar{\rho}\widetilde{u}}{\partial t} + \nabla \cdot \bar{\rho}\widetilde{u}\widetilde{u} = -\nabla \bar{p} + \nabla \cdot \widetilde{\tau} - \nabla \cdot (\bar{\rho}(\widetilde{uu} - \widetilde{u}\widetilde{u})). \tag{3.5}$$

In this equation the subgrid stresses are represented by $\tau_{sgs} = \bar{\rho}(\widetilde{uu} - \widetilde{u}\widetilde{u})$. For this term a subgrid model has to be employed to obtain full closure. This will be discussed in section 3.3.1.

### 3.2.3 The Filtered Conserved Scalar Transport Equation

Filtering the transport equation (2.6) for a scalar without source, $\xi$, leads to the filtered conserved scalar transport equation. The diffusive flux is approximated by a gradient transport model,

$$\frac{\partial \bar{\rho}\widetilde{\xi}}{\partial t} + \nabla \cdot \bar{\rho}\widetilde{u}\,\widetilde{\xi} = \nabla \cdot (\bar{\rho}D\nabla\widetilde{\xi}) - \nabla \cdot (\bar{\rho}(\widetilde{u\xi} - \widetilde{u}\,\widetilde{\xi})). \tag{3.6}$$

## 3.3 Subgrid Scale Modelling

Equations (3.5) and (3.6) contain unclosed terms, which have to be modelled. They describe the small, subgrid scale features of velocity or the conserved scalar, respectively. These terms also describe quantitatively the influence of those small

scales on the large, resolved scales. Since LES resolves a large part of the turbulent spectrum, the small, unresolved scales at the dissipative end of the spectrum are thought to behave more universally. Hence, fairly simple, algebraic models for these subgrid scale term have been developed.

### 3.3.1 The Subgrid Scale Stresses

#### The Smagorinsky Model

The commonly used model for the anisotropic part subgrid scale stresses,

$$\tau_{sgs} = \bar{\rho}(\widetilde{uu} - \tilde{u}\tilde{u}), \tag{3.7}$$

was developed by Smagorinsky [69]. He proposed a turbulent viscosity to be computed as

$$\nu_t = \mu_t/\bar{\rho} = (C_S\Delta)^2 \mid \tilde{S} \mid, \tag{3.8}$$

where $C_S$ is the so called Smagorinsky constant and $\Delta$ the filter width, usually taken to be proportional to the local grid spacing. Originally this model was proposed as a model for incompressible flow, but it is straightforwardly generalised to constitute a model for variable density flow. This form is presented here.

This model proved to work reasonably well in many flow configurations, with values for the modelling constant in the range of $C_S = 0.1 - 0.23$. A brief review of studies into the specific value is given in the introduction of the paper by Germano et al. [29].

Given the turbulent viscosity, the subgrid scale stresses are then modelled as

$$\tau_{sgs} - \frac{1}{3}\tau_{sgs} I = -2\mu_t \widetilde{S}. \tag{3.9}$$

## Dynamic Subgrid Scale Modelling

A breakthrough in the area of large eddy simulation came with the dynamic model first proposed by Germano et al. [29]. In this model the turbulent viscosity is still computed by equation (3.8), but the parameter rather than constant, $C_S$, is determined dynamically. This method employs a second filtering operation applied to equation (3.5). This operation will be denoted with a hat, $\widehat{\bullet}$, and is often referred to as test-filtering.

The test-filtered momentum equation contains a subgrid scale stress tensor, $T$, of the form:

$$T = \widehat{\widetilde{u}\widetilde{u}} - \widehat{\widetilde{u}}\widehat{\widetilde{u}}, \tag{3.10}$$

which can be related to the subgrid scale stresses as given in equation (3.7) by

$$\mathcal{L} = \widehat{\widetilde{u}\widetilde{u}} - \widehat{\widetilde{u}}\widehat{\widetilde{u}} = T - \widehat{\tau_{sgs}}. \tag{3.11}$$

This term has been labelled Leonard term. It can be interpreted as the part of the turbulent energy spectrum between the length scale $\widehat{\Delta}$, dictated by the test-filter and the filterwidth $\Delta$. The Leonard term can be explicitly computed since it involves only resolved quantities. Subsequently, the Smagorinsky approach, equation (3.9), is applied to both $T$ and $\tau_{sgs}$. Taking into account the identity (3.11), the follwing relation can be derived and serve as a starting point for the

determination of $C_S$:

$$\mathcal{L} - \frac{1}{3}\mathcal{L}I = \alpha C_S - \widehat{\beta C_S}, \tag{3.12}$$

with

$$\alpha = -2\widehat{\Delta}^2 \mid \widehat{\widetilde{S}} \mid \widehat{\widetilde{S}} \tag{3.13}$$

$$\beta = -2\Delta^2 \mid \widetilde{S} \mid \widetilde{S}. \tag{3.14}$$

Plenty of different techniques have been proposed, invoking several assumptions to solve equation (3.12) for $C_S$ [29, 51, 61, 30, 54]. For the present study, the version proposed by Piomelli and Liu [61] was used, which utilises the value of $C_S$ from the previous timestep so solve equation (3.12).

The idea of dynamic modelling greatly improves the generality of large eddy simulation since no modelling parameter has to be specified a priori and configuration dependent. The only degree of freedom with this method is the ratio of filter widths, $r_\Delta = \widehat{\Delta}/\Delta$, which is usually taken to be 2. This assumption is much less restrictive than specifying a constant value of $C_S$ for the entire domain.

### 3.3.2 The Subgrid Scale Flux of Conserved Scalar

An equivalent to the dynamic model for the turbulent viscosity, as described in the previous section, was proposed by Pierce and Moin [58] for the modelling of the turbulent, subgrid scale conserved scalar flux, $J_{sgs} = (\bar{\rho}(\widetilde{u\,\xi} - \widetilde{u}\,\widetilde{\xi}))$. A gradient transport model of the form:

$$J_{sgs} = -D_t \nabla\widetilde{\xi}, \tag{3.15}$$

is used and a dynamic procedure utilised to obtain the turbulent diffusivity. However, since approaches that choose to relate the turbulent diffusivity to the turbulent viscosity via an assumption for a turbulent Schmidt number

$$D_t = \frac{\mu_t}{\bar{\rho} Sc_t} \tag{3.16}$$

have proven to work reasonably well [65], a constant turbulent Schmidt number was used in the present study. Sensitivity of the presented method on the specific value for $Sc_t$ will be presented in chapter 6.

## 3.4 Boundary conditions

The solution of a partial differential equation requires the specification of appropriate boundary conditions. In the case of turbulence simulations this can be problematic, since it may not be feasible to extend the computational domain to a point or bounding surface where boundary conditions are well defined.

### 3.4.1 Inflow Boundary Treatment

Most commonly, boundary conditions have to be prescribed for an inflow position where significant turbulence levels are observed experimentally. Although some components of the turbulent stress tensor are routinely recorded experimentally, the question remains how to synthesize a velocity signal that has the observed one-point statistics and where all components of the stress tensor are correlated.

Many studies employ Gaussian noise with the observed means and variances [15]

but this provides uncorrelated velocity signals, of which the oscillations are quickly damped by viscous effects upon entering the domain. Clayton [15] argues, that in cases where turbulence produced during the breakup of a jet or some mixing layer much exceeds the inflow turbulence, the turbulent characteristics at the inflow become irrelevant, and the natural turbulence production of the shear flow suffices to give satisfactory results. However, it is hard to predict under which circumstances this criterion holds and other methods are desireable.

Pierce and Moin [59] developed a forcing method that enabled them to provide inflow conditions for a coannular jet simulation by carrying out a periodic pipe flow calculation which yields the experimentally observed statistics. This is an elegant but computationally relatively expensive method.

Recently, Klein et al. [42] developed a new approach to this problem that was further modified and tested by di Mare et al. [19]. In this approach, a digital filter is used to provide correlated velocity signal components. Subsequently, the observed correlations given by the measured components of the stress tensor are used to scale the correlated signal to yield a realistic estimation of the turbulent flow entering the computational domain. This is the method used for the present work, with the inlet velocity data taken from the sources of the TNF workshop [21, 1].

### 3.4.2 Outflow Boundary Treatment

At the outflow plane a convective outflow boundary condition is imposed.

$$\frac{\partial \phi}{\partial t} + U_{convective} \frac{\partial \phi}{\partial x_n} = 0, \tag{3.17}$$

where $x_n$ denotes the direction normal to the outflow boundary, and $U_{convective}$ is some convective outflow velocity. For the present study this velocity was taken as the bulk velocity resulting from a global mass balance.

Chapter 4

# Conditional Moment Closure

A fundamental challenge for the modelling of combustion is the wide range of length and time scales involved as outlined in section 2.3. While the large scales of the flow and mixing fields are largely governed by the geometry of the specific setup, turbulent dissipation takes place at the Kolmogorov scale, $\ell_\eta$, which is several orders of magnitude smaller. But even this is large compared to the scales introduced by the chemical conversion of species. The thickness of flames might be even smaller, and time scales can vary heavily depending on the reactiveness of single species. This is problematic for the modelling of these processes, since one cannot afford to resolve all scales involved numerically. Therefore models have to account for the effects of the unresolved scales.

Due to the nonlinearity of the equations describing the chemical system, those effects are of particular importance when trying to model combustion. Therefore several closures for the chemical source have been proposed in the past.

## 4.1 Conserved Scalar Approaches to Turbulent Combustion Modeling

It has been realised for a long time that in nonpremixed combustion systems, where fuel and oxidizer are initially separated, the fluctuations occurring in quantities like species mass fractions and temperature or enthalpy are closely linked to the fluctuations of a conserved scalar, the mixture fraction. For a two feed system, Bilger [2] proposed the following definition for this quantity

$$\xi = \frac{\frac{2(Z_C - Z_{C,O})}{M_C} + \frac{(Z_H - Z_{H,O})}{2\,M_H} + \frac{(Z_O - Z_{O,O})}{M_O}}{\frac{2(Z_{C,F} - Z_{C,O})}{M_C} + \frac{(Z_{H,F} - Z_{H,O})}{2\,M_H} + \frac{(Z_{O,F} - Z_{O,O})}{M_O}}, \tag{4.1}$$

with $Z_i$ denoting element mass fractions of element $i$, $M_i$ being the element's atomic weight and $O$ and $F$ denoting oxidizer and fuel stream respectively. This definition is used to compute the local mixture fraction based on experimental data. For numerical simulations it is sufficient to state that mixture fraction is a conserved scalar, that is a scalar without sources, and to impose consistent boundary conditions.

The mixture fraction describes the local ratio of elemental mass originating from the fuel stream to the elemental mass originating from the oxidizer stream. More intuitively it describes the degree of mixing of the two fluid streams. As they mix, on large scales by convection and on small scales by molecular diffusion, conversion of species by chemical reaction takes place and releases heat. This causes the density to drop and the fluid mixture to become more viscous. It is this phenomenon that constitutes the fluid-chemistry coupling. Fluid dynamics determine the mixing for the combustion to take place, and combustion determines

the change in thermodynamic properties feeding back to fluid dynamics.

Since most combustion systems of industrial relevance operate under turbulent flow conditions in order to enhance mixing, one can imagine that further fluctuations, stemming from the turbulence, have great influence on the small scale mixing and therefore on the chemistry. This is commonly known as turbulence-chemistry interaction.

As mentioned in the introduction, several combustion closures utilise the conserved scalar approach, describing chemistry in terms of its mixture fraction dependence. However, most of them are local models, assuming infinitely fast chemistry and an equilibrium between diffusion and reaction across the flame.

No such assumptions are invoked in conditional moment closure (CMC). The equations are exact and the modelling is introduced through some asymptotic analysis of terms that vanish in the high Reynolds number limit. Furthermore the diffusive flux in mixture fraction space is approximated by analogy with a Markov process.

## 4.2 Background for the Conditional Moment Closure Equations

In this section, an outline of the ideas behind the derivation of the conditional moment closure equations for LES will be presented. The joint p.d.f. transport equation is given to highlight the ties of CMC with p.d.f. methods.

### 4.2.1 The Fine Grained and Joint Probability Density Function

Given a vector of random variables $\phi = (\phi_1, \ldots, \phi_n)$, where $n$ denotes the dimensionality of the vector, with phase or sample space $\eta = (\eta_1, \ldots, \eta_n)$ the so called fine grained probability density function (p.d.f.) is given by:

$$\psi = \prod_{i=1}^{n} \delta(\eta_i - \phi_i), \tag{4.2}$$

where $\delta$ denotes the Dirac delta function. With this definition, probability theory provides the joint probability density function of this random variable, $P(\eta)$, as some average of the fine grained p.d.f.:

$$P(\eta) = \overline{\psi}, \tag{4.3}$$

where the overbar indicates the averaging process. This average may be an ensemble average as in the context of the RANS methodology, or a spatial average or filtering as encountered in the LES framework.

### 4.2.2 The Fine Grained Probability Density Function Transport Equation

With the definition of the fine grained p.d.f. in the previous section and some fundamental rules from the theory of generalised functions as well as the generic transport equation for a reactive scalar (2.6), a transport equation for the fine grained p.d.f. can be derived. The total derivative of the fine grained p.d.f. can

be expressed as:

$$\frac{d\psi}{dt} = \sum_{i=1}^{n} -\frac{\partial}{\partial \eta_i}\left(\psi \frac{d\phi}{dt}\right). \tag{4.4}$$

Substituting the total derivative of the random variable on the right hand side of the equation leads to a transport equation for the fine grained p.d.f.:

$$\begin{aligned}\frac{\partial(\rho\psi)}{\partial t} + \nabla\cdot(\rho u\,\psi) &= -\sum_{i=1}^{n}\frac{\partial}{\partial \eta_i}\nabla\cdot(\psi\rho D\nabla\phi_i) \\ &-\sum_{i=1}^{n}\sum_{j=1}^{n}\frac{\partial^2}{\partial\eta_i\partial\eta_j}(\psi\rho D(\nabla\phi_i\cdot\nabla\phi_j)) - \sum_{i=1}^{n}\frac{\partial}{\partial\eta_i}(\psi\rho\omega_i),\end{aligned} \tag{4.5}$$

where $\omega_i$ denotes the volumetric source of random variable $\phi_i$.

### 4.2.3 The Subgrid Scale Joint Probability Density Function and Conditional Filtering

A probability density function, $P(\eta, \mathrm{x}, t)$ can be defined in a way that is consistent with the filtering procedure of the large eddy simulation technique.

$$P(\eta, \mathrm{x}, t) = \int \psi[\eta - \phi(\mathrm{x}', t)]\; G(\mathrm{x} - \mathrm{x}')d\mathrm{x}'. \tag{4.6}$$

A density weighted p.d.f., $\widetilde{P}(\eta, \mathrm{x}, t)$ can be defined as:

$$\widetilde{P}(\eta, \mathrm{x}, t) = \frac{1}{\bar{\rho}(\mathrm{x}, t)}\int \rho(\mathrm{x}', t)\;\psi[\eta - \phi(\mathrm{x}', t)]\; G(\mathrm{x} - \mathrm{x}')d\mathrm{x}'. \tag{4.7}$$

Conditional filtering of a quantity $\phi$ can then be defined as proposed by Steiner and Bushe [70]:

$$\overline{\phi \mid \eta} = \frac{1}{P(\eta, \mathrm{x}, t)} \int \phi \, \psi[\eta - \phi(\mathrm{x}', t)] \, G(\mathrm{x} - \mathrm{x}') d\mathrm{x}' \tag{4.8}$$

Density weighted conditional filtering of a quantity $\phi$ follows as:

$$\widetilde{\phi \mid \eta} = \frac{\overline{\rho \phi P \mid \eta}}{(\overline{\rho \mid \eta}) P(\eta)} = \frac{\overline{\rho \phi P \mid \eta}}{\overline{\rho} \widetilde{P}(\eta)} \tag{4.9}$$

With this definition, the p.d.f. constitutes a subgrid scale p.d.f., describing the small scale features of the flow. Mathematically, this p.d.f. has the same properties as the temporal p.d.f. in Reynolds averaged flow simulations (RANS), where the p.d.f. describes the unsteady features of the flow. Since the present work is concerned with the large eddy simulation of turbulent combustion, the former p.d.f. will be used for the remainder of the text, but all conclusions have their equivalent in the RANS context.

### 4.2.4 The Subgrid Scale Joint Probability Density Function Transport Equation

Applying the definition of the subgrid scale density weighted p.d.f., convoluting equation (4.5) with the spatial filter and rearranging yields a transport equation

for this p.d.f.:

$$\frac{\partial(\bar{\rho}\,\widetilde{P}(\eta))}{\partial t} + \nabla\cdot(\bar{\rho}\,\widetilde{(u\mid\eta)}\,\widetilde{P}(\eta)) = \tag{4.10}$$
$$-\sum_{i=1}^{n}\sum_{j=1}^{n}\frac{\partial^2}{\partial\eta_i\partial\eta_j}\left\{\bar{\rho}\,\widetilde{(D\,\nabla\phi_i\nabla\phi_j\mid\eta)}\widetilde{P}(\eta)\right\}$$
$$-\sum_{i=1}^{n}\frac{\partial}{\partial\eta_i}\left\{\bar{\rho}\,\widetilde{(\dot{\omega}_i\mid\eta)}\,\widetilde{P}(\eta)\right\} - \sum_{i=1}^{n}\frac{\partial}{\partial\eta_i}\nabla\cdot(\bar{\rho}\,\widetilde{(D\nabla\phi_i\mid\eta)}\,\widetilde{P}(\eta))$$

Similar forms of this equation have been proposed by Gao et al. [26], Colucci et al. [16] as well as Jones and Navarro-Martinez [35].

### 4.2.5 Conditional Expectation

The first statistical moment, also referred to as the mean or expectation , $Q$, of a random variable $\phi$ with p.d.f. $P(\eta)$, where $\eta$ is the sample or phase space of that random variable is defined as:

$$Q = \int_{-\infty}^{+\infty}\eta\,P(\eta)d\eta. \tag{4.11}$$

For a system involving multiple random variables, the *conditional* first moment, or the *conditional* mean of one of these random variables, conditioned on the remaining variables is often of interest.

To illustrate this concept, consider the system of $n+1$ random variables $\phi = (Y,\xi) = (Y,\xi_1,\ldots,\xi_n)$. The sample or phase space of these random variables will be denoted by $\Phi = (y,\eta) = (y,\eta_1,\ldots,\eta_n)$. In that case the joint p.d.f. of all random variables, $P(\Phi) = P(y,\eta)$, fully describes the state of the system. If the conditional expectation or conditional mean, $Q = \langle Y \mid \xi = \eta\rangle$, of the random

variable $Y$, is of interest, equation (4.11) can be straightforwardly be generalised to this multi dimensional case as:

$$Q = \langle Y \mid \xi = \eta \rangle = \frac{1}{P(\eta)} \int y \, P(y, \eta) \, dy. \tag{4.12}$$

The idea of the conditional mean of a random variable together with the transport equation for a joint p.d.f. of multiple random variables (4.10) and the fine-grained p.d.f., equation (4.2.2), provides the framework necessary to derive the conditional moment closure equations for large eddy simulation.

The CMC equations provide a strong reduction of the dimensionality of the system, since chemical quantities are now only a function of space, time and the chosen conditioning variables, $4 + N_c$, with $N_c$ denoting the number of conditioning variables. Recall that equation (4.10) is of dimensionality $4 + N$, where $N$ denotes the number of chemical species in the system.

## 4.3 The Conditional Moment Closure Equations

Following the idea presented in the previous section the conditional moment closure equations for large eddy simulation can be derived as shown in great detail in Navarro-Martinez et al. [55].

### 4.3.1 The Singly Conditional Moment Closure Equation

If only one conserved scalar is considered as conditioning variable and usual assumptions regarding high Reynolds number flows are employed, the singly condi-

tioned moment closure equations as derived and presented by Klimenko and Bilger [44] and derived for the LES context by Navarro-Martinez et al. [55]. The evolution of the density weighted conditional mean, $Q_i = \widetilde{\langle Y_i \mid \eta \rangle} = \widetilde{\langle \rho Y_i \mid \eta \rangle} / \langle \bar{\rho} \mid \eta \rangle$, of a reactive scalar $Y_i$ conditioned on a conserved scalar with sample space variable $\eta$ reads:

$$\frac{\partial Q_i}{\partial t} + \widetilde{\langle u \mid \eta \rangle} \cdot \nabla Q_i = \widetilde{\langle w_i \mid \eta \rangle} + \frac{1}{2} \widetilde{\langle \chi \mid \eta \rangle} \frac{\partial^2 Q_i}{\partial \eta^2} + e_y, \tag{4.13}$$

with $\chi = 2D|\nabla \xi|^2$ and $e_y$ defined as

$$e_y \equiv \frac{\nabla \cdot \left[ \langle \rho \mid \eta \rangle \left( \widetilde{\langle u \mid \eta \rangle} \widetilde{\langle Y_i \mid \eta \rangle} - \widetilde{\langle u Y_i \mid \eta \rangle} \right) \widetilde{P}(\eta) \right]}{\langle \rho \mid \eta \rangle \widetilde{P}(\eta)}. \tag{4.14}$$

This term describes the influence of fluctuations about the conditional mean. Usually subgrid contributions in LES are modelled by gradient transport approaches and that practice is applied for this term

$$e_y = -\nabla \cdot (\langle D_t \mid \eta \rangle \nabla Q_i). \tag{4.15}$$

### 4.3.2 The Doubly Conditioned Moment Closure Equation

For the case of local extinction and reignition a progress variable should be taken into account. In this case the evolution of the doubly conditioned mean, $Q_i = \langle Y_i \mid \eta, \zeta \rangle$ of a reactive scalar $Y_i$, conditioned on a conserved scalar $\xi$ and a reactive scalar $c$, with sample space variables $\eta$ and $\zeta$ respectively, is given by Kronenburg

[45] and reads:

$$\begin{aligned}
\langle \rho \mid \eta,\zeta\rangle \frac{\partial Q_i}{\partial t} \;+\; & \langle \rho u \mid \eta,\zeta\rangle \cdot \nabla Q_i = \langle w_i \mid \eta,\zeta\rangle - \langle w_c \mid \eta,\zeta\rangle \frac{\partial Q_i}{\partial \zeta} \\
+\; & \frac{1}{2}\langle \rho\chi \mid \eta,\zeta\rangle \frac{\partial^2 Q_i}{\partial \eta^2} + \langle \rho D\, \nabla c \nabla c \mid \eta,\zeta\rangle \frac{\partial^2 Q_i}{\partial \zeta^2} \\
+\; & 2\,\langle \rho D\, \nabla \xi \nabla c \mid \eta,\zeta\rangle \frac{\partial^2 Q_i}{\partial \eta \partial \zeta} + e_q + e_y
\end{aligned} \tag{4.16}$$

with

$$\begin{aligned}
e_q \;\equiv\; & \langle \nabla \cdot (\rho D_i \nabla Q_i) + \rho D_i \nabla \xi \cdot \nabla \frac{\partial Q_i}{\partial \eta} + \rho D_i \nabla c \cdot \nabla \frac{\partial Q_i}{\partial \zeta} \\
+\; & \nabla \cdot (\rho (D_i - D_\xi) \nabla \xi) \frac{\partial Q_i}{\partial \eta} + \nabla \cdot (\rho (D_i - \alpha) \nabla c) \frac{\partial Q_i}{\partial \zeta} \mid \eta,\zeta\rangle, \\
e_y \;\equiv\; & -\langle \rho \frac{\partial Y''}{\partial t} + \rho u \nabla Y'' - \nabla \cdot (\rho D_i \nabla Y'') \mid \eta,\zeta\rangle.
\end{aligned} \tag{4.17}$$

Here, $Y''$ denotes the fluctuations about the conditional mean. These equations can be simplified for unity Lewis number cases, where $D_i = D_\xi = \alpha$. An order of magnitude estimation suggests that $e_y$ can often be neglected as practised by Kronenburg [45] for DNS of homogeneous, decaying turbulence. In the context of the present work these equations are presented for reference and to highlight the main differences and common features of the singly and double conditional moment closure equations. For the use of the doubly conditioned moment closure equations, closure of the dissipation rates involving gradients of the progress variable, $c$, will not be straightforward and is the main problem for the solution of these equations.

## 4.4 The Conserved Scalar Subgrid Scale p.d.f.

The solution of equation (4.13) provides the conditional moments of chemical quantities. Unconditional values are then given by the convolution of the conditional moments with the density weighted subgrid scale p.d.f. of mixture fraction, $\widetilde{P}(\eta)$, as:

$$\widetilde{Y}_i = \int_{\eta=0}^{1} Q_i \, \widetilde{P}(\eta) \, d\eta. \tag{4.18}$$

To obtain $\widetilde{P}(\eta)$ it is possible to seek a numerical solution to the subgrid scale p.d.f. transport equation (4.10) for a conserved scalar as sole random variable. However, due to the computational cost of this approach and the notion that in the LES context variance should be rather small, the p.d.f. is often approximated by a $\beta$-function. It has been shown that this is a reasonably good approximation to the p.d.f. [34, 17].

The $\beta$-p.d.f. is given by [17]:

$$\widetilde{P}(\eta) = \frac{\eta^{a-1}(1-\eta)^{(b-1)}}{\int_0^1 \gamma^{a-1}(1-\gamma)^{b-1} d\gamma}, \tag{4.19}$$

with

$$a = \widetilde{\xi}\left(\frac{\widetilde{\xi}(1-\widetilde{\xi})}{\widetilde{\xi''^2}} - 1\right) \tag{4.20}$$

$$b = (a/\widetilde{\xi}) - a. \tag{4.21}$$

A subtlety worth mentioning in this context is the somewhat counter-intuitive equation to determine the unconditional density. Since the p.d.f. is density

weighted, unconditional density is obtained as:

$$\frac{1}{\bar{\rho}} = \int_{\eta=0}^{1} \frac{1}{\langle \rho \mid \eta \rangle} \widetilde{P}(\eta)\, d\eta. \tag{4.22}$$

For an explanation of this relation, the reader is referred to Appendix A.

### 4.4.1 Subgrid Scale Modelling

#### The Conserved Scalar Variance

The $\beta$-function is determined by its first two statistical moments. The mean is given by the solution of equation (3.6). The variance is a characteristic quantity, it determines the structure of the conserved scalar field and has to be accounted for by a subgrid scale model. A lot of work has been and still is being devoted to devise subgrid scale models for large eddy simulation. In analogy to Smagorinsky's [69] model for the subgrid scale stresses Branley and Jones [6] devised a model for the subgrid scale variance of a conserved scalar that reads:

$$\widetilde{\xi''^2} = C_\xi \Delta^2 |\nabla \widetilde{\xi}|^2. \tag{4.23}$$

Pierce and Moin [58] proposed a dynamic procedure to obtain the coefficient $C_\xi$ but that method has not been adopted in the present work. Instead a constant value of $C_\xi$ is used. For the present work, it was taken to be $C_\xi = 0.09$ as suggested by Navarro-Martinez et al. [55].

### The Conserved Scalar Dissipation Rate

The filtered scalar dissipation rate, $\widetilde{\chi} = \widetilde{2D|\nabla\xi|^2}$ can be split into the resolved, $\chi_{res} = 2D|\nabla\widetilde{\xi}|^2$, and the residual or subgrid scale part, $\chi_{sgs}$, which requires modelling. Following Pierce and Moin [58] this contribution is taken to be

$$\chi_{sgs} = 2D_t|\nabla\widetilde{\xi}|^2 = 2\,\frac{\mu_t}{\bar{\rho}\,Sc_t}\,|\nabla\widetilde{\xi}|^2, \tag{4.24}$$

such that

$$\widetilde{\chi} = \chi_{res} + \chi_{sgs} = 2\,\left(D + \frac{\mu_t}{\bar{\rho}\,Sc_t}\right)\,|\nabla\widetilde{\xi}|^2 \tag{4.25}$$

## 4.5 Closures

The conditional moment closure equations (4.13,4.16) involve conditional quantities like the conditionally filtered velocity or scalar dissipation rate that are unclosed. Modelling these quantities poses serious difficulties in the context of RANS simulations, where conditional quantities have to be approximated based on only two parameters, the mean and the variance. Since in LES-CMC it is common practise to solve the CMC equations for much larger control volumes than unconditional quantities, such as velocities and scalars, it is possible to derive a straightforward model for conditional quantities, which involves little a priori knowledge or assumptions.

The basic idea is expressed mathematically as follows:

$$\widetilde{\langle\phi \mid \eta\rangle} = \langle\widetilde{\phi} \mid \eta\rangle \tag{4.26}$$

As will be outlined in section 4.6.1, every CMC cell volume coincides with several hundred LES cells. That means several hundred values of the Favre averaged quantity $\widetilde{\phi}$ are available within this volume. This offers a straightforward way to model conditional quantities. With the assumption of local homogeneity within one CMC control volume, these terms are simply approximated as the conditional average of the LES quantity.

$$\langle \widetilde{\phi} \mid \eta \rangle = \frac{\sum_{(CV_{\mathbf{x}} \subset CV_{CMC}) \wedge (\eta - \Delta\eta \leq \widetilde{\xi}(\mathbf{x}) < \eta + \Delta\eta)} \widetilde{\phi}(\mathbf{x})}{\sum_{(CV_{\mathbf{x}} \subset CV_{CMC}) \wedge (\eta - \Delta\eta \leq \widetilde{\xi}(\mathbf{x}) < \eta + \Delta\eta)} 1} \tag{4.27}$$

This method has proven successful in a LES-CMC computation of Sandia flame D [55]. However, it has to be stressed that in order for this model to be advantageous over others, it needs to be made sure that a sufficiently large part of conserved scalar space is covered by the respective CMC control volumes. This is to ensure that samples exist for the most part of conserved scalar space. Otherwise the modelling is not straightforward at those points in mixture fraction space. Without information from the flow field, assumptions about the functional form of the conditional quantity have to be employed. Whenever this was the case in the present work, linear interpolation was used to provide a non-zero value for $\widetilde{\langle \phi \mid \eta \rangle}$ for the entire range of $0 \leq \xi \leq 1$. Since those occurrences are avoided where possible, this only occurred on the rich side of conditional quantities far downstream, since the conserved scalar diffuses, which causes the maximum possible value for this conserved scalar to decrease below $\xi = 1$ with increasing downstream distance.

## 4.6 Numerical Solution of the CMC Equations

The set of equations consisting of the singly conditioned moment closure equation (4.13), formulated for all chemical species in the system and enthalpy, cannot be solved analytically. Therefore a numerical solution at discrete points in time and space is sought.

### 4.6.1 The Computational Mesh

Since the conditional moment closure equations require the resolution of an additional dimension that represents conserved scalar space, the computational costs of and the memory requirements for solving these equations are high.

However, since conditional moments of reactive quantities are expected to vary less rapidly as unconditional quantities, Navarro-Martinez et al. [55] argued that the CMC equations can be solved on a much coarser mesh than that of unconditional quantities like velocity or the conserved scalar. This procedure implicitly assumes homogeneity of conditional moments in the respective control volumes, which seems reasonable. This procedure has proven to work well for the LES-CMC simulation of piloted jet flames [55] and is adopted for the present work. Figure 4.1 illustrates the mesh arrangement, where the control volumes for the conditional moments contain up to hundreds of LES control volumes. This mesh design makes the modelling of conditional quantities as described in Section 4.5 possible.

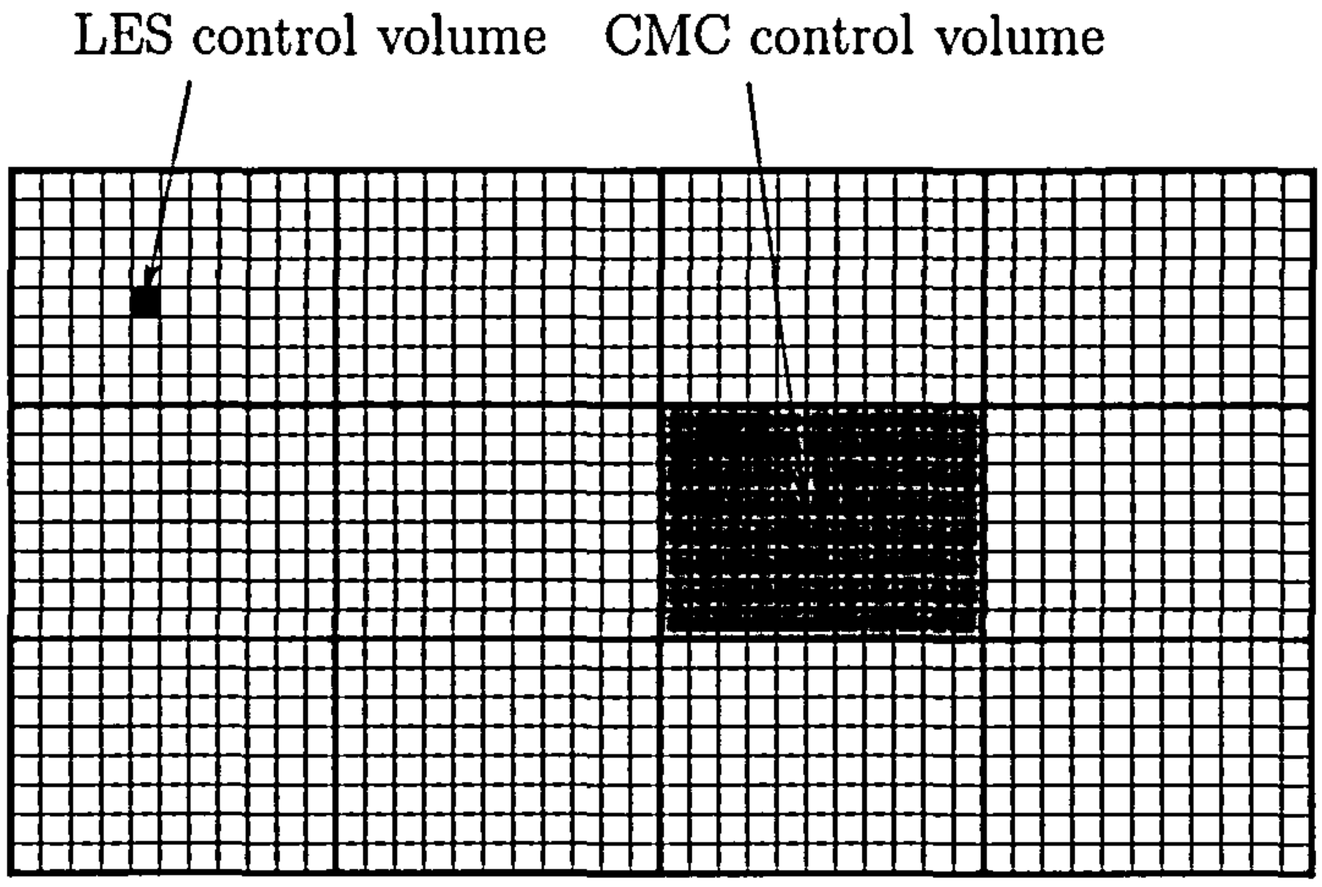


Figure 4.1: Mesh arrangement

### 4.6.2 Boundary Conditions

For the present study of piloted jet flames three points in mixture fraction space for reactive quantities are specified by the fuel composition at $\xi = 1$, the oxidizer composition at $\xi = 0$ and the pilot composition at $\xi = 0.27$. Therefore, a triangular profile is constructed and applied as boundary condition for conditional moments at the inflow plane. All other boundaries are treated as Neumann boundaries, hence

$$\left.\frac{\partial Q}{\partial x_{normal}}\right|_{\text{Boundary plane}} = 0 \tag{4.28}$$

is enforced.

### 4.6.3 Discretization

The convective term in equation (4.13) is discretized with a standard central difference scheme and treated explicitly.

The model for term (4.14), equation (4.15), is discretized by a standard finite difference, second derivative approximation. This term is treated explicitly as well.

Diffusion in scalar space is equally discretized by a three-point, finite difference, second derivative approximation. This term is the only transport term which is treated implicitly. It yields a three point stencil, thus a tridiagonal matrix. This makes it possible to use for the solution of the linear system the Thomas or tridiagonal matrix algorithm (TDMA), which is a direct solution method and is extremely efficient and scalable.

Details of all the mentioned discretization schemes and the TDMA can be found in standard textbooks such as Ferziger and Peric [24]. All schemes chosen are of second order accuracy.

### 4.6.4 Solution Procedure

The numerical solution of equation (4.13) is challenging since it involves the chemical source term which causes the system of equations to be stiff and poses unacceptable constraints on the possible time step size if treated in the simplest, explicit manner. Additionally, it is desireable to achieve a certain degree of modularity in the solver, so that independent changes of the numerical treatment of a single term can be implemented without the necessity to review the remaining parts, for which a satisfactory solution might be at hand.

For these reasons, the method of fractional steps has been used to advance the numerical solution of equation (4.13) in time. This method was developed by

Yanenko [82] and has found widespread use as in Kim and Moin [37].

### The Method of Fractional Steps

To introduce the method of fractional steps, consider the conditional moment closure equation (4.13), written in terms of numerical operators.

$$\frac{\partial Q}{\partial t} = W(Q) + T(Q), \tag{4.29}$$

where $W$ denotes the operator accounting for the chemical source of conditional moments, and $T$ subsumes all remaining transport terms. The entire equation can then be split into the various contributions of different physical processes, so that they can be integrated individually. In the present case, the operator splitting method proposed by Strang [71], often referred to as Strang-splitting, is used, which involves the following steps:

Step 1:

$$\frac{Q^* - Q^t}{(1/2\ \Delta t)} = T(Q^t) \tag{4.30}$$

Step 2:

$$\frac{Q^{**} - Q^*}{\Delta t} = W(Q^*) \tag{4.31}$$

Step 3:

$$\frac{Q^{t+\Delta t} - Q^{**}}{(1/2\ \Delta t)} = T(Q^{**}) \tag{4.32}$$

This sequence completes the advancement in time. This method, as originally proposed by Strang, is of second order accuracy in time. However, his analysis did

not include a chemical reaction operator and was concerned with a pure advection equation in two spatial dimensions. Carrayrou et al. [9] consider very simple reaction models and their implications on the errors of the numerical solution of reactive transport equations such as the CMC equations.

### 4.6.5 Implicit Integration of the Chemical Source Term

The stiffness of the equations describing chemical kinetics makes it necessary to treat the chemical source term in the conditional moment closure equations with care. A simple explicit integration leads to impractically small times steps to ensure stability. Therefore a more sophisticated method which utilises a Newton linearisation of the chemical source term is used for the integration. The mathematical form of this method will be outlined below.

A solution is sought for the following differential equation describing a chemical system of $i = 1, \ldots, n$ species and $m$ elementary reactions

$$\frac{\partial Y_i}{\partial t} = w_i \tag{4.33}$$

The chemical source term $w_i$ of chemical species $i$ as function of the composition vector $Y_i$, pressure $p$ and temperature $T$, can be expanded in a Taylor series in

the following way:

$$\begin{aligned} w_i(Y_j, T, p) &= w_i(Y_{j,0}, T_0, p_0) \\ &\quad + \frac{\partial w_i}{\partial Y_j}\,\Delta Y_j + \frac{\partial^2 w_i}{\partial Y_j^2}\,\frac{(\Delta Y_j)^2}{2!} + \overbrace{\cdots}^{\text{higher order terms}} \\ &\quad + \frac{\partial w_i}{\partial T}\,\Delta T + \ldots + \frac{\partial w_i}{\partial p}\,\Delta p + \ldots \end{aligned} \tag{4.34}$$

Terminating the series after the linear term and discarding influences of varying temperature $T$ and pressure $p$ comprises a linearised form of this equation, giving:

$$w_i(Y_j) = w_i(Y_{j,0}) + \frac{\partial w_i}{\partial Y_j}\,\Delta Y_j \tag{4.35}$$

Considering Arrhenius kinetics, an irreversible reaction involving $l$ species being converted, the rate of reaction of species $i$ can be expressed as

$$w_i = k(T) \cdot Y_i^{C_i} \cdot \sum_{j=1}^{l-1} Y_j^{C_j} \tag{4.36}$$

Given this, the Jacobian $\frac{\partial w_i}{\partial Y_j}$ is readily evaluated analytically as

$$\frac{\partial w_i}{\partial Y_j} = k(T) \cdot C_j \cdot Y_j^{C_j - 1} \cdot \sum_{k=1}^{l-1} Y_k^{C_k} \tag{4.37}$$

Discretizing equation 4.33 and introducing equation 4.35 expanded about $t_0 = t^*$,

with $t^*$ being the last intermediate time level leads to

$$\begin{aligned}
\frac{Y_i^{t+\Delta t} - Y_i^t}{\Delta t} &= w_i(Y^{t^*}) + \left.\frac{\partial w_i}{\partial Y_j}\right|^{t^*} (Y_j^{t+\Delta t} - Y_j^{t^*}) \\
Y_i^{t+\Delta t} - Y_i^t &= w_i(Y^{t^*})\,\Delta t + \left.\frac{\partial w_i}{\partial Y_j}\right|^{t*} (Y_j^{t+\Delta t} - Y_j^{t^*})\,\Delta t \\
Y_i^{t+\Delta t} - Y_i^t &= w_i(Y^{t^*})\,\Delta t \\
&\quad + \left.\frac{\partial w_i}{\partial Y_i}\right|^{t^*} (Y_j^{t+\Delta t} - Y_j^{t^*})\,\Delta t + \left.\frac{\partial w_i}{\partial Y_j}\,(\Delta Y_j)\right|_{j\neq i}^{t^*} \Delta t \\
(1 - \left.\frac{\partial w_i}{\partial Y_i}\right|^{t^*})\, Y_i^{t+\Delta t} &= w_i(Y^{t^*})\,\Delta t \\
&\quad + \left.\frac{\partial w_i}{\partial Y_j}\,(\Delta Y_j)\right|_{j\neq i}^{t^*} \Delta t - \left.\frac{\partial w_i}{\partial Y_i}\right|^{t^*} Y_i^{t^*} + Y_i^t \qquad (4.38)
\end{aligned}$$

where the coefficients for the linearised system of the form $\mathbf{A}x = b$ can easily be identified.

That constitutes a fully implicit integration of the form

$$\frac{\partial Y_i}{\partial t} = w_i^{t+\Delta t} \qquad (4.39)$$

since for the converged solution $Y_j^{t+\Delta t} = Y_j^{t^*}$ holds, and the difference $Y_j^{t+\Delta t} - Y_j^{t^*}$ vanishes. This leaves the Newton linearisation as a numerical construct to improve stability of the integration.

For an interpretation of this procedure it is more convenient to consider the integral form of equation (4.33).

$$\int_t^{t+\Delta t} \frac{\partial Y_i}{\partial t} dt = Y_i^{t+\Delta t} - Y_i^t = \int_t^{t+\Delta} \left( w_i(Y^t) + \int \frac{\partial w_i}{\partial Y_j}\, dY(t) \right)\, dt \qquad (4.40)$$

An explicit integration of this equation, with $w_i = w_i(Y^t)$ would assume the

rate of reaction to be constant even though the species mass fractions $Y$ might vary considerably. Given the highly nonlinear nature of chemical kinetics, explicit integration is unstable and therefore useless for practical purposes. By implicit integration with the present method, rates of reaction are still assumed constant within one time step but stability of the integration is greatly improved. The method and a graphical interpretation of the integral equation (4.40) is illustrated in figure 4.2.

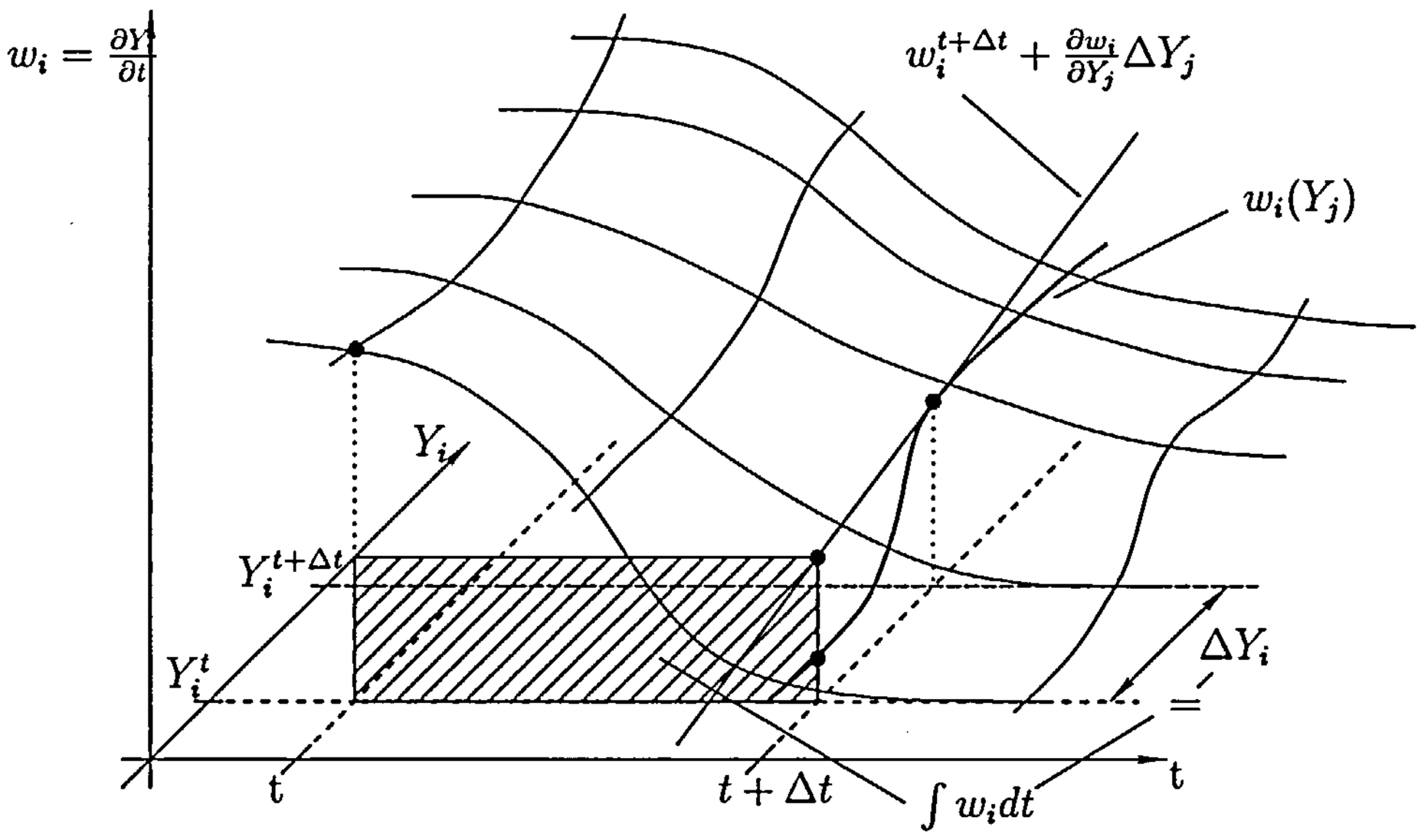


Figure 4.2: Source term integration

Chapter 5

# Extended Conditional Moment Closure

Doubly conditional moment closure provides a mathematically sound framework for scenarios where a single conditioning variable might not be sufficient to capture the main parameters governing the combustion process. In the case of extinction and reignition, mixture fraction accounting for the mixing process of fuel and oxidizer is not the only characteristic parameter. Fluctuations about the singly conditioned mean will be large, and the finite progress of chemical reaction has to be considered. Whereas a first order evaluation of the chemical source term based on conditional mean quantities might be sufficient for pure diffusion flames, for the case of such highly unsteady scenarios like local extinction and reignition, it is necessary to quantify the reaction progress and include this additional knowledge in the approximation of the source term. The reaction progress can be quantified by considering a suitably chosen progress variable. This progress variable parameterises the transition of a mixture of fixed mixture fraction, or equivalence ratio respectively, from mixed reactants at ambient temperature to products at the specific adiabatic flame or equilibrium temperature.

## 5.1 Extended Source Term Closure

The aim of the extended conditional moment closure method is to approximate the effect of double conditioning on the chemical source term in equation (4.13). It is obvious from equation (2.24) that temperature, sensible enthalpy, or therefore any other progress variable parameterising the transition from mixed oxidant and reactants at ambient conditions to chemical equilibrium, has a strongly nonlinear influence on the rate of reaction. Therefore, taking into account variations in conditional temperature should improve chemistry predictions for cases with local extinction and reignition events.

For this, doubly conditioned moments of the chemical species of the system have to be approximated. The present work uses a precomputed, doubly conditioned reference field, $Q^{d,0}(\eta, \zeta)$, where superscript $d$ denotes double conditioning and $\eta$ and $\zeta$ are the sample space variables of mixture fraction and progress variable, respectively. Section 5.2 elaborates on the choice of progress variable for the present work. Section 5.3 discusses issues and the approximation of the conditional p.d.f. and section 5.4 describes the construction of the reference field $Q^{d,0}(\eta, \zeta)$.

The reference field $Q^{d,0}(\eta, \zeta)$ provides an educated guess for the functional dependence of conditional moments on a progress variable but is not necessarily consistent with the instantaneous, local, singly conditioned moments stemming from the solution of equation (4.13). The joint probability density function of mixture fraction and progress variable, $P(\eta, \zeta)$, can be decomposed according to Bayes' theorem

$$P(\eta, \zeta) = P(\eta)\, P(\zeta \mid \eta). \tag{5.1}$$

With this p.d.f. given, doubly conditioned moments, $Q^d(x,t,\eta,\zeta)$, are related to singly conditioned moments, $Q^s(x,t,\eta)$, and have to satisfy the following condition:

$$Q^s(x,t,\eta) = \int_{\zeta=0}^{1} Q^d(x,t,\eta,\zeta)\, P(\zeta \mid \eta)\, d\zeta. \tag{5.2}$$

In the proposed method we seek an estimation for these doubly conditioned moments $Q^d$ by a reference field $Q^{d,ref}$ for which the constructed reference field $Q^{d,0}$ provides the functional shape. In order to ensure consistency as defined by equation (5.2), the constructed reference field is scaled, such that this relation is satisfied. The scaled reference field, $Q^{d,ref}(x,t,\eta,\zeta)$, which is used to calculate the doubly conditioned chemical source term, is computed as

$$Q^{d,ref}(x,t,\eta,\zeta) = g(x,t,\eta) \cdot Q^{d,0}(\eta,\zeta). \tag{5.3}$$

The scaling factor $g(x,t,\eta)$ enforces that equation (5.2) holds and is obtained from

$$g(x,t,\eta) = \frac{Q^s(x,t,\eta)}{\int_{\zeta=0}^{1} Q^{d,0}(\eta,\zeta)\, P(\zeta \mid \eta)\, d\zeta}, \tag{5.4}$$

where $Q^s(x,t,\eta)$ denotes the current solution of the standard CMC equations.

Based on the scaled reference field, $Q^{d,ref}(x,t,\eta,\zeta)$, the doubly conditioned chemical source term can be calculated as

$$\langle w_i \mid \eta,\zeta \rangle = w_i(Q^{d,ref}(x,t,\eta,\zeta), p, T), \tag{5.5}$$

via

$$w_i = \sum_{k=1}^{r} (\nu''_{i,k} - \nu'_{i,k}) \left[ k_f \prod_{j=1}^{N} C_j^{\nu'_{j,k}} - k_b \prod_{j=1}^{N} C_j^{\nu''_{j,k}} \right], \tag{5.6}$$

where $Q^{d,ref}(x,t,\eta,\zeta)$ provides the concentrations $C_i$. The thermodynamical state of the system is specified by the composition, the pressure and the enthalpy. The temperature $T$ is then determined by an iterative procedure, where the temperature is sought, which, for the composition given by $Q^{d,ref}(x,t,\eta,\zeta)$ yields the enthalpy given by

$$h = \zeta\,(h_{s,max} - h_{s,min}) + \sum_{i=1}^{N} Q_i^{d,ref}(x,t,\eta,\zeta)\cdot h^{\circ}_{f,i}. \tag{5.7}$$

The temperature influences the chemical source term through the Arrhenius reaction rate constant

$$k = B\,T^n\,e^{-\frac{E}{RT}}. \tag{5.8}$$

Subsequently the doubly conditioned source term is integrated in progress variable direction to yield the singly conditioned source term, which appears in the CMC equation (4.13).

$$\langle w_i \mid \eta\rangle = \int_{\zeta=0}^{1} \langle w_i \mid \eta,\zeta\rangle\; P(\zeta \mid \eta)\; d\zeta \tag{5.9}$$

The above flow chart, figure 5.1, illustrates and summarises the method and the sequence of computations.

## 5.2 The Progress Variable

Many choices are plausible for a progress variable. The most obvious is temperature which has been used in a number of studies [10, 60, 64]. Others choose a linear combination of certain species [25, 20, 78]. These studies use the sum of

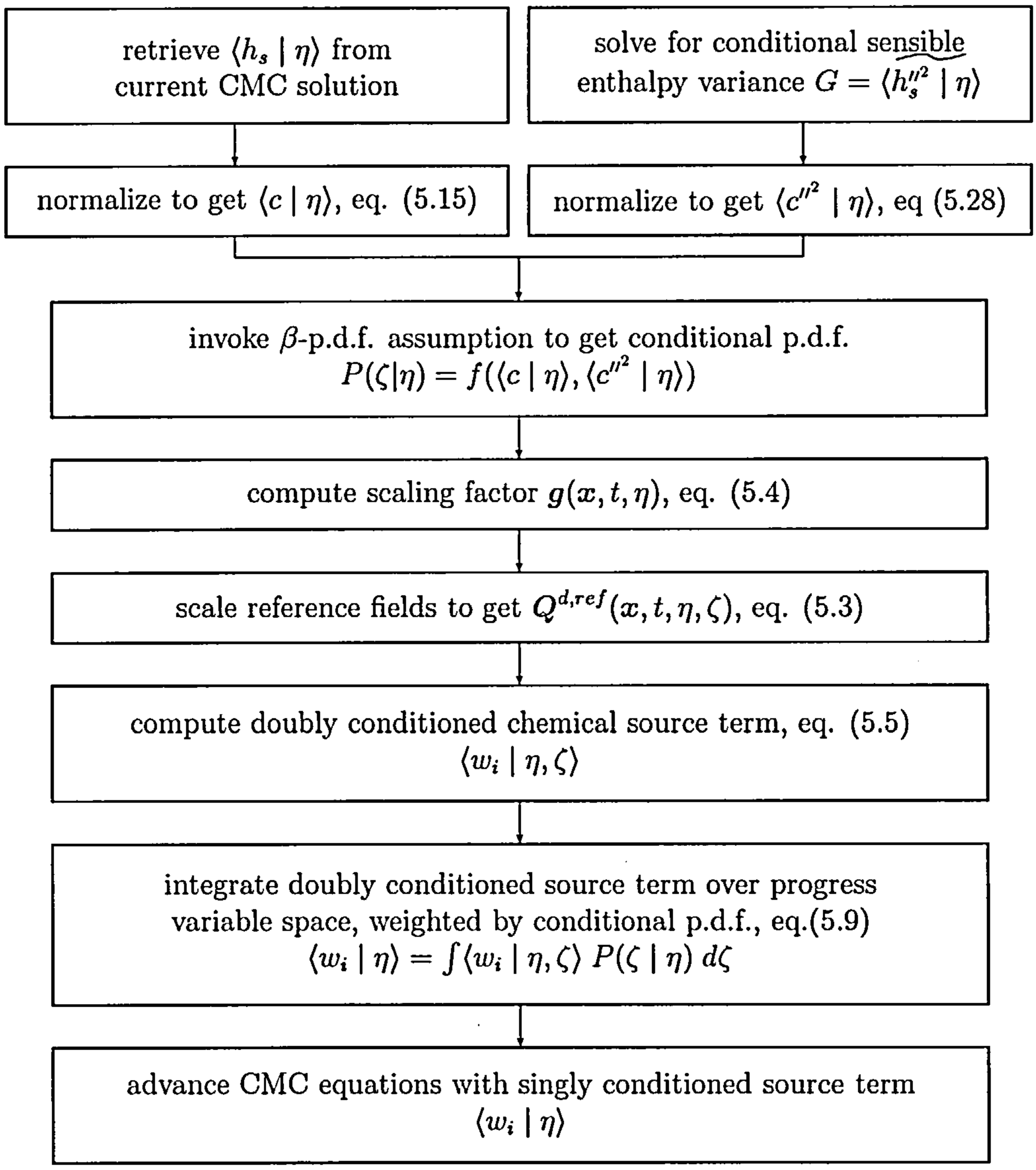


Figure 5.1: Flow chart of CMCe methodology

$CO_2$ and CO mass fractions to ensure a monotonous parameterisation of progress variable space. For the present work sensible enthalpy was chosen as progress variable.

Enthalpy of a multicomponent mixture comprises two contributions. On one hand the enthalpy of formation; the enthalpy required to form the species of the mixture from their elements at standard conditions. Standard condition is usually accepted as $T° = 25°C$ and $p° = 1\,atm = 101.325\,kPa = 1.01325\,bar$. On the other hand there is sensible enthalpy, which is the amount of enthalpy that is needed to heat the mixture from standard temperature, $T°$, to the actual temperature encountered, $T$.

$$h(T,p) = \underbrace{h_f(T°,p)}_{Enthalpy\,of\,formation\,at\,standard\,condition} + \underbrace{\int_{T°}^{T} c_p\,dT}_{sensible\,enthalpy} \tag{5.10}$$

For the present work, sensible enthalpy, $h_s$, as defined by Eq. (5.10) and calculated according to Eq.(5.11) is used.

$$h_s = h - \sum_{i=1}^{N} Y_i \cdot h°_{f,i} \tag{5.11}$$

Kronenburg [45] argues, that this is a good choice because it yields a straight-forward calculation of the progress variable source term. The calculation of the source term for the case of temperature as progress variable would be more difficult because of temperature dependence of the specific heat.

If volume forces, pressure fluctuations and shear stresses are negligible, and unity Lewis number is assumed, which is standard practice, the sensible enthalpy source

term is given by

$$w_{h_s} = -\sum_{i=1}^{N} w_i \cdot h^{\circ}_{f,i} + q_R. \tag{5.12}$$

Heat release goes along with the system approaching or retreating from chemical equilibrium. Therefore sensible enthalpy provides a monotonous and continuous parameterisation of the reaction.

The extended CMC methodology solely focuses on the closure of the chemical source term. Mixture fraction and sensible enthalpy are identified to be the two parameters with which fluctuations of the source term can be associated. To capture the effect of varying sensible enthalpy, representing a non-zero probability of states of reaction progress from unburnt to fully burnt, this probability has to specified.

## 5.3 The Conditional p.d.f.

Since the dependence of the chemical source term on mixture fraction and progress variable will be considered, the joint p.d.f., $P(\eta, \zeta)$, of those two parameters has to be approximated. Invoking Bayes' theorem, a joint p.d.f. can be expressed as the product of a the marginal p.d.f. of one variable, $P(\eta)$, and the conditional p.d.f., $P(\zeta \mid \eta)$, of the other.

$$P(\eta, \zeta) = P(\eta)\, P(\zeta \mid \eta). \tag{5.13}$$

In this way, both terms on the right hand side can be treated separately. The marginal p.d.f. of mixture fraction, $P(\eta)$, is approximated as shown in section

4.4.

For the conditional p.d.f., $P(\zeta \mid \eta)$, Vervisch et al. [78] have shown that, with the mean and variance (the first and second statistical moment of a p.d.f.) known, a $\beta$-function is a good approximation, as long as the progress variable is normalized. This is to ensure that for every point in mixture fraction space, the progress variable is allowed to vary between a local minimum and a locally achievable maximum. This represents a stretching of progress variable space, in order to cover only accessible regions of mixture fraction-progress variable space.

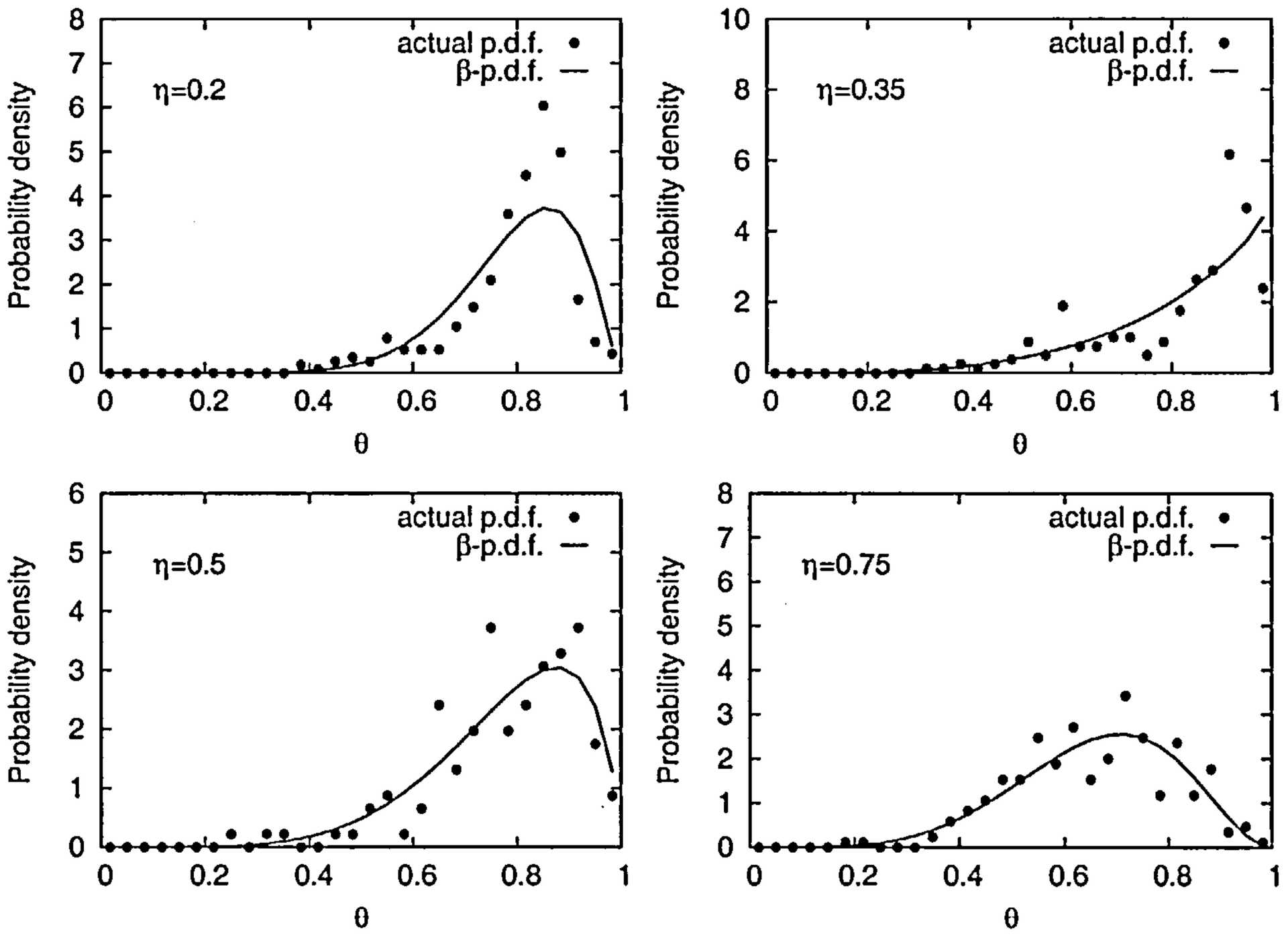


Figure 5.2: Assessment of the validity of the $\beta$-p.d.f. assumption for the conditional p.d.f. of the progress variable.

To stress the validity of this approach, figure 5.2 shows a test of the $\beta$-p.d.f. assumption, based on the data from Sandia flame E. Temperature data was nor-

malized by the maximum value for a specific mixture fraction value, $T_{max}$, and the minimum temperature of the coflow, $T_{min} = 291K$,

$$\theta = \frac{T - T_{min}}{T_{max} - T_{min}}, \tag{5.14}$$

where $\theta$ denotes normalized temperature.

The conditional mean and variance for that point in mixture fraction space was computed and based on those values the $\beta$-p.d.f. was obtained.

It can be seen that with the correct prediction of conditional mean and variance as well as a suitable normalization, the $\beta$-p.d.f. is indeed a good approximation to the true conditional probability density function.

### 5.3.1 The Conditional Mean of the Progress Variable

At any given value of mixture fraction, or equivalence ratio respectively, there is only a finite amount of chemically bound energy available to be released through chemical reaction. The adiabatic flame temperature, or equilibrium temperature is a function of mixture fraction, and temperature above those will generally not be encountered in absence of heat sources.

For the present study, sensible enthalpy is therefore normalized as

$$\langle c \mid \eta \rangle = \frac{\langle h_s \mid \eta \rangle - h_{s,min}(\eta)}{h_{s,max}(\eta) - h_{s,min}(\eta)}, \tag{5.15}$$

in order to invoke the $\beta$-p.d.f. assumption for the conditional p.d.f., with

$$h_{s,min}(\eta) = h(\eta) - \sum_{i=1}^{N} [Y_{i,O} + \eta \cdot (Y_{i,F} - Y_{i,O})] \cdot h_f^\circ, \tag{5.16}$$

and $h_{s,max}(\eta)$ taken from the solution of a flamelet calculation with scalar dissipation rate of $20\frac{1}{s}$ at stoichiometric and an error-function dependence on mixture fraction.

With the conditional mean, $\langle c \mid \eta \rangle$, given by equation (5.15), only the conditional variance of the progress variable has to be approximated to specify a $\beta$-function as model for the conditional p.d.f..

### 5.3.2 The Conditional Variance of the Progress Variable

#### Modelling approaches

To estimate the conditional variance of the progress variable, current practice in LES suggests a few straightforward ideas.

Firstly, the well established model for the variance of a conserved scalar was tested for this case,

$$\widetilde{h_s''^2} = C_{h_s} \Delta^2 |\nabla \widetilde{h}_s|^2. \tag{5.17}$$

as well as the formulation taking into account the source correlation, as suggested by Pierce and Moin [58]:

$$\widetilde{h_s''^2} = C_1 \left( C_{h_s} \Delta^2 |\nabla \widetilde{h}_s|^2 + \widetilde{w_{h_s}'' \, h_s''} / |\widetilde{S}| \right). \tag{5.18}$$

Also, in a further attempt, the unconditional variance equation was solved.

$$\frac{\partial \bar{\rho}\,\widetilde{h_s''^2}}{\partial t} + \nabla \cdot \bar{\rho}\tilde{u}\,\widetilde{h_s''^2} = \nabla \cdot \bar{\rho} D_{eff} \nabla\,\widetilde{h_s''^2} - \bar{\rho}\,\chi_{h_s,sgs} + 2\bar{\rho}\,\widetilde{w_{h_s}'' h_s''} + 2\bar{\rho}\,D_t |\nabla \tilde{h}_s|^2, \quad (5.19)$$

where $D_{eff}$ denotes an effective diffusivity, obtained as $D_{eff} = D_{molecular} + D_t$.

After obtaining those variances, they were conditioned as described in section 4.5, to yield conditional variances.

However, it was not possible to obtain reasonable results in this way. The peak of conditional variances of temperature around stoichiometric, which can be observed in the experiments could never be reproduced. In fact, conditional variances predicted by any of the above methods showed unnaturally strong underprediction of conditional variances around stoichiometric.

It was found that a fundamental flaw in the practice described above, was the reason behind this originally puzzling behaviour. Firstly, unconditional and conditional variances are fundamentally different quantities. The latter is a measure of fluctuations about the conditional mean; therefore modelling of this quantity should not be based solely on unconditional quantities, since they contain the fluctuations of the conditioning variable. The main issue however is the following.

If the conditional variance, $\widetilde{\langle h_s''^2 \mid \eta \rangle}$, of a conditional quantity like sensible enthalpy, $\widetilde{\langle h_s \mid \eta \rangle}$, in the present formulation is sought, it has to be kept in mind, that the unconditional quantity $h_s$ is not independent, but a function of the conditioning variable; in the present case $\xi$. The dependence is formally given by equation (4.18). If the conditional variance is now attempted to be modelled based on the gradients of the unconditional $h_s$-field a simple analysis highlights

the problems.

Considering the most basic model, equation (5.17), and introducting the functional dependence of $h_s$ on $\widetilde{\xi}$ and $\widetilde{\xi''^2}$, the model reads:

$$\widetilde{h_s''^2} = C_{h_s}\Delta^2|\nabla\widetilde{h}_s|^2 = C_{h_s}\Delta^2|\nabla f(\widetilde{\xi},\widetilde{\xi''^2})|^2. \tag{5.20}$$

Applying the chain rule of differentiation and assuming a narrow mixture fraction p.d.f., the model can be written as:

$$C_{h_s}\Delta^2|\nabla f(\widetilde{\xi},\widetilde{\xi''^2})|^2 \approx C_{h_s}\Delta^2\left|\left(\frac{\partial h_s}{\partial\eta}\right)\nabla\widetilde{\xi}\right|^2. \tag{5.21}$$

Considering now a typical profile of conditional temperature, which is strongly linked to conditional sensible enthalpy, with the maximum temperature close to the stoichiometric mixture and decreasing temperatures towards both limits of conserved scalar space; yielding the pure fuel or pure oxidizer temperature respectively, the problem is evident. Because

$$\frac{\partial f(\eta)}{\partial\eta} = 0 \tag{5.22}$$

at a maximum of any function $f(\eta)$, this entire term (5.21) will approach zero around the physically crucial area of the stoichiometric mixture in conserved scalar space. Due to the fact that this term is expected to be the main source of variance, referred to as the 'production'-term by many authors, it is not surprising that conditional variance is underpredicted around stoichiometric by the above procedures.

It shall be noted that the source correlation term $\widetilde{w''_{h_s}\, h''_s}$ is no solution to the problem, since it was found to be mostly negative or of insignificant magnitude compared with the previously discussed term. Furthermore, none of the other terms in the unconditional variance transport equation (5.19) are variance producing.

In another attempt, sensible enthalpy was treated as an independent variable and the unconditional sensible enthalpy transport equation

$$\frac{\partial \bar{\rho}\, \widetilde{h}_s}{\partial t} + \nabla \cdot \bar{\rho} \widetilde{u}\, \widetilde{h}_s = \nabla \cdot \bar{\rho} D_{eff} \nabla\, \widetilde{h}_s + \widetilde{w}_{h_s}, \tag{5.23}$$

along with the unconditional sensible enthalpy variance equation (5.19) was solved.

The heat release rate, $\widetilde{w}_{h_s}$, appearing in this equation was obtained from the doubly conditioned heat release rate and the integration with the marginal mixture fraction p.d.f. and the conditional p.d.f. of normalized sensible enthalpy

$$\widetilde{w}_{h_s} = \int \int \langle w_{h_s} \mid \zeta, \eta \rangle\; P(\eta)\; P(\eta \mid \zeta)\;\; d\eta\; d\zeta. \tag{5.24}$$

The sensible enthalpy mean and variance were conditionally averaged, following equation (4.27), and subsequently used to determine the conditional p.d.f. invoking the $\beta$-p.d.f. assumption.

As with the previously discussed methods, it did not lead to physically useful predictions. The heat release obtained in this way led to a globally extinguished flame. Since for the case of sensible enthalpy being an independent variable, the doubly conditioned moment closure equations describe the chemical system, it was also attempted to incorporate the term $-\langle w_c \mid \eta, \zeta \rangle \frac{\partial Q_i}{\partial \zeta}$ through a rather crude

approximation of the form

$$\langle w_c \mid \eta, \zeta \rangle \frac{\partial Q_i}{\partial \zeta} \approx \langle w_c \mid \eta \rangle \frac{Q_i - Q_{i,mixing}}{\langle c \mid \eta \rangle - 0}, \tag{5.25}$$

where $Q_{i,mixing}$ denotes the boundary condition of doubly conditioned moments, which is assumed to be given by pure mixing of fuel and oxidizer according to the specific mixture fraction value

$$Q_{i,mixing} = \langle Y_{i,mixing} \mid \eta \rangle = \tag{5.26}$$
$$Y_{i,Oxidizer} + \eta \cdot (Y_{i,Fuel} - Y_{i,Oxidizer}).$$

This method also proved to be of no practical use. Again the heat release obtained in this case led to a globally extinguished flame. Therefore, the following approach was adopted.

### Current Model

Due to the problems described in the previous section, the following model yielded the most useful predictions.

Sensible enthalpy was not treated as an independent variable, but remained a function of mixture fraction. To approximate the conditional variance of the progress variable, the following equation for the conditional variance of sensible enthalpy, $G = \langle \widetilde{h_s''^2} \mid \eta \rangle$, is solved [44]

$$\frac{\partial G}{\partial t} + \widetilde{\langle u \mid \eta \rangle} \nabla G = \langle D \widetilde{\nabla \xi \nabla \xi} \mid \eta \rangle \frac{\partial^2 G}{\partial \eta^2} + 2 \langle \widetilde{w_{h_s}'' h_s''} \mid \eta \rangle + \tag{5.27}$$
$$\langle \widetilde{\chi_\xi'' h_s''} \mid \eta \rangle \frac{\partial^2 Q_{h_s}}{\partial \eta^2} - 2 \langle D \widetilde{\nabla h_s \nabla h_s} \mid \eta \rangle - 2 \langle \widetilde{u'' h_s''} \mid \eta \rangle \nabla Q_{h_s} + \frac{1}{\bar{\rho} \widetilde{P}(\eta)} \frac{\partial J_G}{\partial \eta}$$

In order to invoke a $\beta$-p.d.f. the variance has to be normalized as well. This is done in the following way

$$\langle c''^2 \mid \eta \rangle = \frac{G}{(h_{s,max}(\eta) - h_{s,min}(\eta))^2}. \tag{5.28}$$

Several of the terms of the r.h.s. of this transport equation have to be modelled. For the employed closure of the first term on the r.h.s. the reader is referred to chapter 4.

### The Source-Scalar Correlation

Strictly, the correlation of the scalar source $w_{h_s}$ and the scalar $h_s$, the second term on the r.h.s., does not need modelling. The present extension to the CMC method, with the presumed conditional p.d.f. along with the doubly conditional source term from equation (5.5), provides a consistent way to compute the correlation directly:

$$\langle \widetilde{w''_{h_s} h''_s} \mid \eta \rangle = \int w''_{h_s} \, h''_s \, P(\zeta \mid \eta) d\zeta, \tag{5.29}$$

with

$$w''_{h_s} = \langle w_{h_s} \mid \eta, \zeta \rangle - \langle w_{h_s} \mid \eta \rangle \tag{5.30}$$

and

$$h''_s = (h_s(c) - \langle h_s \mid \eta \rangle). \tag{5.31}$$

Singly conditional quantities like $\langle w_{h_s} \mid \eta \rangle$ are obtained via weighting with the conditional p.d.f. and integration in progress variable space as exemplified in equation (5.9).

### The Scalar Dissipation-Scalar Correlation

The third term on the r.h.s. of equation (5.27) needs to be modelled. However, since there is no direct dependence of sensible enthalpy on scalar dissipation, approximating this correlation is not straightforward.

Scalar dissipation as a parameter appears in most conserved scalar approaches to turbulent combustion and the S-shaped curve is a well established outcome. The S-shaped curve gives the temperature, usually at stoichiometric, as a function of the *log* of scalar dissipation and has three distinct branches. The uppermost branch corresponds to burning *flamelets* (one dimensional, non-premixed diffusion flames) and shows decreasing temperature with increasing scalar dissipation. The lowest branch corresponds to an extinguished non-premixed flame, and these two are connected by an unstable branch. This unstable branch corresponds to the transition or extinction and reignition. Therefore, in this crucial region, there is no physical connection between a certain value of scalar dissipation and temperature.

Because of these uncertainties, a rough estimation to model this term is taken for the present work. The sign of this correlation is given from the negative influence of increasing scalar dissipation on temperature for non-premixed flames. The magnitude is approximated by the product of the root-mean-square of conditional scalar dissipation and conditional sensible enthalpy.

$$\widetilde{\langle \chi''_\xi h''_s \mid \eta \rangle} = -\widetilde{\langle \chi''^2_\xi \mid \eta \rangle}^{(1/2)} G^{(1/2)} \tag{5.32}$$

Li and Bilger [50] proposed a slightly different model for this term. Their approach is formulated in terms of the conditional mean scalar dissipation rate. Since LES-

CMC provides a quantification of conditional scalar dissipation rate fluctuations due to the large CMC control volumes, the present method takes advantage of this fact. It is however, only a first step until further understanding of this correlation provides an improved approach.

This term turns out to be of particular importance and is included in all studies where a conditional variance equation is solved, such as Kim et al. [41, 40, 39], Fairweather and Woolley [22] as well as Kronenburg et al. [46] or Mastorakos and Bilger [52]. Studies into the behaviour of conditional variance equations by Swaminathan and Bilger [72, 73] and Kim [38] confirm the importance of this term. It shall be stressed however, that most of the published work on conditional moment closure and conditional variance equations has been carried out with the time-averaged formulation and a RANS flow solver. It is not clear whether conclusions drawn under these circumstances can be adopted for the space-average LES case. Nevertheless, the fact that trends seem to agree in both cases, provides encouragement for the current practice. Further research into the differences between RANS-CMC and LES-CMC and implications for modelling is welcome.

Since in the proposed methodology the progress variable is not treated as an independent scalar and remains a function of the conserved scalar, the turbulent production term, $\widetilde{\langle u'' h_s'' \mid \eta \rangle} \nabla Q_{h_s}$, modelled by a gradient transport assumption in the standard way is not sufficient to produce realistic variances, especially around stoichiometric, as described in section 5.3.2. It is the scalar dissipation-scalar correlation that is the key to a physically meaningful estimation of these conditional variances.

## The Reactive Scalar Dissipation Rate

The fourth term on the r.h.s. is the rate of dissipation of sensible enthalpy. Although a lot of work has been done to model the conserved scalar dissipation rate, it is still a matter of controversy how to approximate the dissipation rate of a reactive scalar. The influence of the reaction term on the dissipation is not yet understood well enough to devise reasonably universal models. However, work is being done to gain fundamental understanding of the processes involved . These studies investigate the contributions of various terms in a transport equation for the reactive scalar dissipation rate for the case of a turbulent premixed flame. Swaminathan and Bray [74] propose a model incorporating the effect of flame propagation on the reactive scalar dissipation rate. Swaminathan and Grout [75] propose a similar model and introduce the Damköhler number to account for flame propagation effects. Chakraborty and Swaminathan [12, 13] investigate further the influence of the Damköhler number on the reactive scalar dissipation rate. These are interesting developments and it will be interesting to study the effect of these new approaches for the present work. However, since the present work is concerned with a new chemical source term closure, focus is not on reactive scalar dissipation rate modelling. Nevertheless, this provides interesting considerations for further research.

For these reasons, as a first step, a simple relation between time scales for conserved and reactive scalar mixing is assumed [32, 20, 47]. For the present work, the following considerations lead to a simple, one-parameter model for the conditional reactive scalar dissipation rate.

A time scale for the mixing of the conserved scalar can be defined as:

$$t_\xi = \frac{\widetilde{\xi''^2}}{\widetilde{\chi}_\xi}. \tag{5.33}$$

A conditional time scale, $\langle t_\xi \mid \eta \rangle$, is then obtained through conditioning of the unconditional values, as described in Section 4.5, assuming spatial homogeneity of this time scale.

Introducing the notation $\langle \widetilde{\chi_{h_s}} \mid \eta \rangle$ for the dissipation rate of sensible enthalpy, $2 \langle D \widetilde{\nabla h_s \nabla h_s} \mid \eta \rangle$, a conditional time scale for the reactive scalar can be defined as:

$$\langle t_{h_s} \mid \eta \rangle = \frac{G}{\langle \widetilde{\chi_{h_s}} \mid \eta \rangle} \tag{5.34}$$

Assuming proportionality between these two conditional time scales,

$$\langle t_{h_s} \mid \eta \rangle = \gamma_t \langle t_\xi \mid \eta \rangle \tag{5.35}$$

with proportionality factor $\gamma_t$, leads to a model of the form:

$$\langle \widetilde{\chi_{h_s}} \mid \eta \rangle = G \frac{1}{\gamma_t \langle t_\xi \mid \eta \rangle}. \tag{5.36}$$

Specific values for the constant $\gamma_t$ will be given in chapter 6, where all other parameters are given for the specific experimental configuration. Values for $\gamma_t$ have been obtained by matching the conditional fluctuations of temperature, as observed in the experiments. It is acknowledged that this is not a desirable way to model this term, but since the focus of this work is the assessment of the presented chemical source term closure, it is deemed necessary to ensure the parameters influencing the method, such as conditional conserved scalar dissipation and conditional

variance of the progress variable, resemble the physically observed parameters as closely as possible. This procedure yields values for $\gamma_t$ of the order $\mathcal{O}(1)$, which is reassuring and provides confidence that the assumptions made in order to model the various terms are not too far from reality.

### The Turbulent Flux

The fifth term on the r.h.s. describes the production of conditional variance due to turbulent flux of sensible enthalpy. For this term a gradient transport model for the correlation is employed in physical space which is common practice in turbulence modelling and can be found in Ihme and Pitsch [32]

$$\widetilde{u''h_s''} = -D_t \nabla h_s. \tag{5.37}$$

The conditional term is approximated in a way that is consistent with modelling of other conditional quantities in LES-CMC, as described in section 4.5

$$\widetilde{\langle u''h_s'' \mid \eta \rangle} \nabla Q_{h_s} = \langle \, (-D_t \mid \nabla h_s \mid^2) \mid \eta \rangle. \tag{5.38}$$

### The Diffusion of Conditional Variance

For the diffusion flux of sensible enthalpy variance, a gradient transport model as proposed by Kim [38] is employed:

$$J_G = C_G \, \bar{\rho} \, \langle \frac{1}{2} \chi_\xi \mid \eta \rangle \, \widetilde{P}(\eta) \, \frac{\partial G}{\partial \eta}, \tag{5.39}$$

with the constant $C_G$ set to unity.

## 5.4 The Construction of the Reference Field

As briefly outlined in this chapter's introduction the source term evaluation is based on a constructed two-dimensional reference field $Q^{d,0}$.

To construct this field, the second conditioning variable has to be mapped from sensible enthalpy to normalized sensible enthalpy. Figure 5.3 illustrates how this is done. Several steady flamelets are computed, filling the shaded region. Above

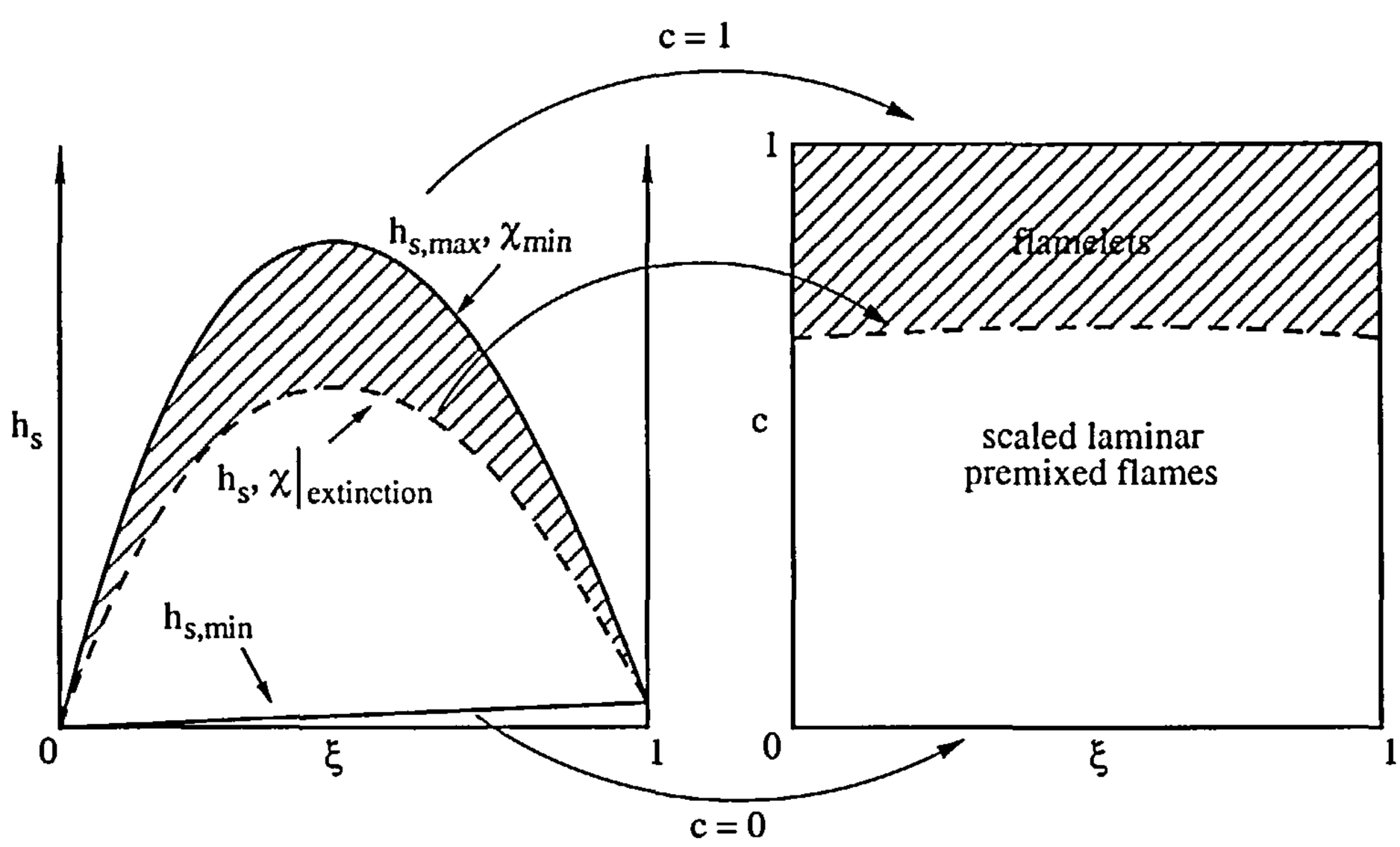


Figure 5.3: Construction of reference field $Q^{d,0}$

a certain limit of scalar dissipation rate, a stable solution of the reaction-diffusion equation does not exist and the flamelets extinguish. However, due to the partially premixed nature of combustion, some chemical conversion will take place in the grey region of figure 5.3. To approximate the functional form of the species mass fractions at sensible enthalpies and temperatures below (or scalar dissipation rate above) the quenching limit, laminar premixed flames at equivalence ratios accord-

ing to the value of mixture fraction were computed and scaled to match the value of flamelets at the quenching point, as illustrated in Fig. 5.4. For this, the ratio of

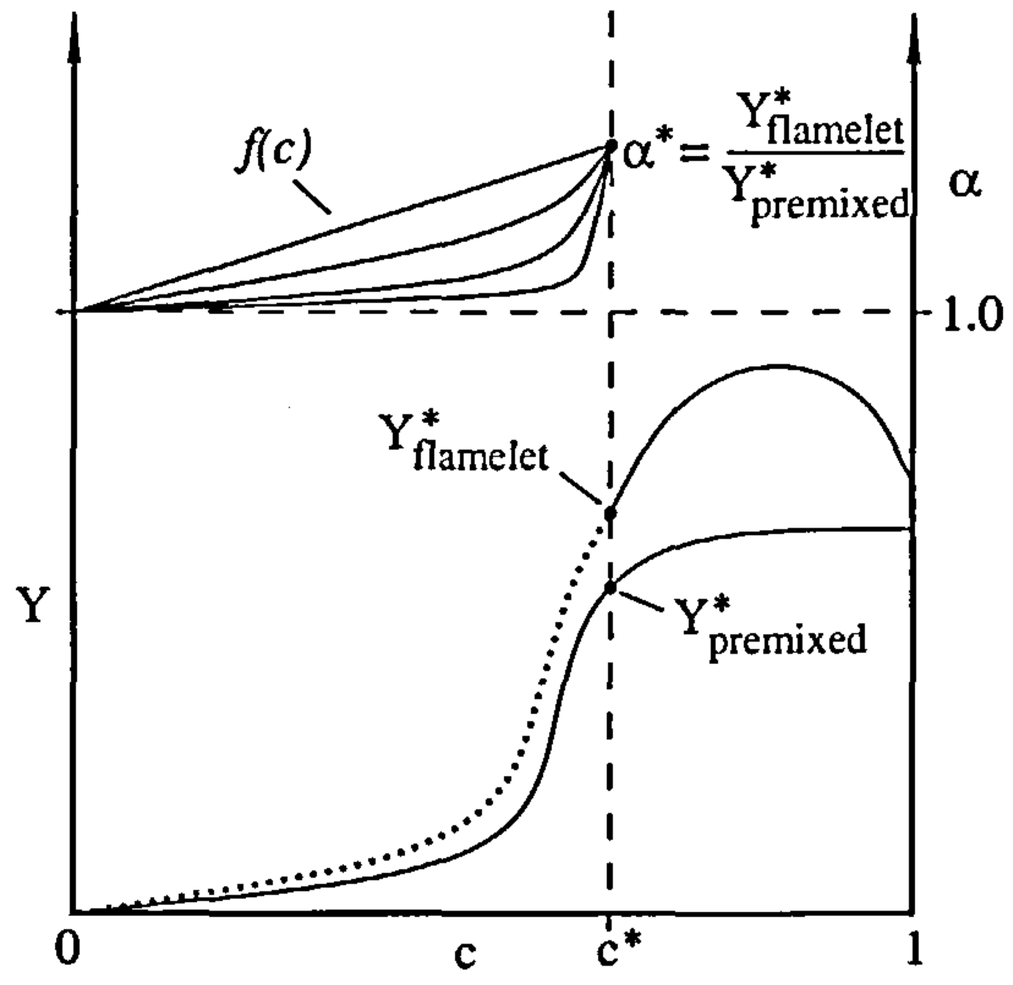


Figure 5.4: Scaling procedure

flamelet and premixed flame mass fractions at the quenching point $c^*$ is computed as:

$$\alpha_i^* = \frac{Y_{i,flamelet}^*}{Y_{i,premixed}^*}, \tag{5.40}$$

and reference field $Q^{d,0}$, below the quenching limit is then constructed as:

$$Q_i^{d,0}(c < c^*, \xi) = \left[1 + f(\frac{c}{c^*}) \cdot (\alpha_i^* - 1)\right] Y_{i,premixed}(c), \tag{5.41}$$

where $f$ is an arbitrary relaxation function yielding $\alpha = \alpha^*$ at $c = c^*$ and $\alpha = 1$ at $c = 0$ to ensure smoothness of the fields. In cases where certain flamelet mass fractions and laminar premixed flame mass fractions differ heavily at $c = c^*$, a linear relaxation might lead to unphysically high values for $Q_i^{d,0}$ at $c < c^*$. In the

present case an exponentially decaying function

$$f(\frac{c}{c^*}) = e^{b(\frac{c}{c^*}-1)}, \tag{5.42}$$

has been used, where $b$ represents a damping factor that controls how quickly the reference field converges to the premixed flame solution in the shaded region. The factor was taken to be $b = 14$ as a compromise between the smoothness of the reference field and a limited region of deviation from the premixed solution. This choice seems justified as the reference field compare reasonably well with the experimental doubly conditioned fields as shown in figures 5.5 and 5.6.

This procedure is applied to all species and this library is the input for our CMCe method. Figures 5.5 and 5.6 show the resulting reference fields for some representative species, together with the doubly conditioned field obtained from experimental data at $x/D = 7.5$ and $x/D = 15$. It can be seen that the constructed reference fields give a rather good approximation to the experimentally observed doubly conditioned moments.

Singly conditional moment closure as described in chapter 4 can be thought of as the presented methodology, CMCe, with vanishing variance of sensible enthalpy, and therefore a Dirac delta p.d.f..

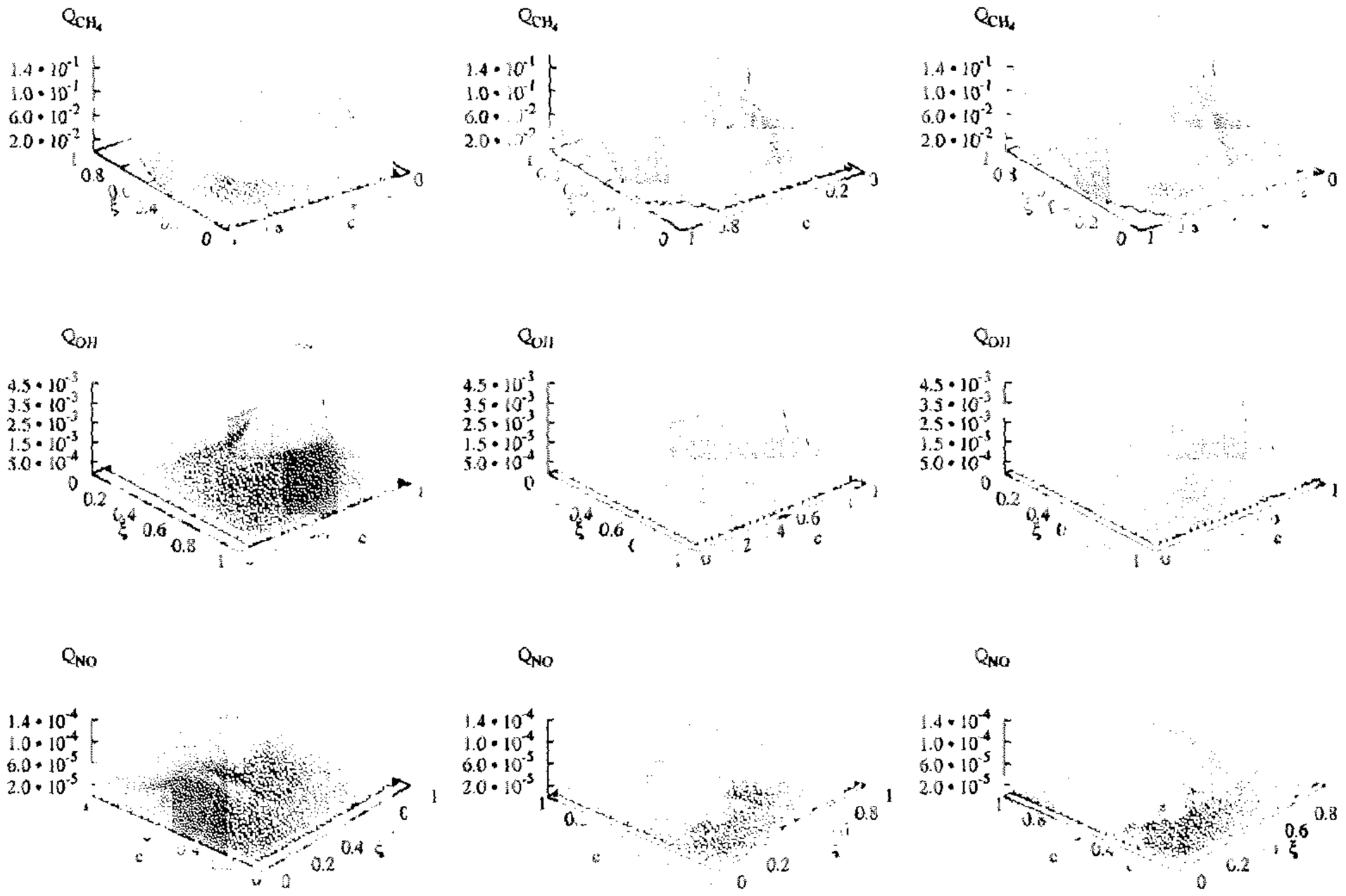


Figure 5.5: Reference fields and doubly conditioned fields from experimental data for methane, hydroxyl radical and nitric oxide (left column: Constructed fields, centre column: Experimental data at $x/D = 7.5$, right column: Experimental data at $x/D = 15$)

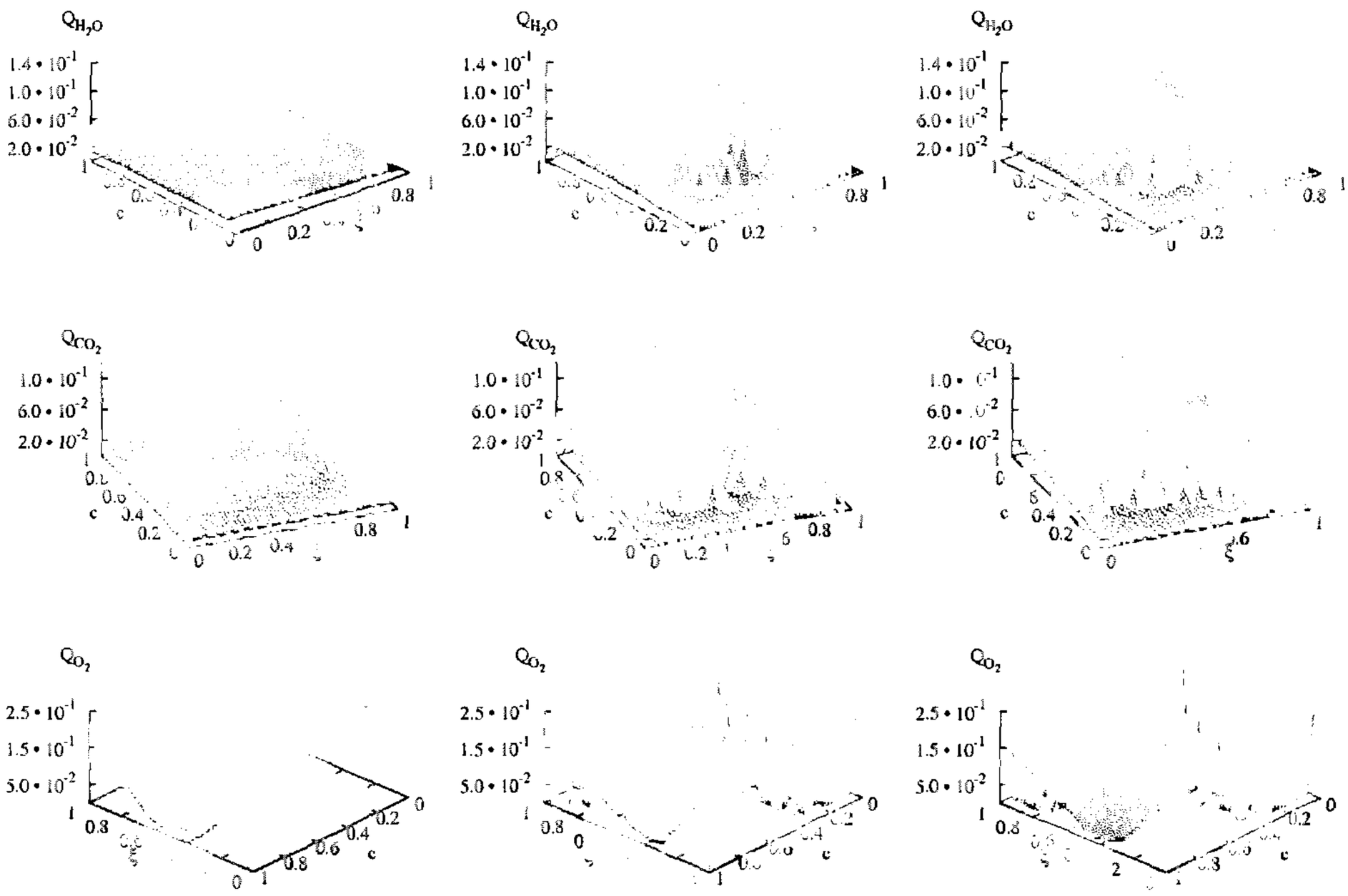


Figure 5.6: Reference fields and doubly conditioned fields from experimental data for water, carbon dioxide and oxygen (left column: Constructed fields, centre column: Experimental data at $x/D = 7.5$, right column: Experimental data at $x/D = 15$)

Chapter 6

# Large Eddy Simulation of Piloted Jet Flames

The presented extended conditional moment closure method is tested for its capability to improve upon standard LES-CMC predictions and its capability to predict local extinction and reignition. The '*International Workshop on Measurement and Computation of Turbulent Nonpremixed Flames*' (TNF)[21] was established in a worldwide, joint effort of combustion researchers to provide a set of standard benchmark flame configurations, such as simple jet, piloted jet, bluff body as well as swirl flames. These different configurations were carefully designed to exhibit various combustion phenomena of interest, and exhaustive, detailed measurements were taken of the flow and mixing fields, as well as chemical species and temperature. These flames serve as benchmark for the majority of new combustion modelling techniques that are validated against them and therefore provide a means of direct comparison of a variety of modelling strategies.

## 6.1 The Sandia Piloted Jet Burner

One of the basic flame configurations in the TNF workshop are the piloted jet flames, Sandia flames A-F.

This burner issues a volumetric mixture of 25% methane ($CH_4$) and 75% air into the surroundings. Barlow and Frank give an insight into the considerations that led to the choice of this composition [1]:

> *"This mixture significantly reduces the problem of fluorescence interference from soot precursors, allowing improved accuracy in the scalar measurements. Partial premixing with air also reduces the flame length and produces a more robust flame than pure $CH_4$ or nitrogen-diluted $CH_4$. Consequently, the flames may be operated at reasonably high Reynolds number with little or no local extinction, even with a modest pilot. The mixing rates are high enough that these flames burn as diffusion flames, with a single reaction zone near the stoichiometric mixture fraction and no indication of significant premixed reaction in the fuel-rich $CH_4$/air mixtures."*

The jet nozzle has a diameter of $D = 7.2\ mm$ and is enclosed by a burning pilot. The outer diameter of the pilot nozzle is $D_{Pilot} = 18.2\ mm$. The pilot operates at a mixture fraction value of $\xi_{Pilot} = 0.27$.

This burner is placed inside a windtunnel that provides a low coflow velocity $u_{Coflow} = 0.9\ m/s$. The geometry is unconfined. Figure 6.1 shows a schematic of the setup and Table 6.1 summarises the main parameters for all flames simulated for this study, flames D-F.

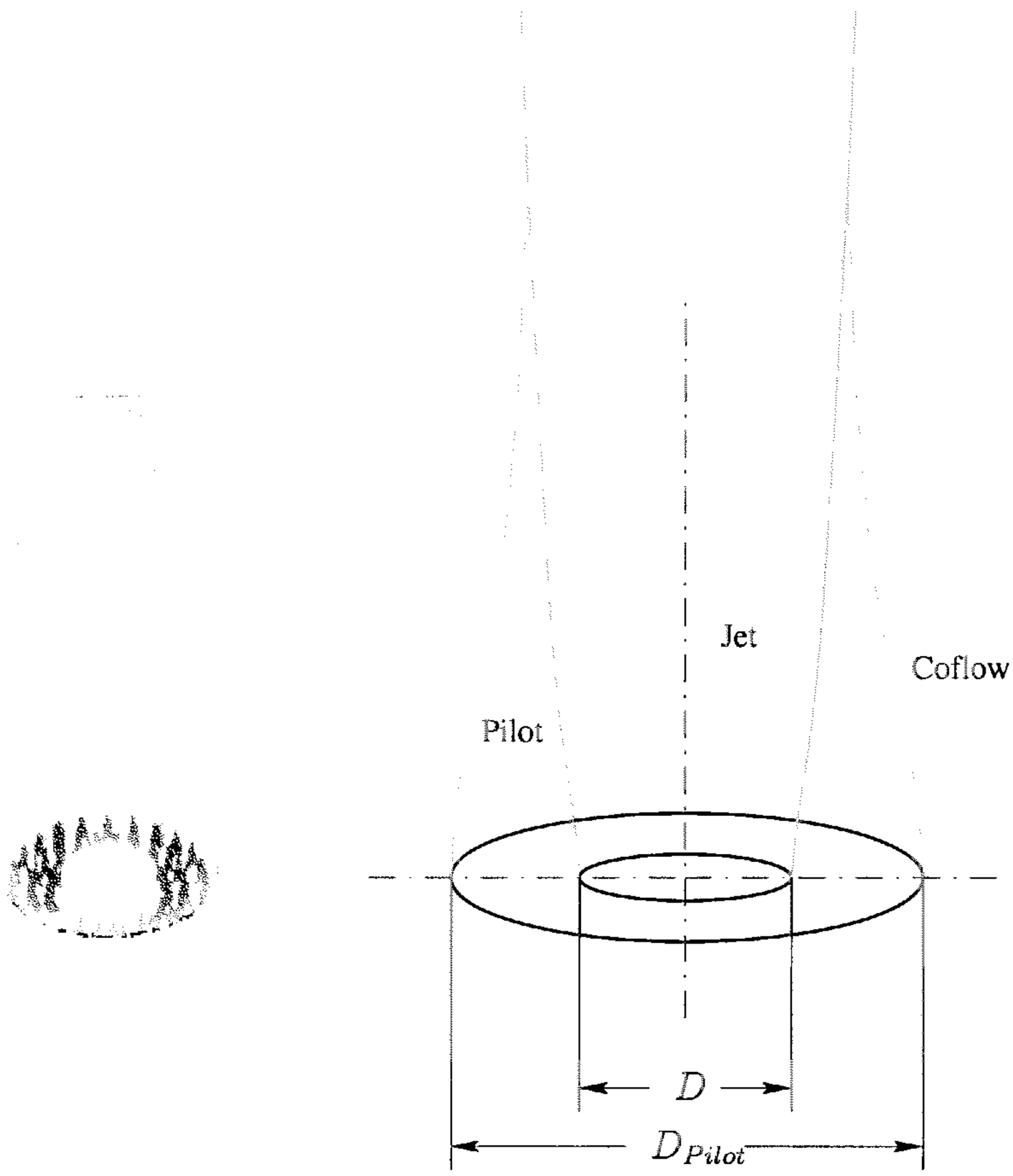


Figure 6.1: Picture of the Sandia piloted jet burner (left), and the corresponding schematic (right)

To quantify the level of local extinction and reignition Xu and Pope [81] define a burning index, B.I., which is the ratio of a scalar such as temperature or species mass fraction and a reference value of a mildly strained, opposed-flow laminar flame

$$B.I. = \frac{\langle T \mid \eta \rangle}{T_{ref}}, \tag{6.1}$$

where $T_{ref}$ is the reference temperature for the laminar flame. This reference value represents the state of a fully burning flame. It is taken from Xu and Pope [81]

| | Jet | Pilot | Coflow |
|---|---|---|---|
| $\xi$ | 1.0 | 0.27 | 0.0 |
| Temperature [K] | 294 | 1880(± 50) | 291 |
| Bulk velocity [m/s]: | | | |
| Flame D | 49.6 (± 2) | 11.4 (± 0.5) | 0.9 (± 0.05) |
| Flame E | 74.4 (± 2) | 17.1 (± 0.75) | 0.9 (± 0.05) |
| Flame F | 99.2 (± 2) | 22.8 (± 1.0) | 0.9 (± 0.05) |
| Reynolds number: | | | |
| Flame D | 22400 | | |
| Flame E | 33600 | | |
| Flame F | 44800 | | |

Table 6.1: Specifications for the Sandia D-F flames series

and has a value of $T_{ref} = 2023K$. The burning index aids in comparing levels of extinction qualitatively, such that these differences amongst the three flames become somewhat more comprehensible.

This burning index is presented for the piloted jet flames D, E and F in figure 6.2 to illustrate the distinct levels of local extinction and reignition. The low levels of extinction of flame D, represented by high values of the burning index are clearly visible. Temperature stays closer to the limit of a weakly strained flame throughout the domain. Flame E shows more pronounced extinction, which is expected given the increased Reynolds number. Flame F shows the lowest burning indices, which is consistent with the highest Reynolds number of the flames series and the flame being close to global extinction.

## 6.2 Computational parameters

The presented extended conditional moment closure method is applied to all three of the above described flames, D,E and F. Flame E exhibits a good balance of a

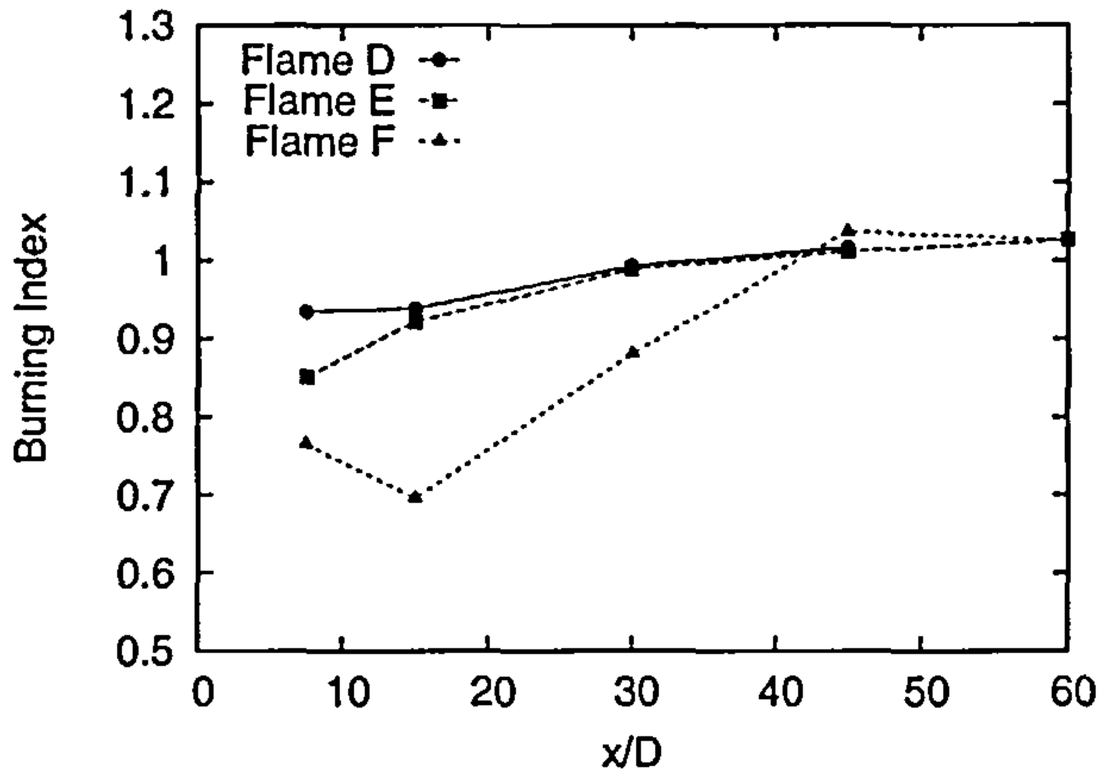


Figure 6.2: Burning indices for Sandia flames D, E and F

substantial level of extinction and reignition, retained stability of the flame and confidence in the boundary conditions. Some authors [76] have found that flame F is close to global extinction and that even relatively small variations of $\sim 20\ K$ in the pilot temperature can cause the entire flame to extinguish. Therefore, all development was carried out on flame E and calculations of flames D and F show the effect of in/decreasing turbulence levels on the predictions.

All calculations were carried out on a $320 \times 96 \times 96$ grid, stretched in main flow as well as the lateral directions. It extends 80 jet diameters in the downstream direction. In cross sectional direction it varies between 10 jet diameters at the inflow plane and 24 jet diameters at the outflow plane, accounting for the jet spreading in downstream direction. Figure 6.3 gives an impression of the domain.

Reference calculations with the standard LES-CMC method have been carried out to serve as a benchmark for the performance of the extended CMC method.

The CMC grid consists of $64 \times 1 \times 1$ points, where grid refinement has shown no

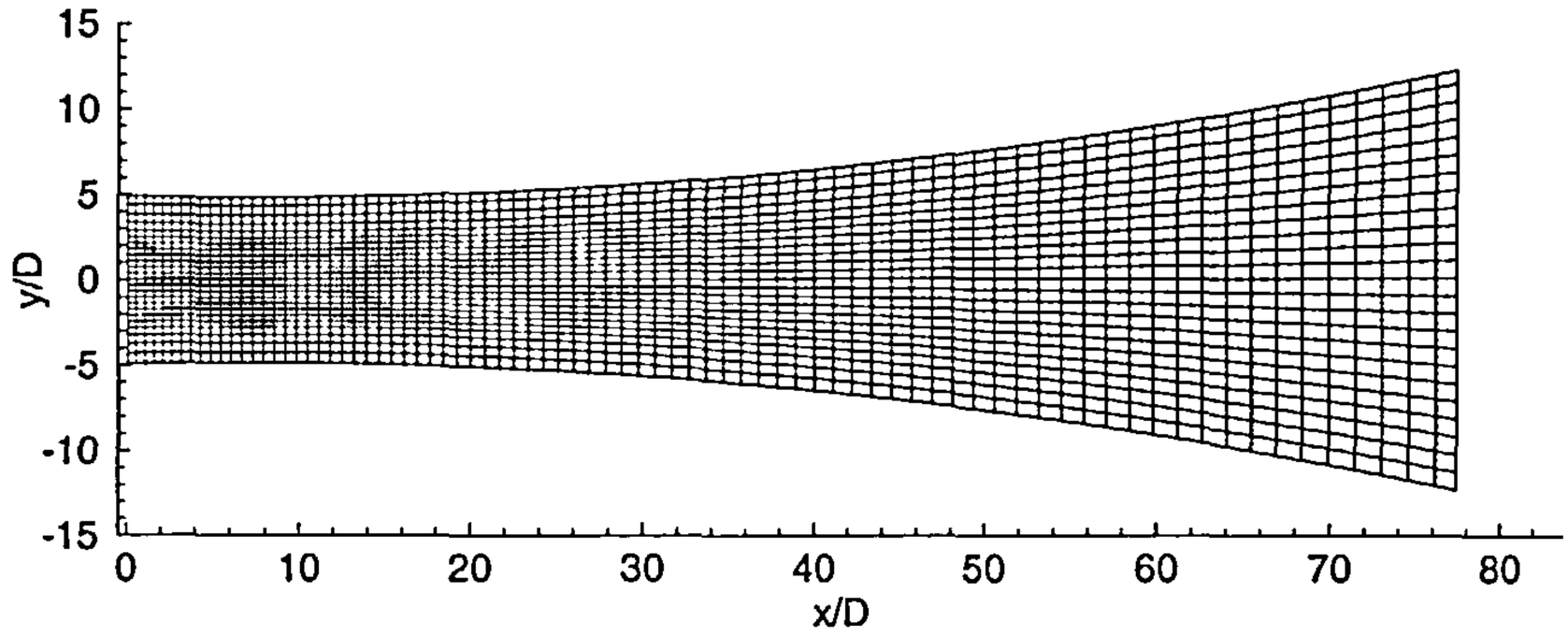


Figure 6.3: Grid used for the present study (only every fourth grid point shown for clarity).

significant improvement of results for both CMC and the extended CMC method. Mixture fraction space is resolved by 50 grid nodes.The reference fields for the CMCe methodology were approximated by 50 points in mixture fraction space and 26 in sensible enthalpy space.

The chemical mechanism used approximates methane combustion with 48 species and 300 elementary reactions and includes $NO_x$ chemistry. For reference the mechanism is given in appendix B. For details the reader is referred to Meyer [53].

The calculations were carried out on a 32 node cluster, equipped with AMD Opteron 2.2 GHz processors and took 8 days to complete for the CMCe cases and 5 days for the LES-CMC cases.

## 6.3 Results

Flame E is the intermediate flame between flame D and flame F. For prediction of flame D, which shows moderate extinction and reignition, conserved scalar approaches like Eulerian flamelets [62] or LES-CMC [55] provide reasonably accurate predictions. Flame F is close to global extinction and regarded as the most challenging flame of the series.

### 6.3.1 Flame E

For the case of flame E, three calculations with the CMCe methodology were carried out.

*Case A*

In the first case, coefficient $\gamma_t$ of the conditional sensible enthalpy variance equation (5.36) was determined as equal to 1.75. This was done by matching the magnitude of experimentally observed, conditional temperature fluctuations at $x/D = 7.5$. It is appreciated that this is somewhat arbitrary. However, since the level of extinction at this location is rather high, as indicated by the low conditional temperatures observed there, it seemed like a reasonable choice to base this study on.

*Case B*

In the second case, coefficient $\gamma_t$ was kept at 1.75, but the turbulent Schmidt number was decreased to $Sc = 0.2$ to study the effect of increased scalar dissipation.

*Case C*

For the third case, $\gamma_t$ was determined such as to match the conditional temperature fluctuations at $x/D = 15$, which resulted in generally higher predictions of conditional temperature fluctuations. In this case, the turbulent Schmidt number was kept equal to the value for the first case, $Sc = 0.4$.

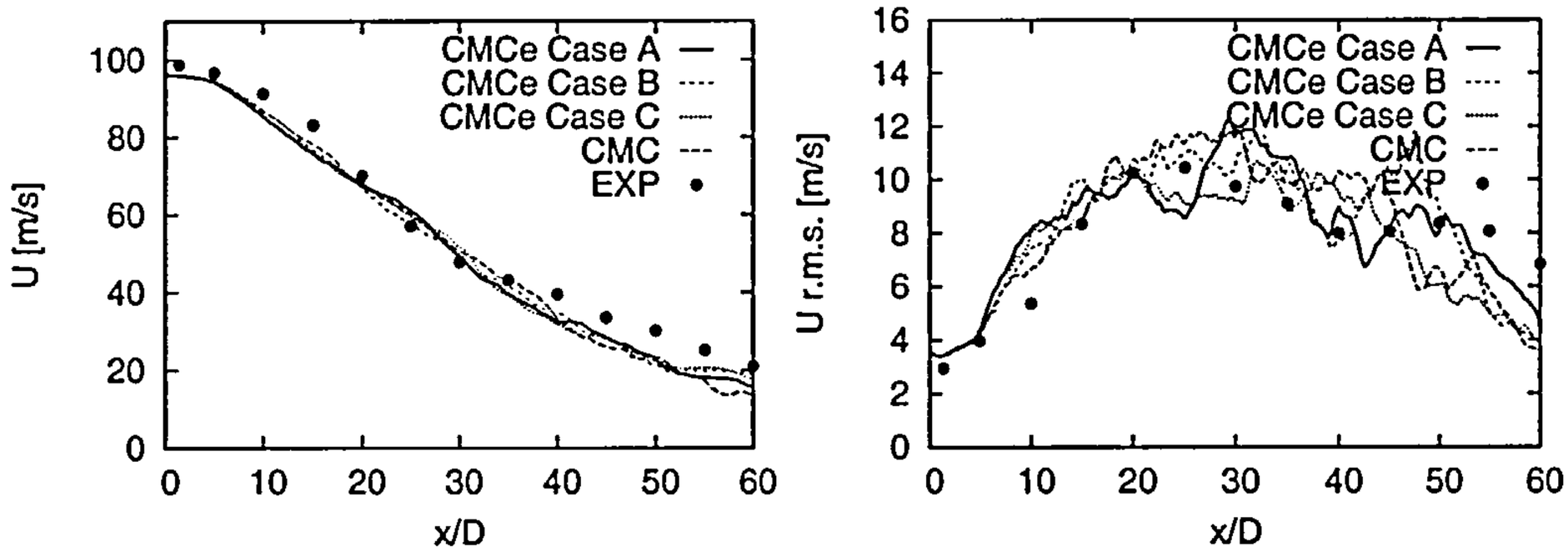


Figure 6.4: Axial velocity mean and r.m.s along the centreline

Figure 6.4 shows the mean and r.m.s. axial velocity component along the centreline. The mean velocity is well captured in the entire domain and the predictions for the r.m.s. velocity are also in reasonable agreement with the experimental values. Even close to the nozzle, r.m.s. velocity predictions agree well with the experimentally observed values. That is further evidence, that the method for generating a correlated quasi turbulent signal as inflow boundary condition, described in section 3.4.1, has its merit. It provides a significant improvement over previous practice, where random fluctuation where scaled according to experimental inflow data, but quickly damped upon entering the domain [42].

Figure 6.5 shows the mean and r.m.s. mixture fraction along the centreline. It can be seen, that the mean mixture fraction is somewhat underpredicted from approximately $x/D = 15$ on downwards. This might be attributed to the TVD scheme used to treat the convective term of scalar transport equations, which is

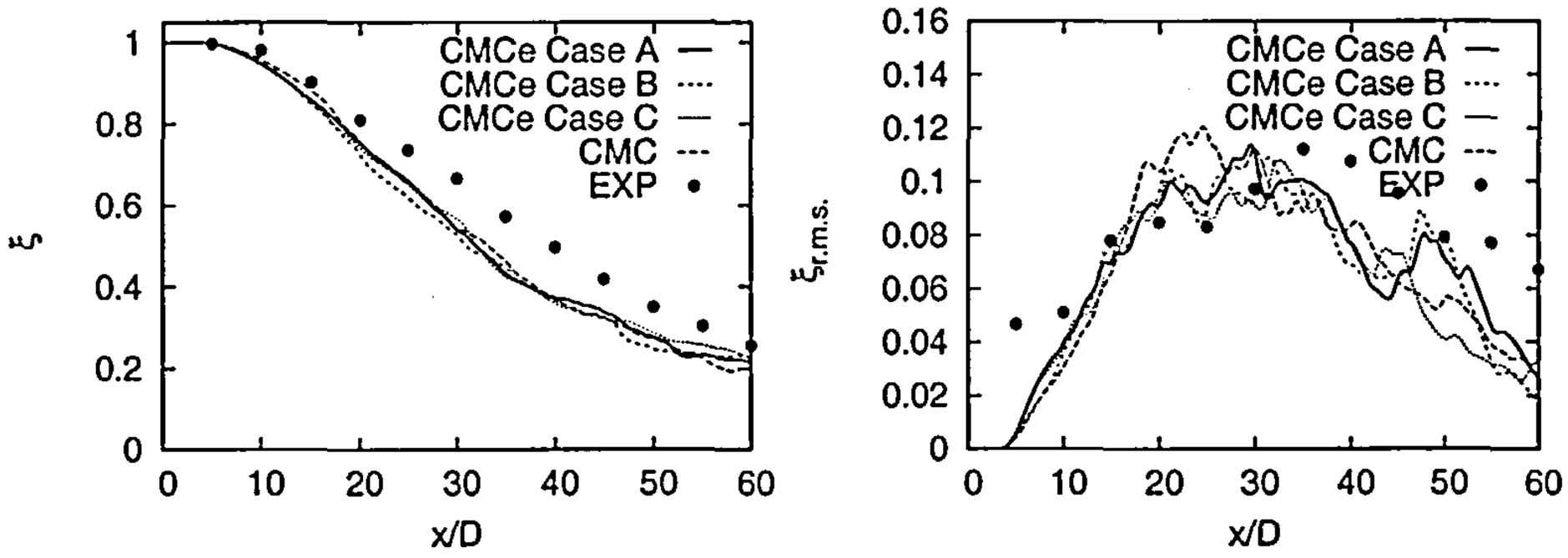


Figure 6.5: Mixture fraction mean and r.m.s. along the centreline

strongly dissipative, but ensures boundedness. The root mean square mixture fraction is well captured after the breakup of the jet has occurred around $x/D = 15$, as indicated by the change in curvature of the mean mixture fraction and mean velocity profile. The discrepancy of the predicted value of the r.m.s. mixture fraction closer to the nozzle $x/D < \sim 15$ is easily explained. Since most of these points lie within the jet core which is still largely intact in this area, no fluctuations of the mixture fraction are expected from a physical point of view. The measured fluctuations in that region can be attributed to experimental noise and largely discarded.

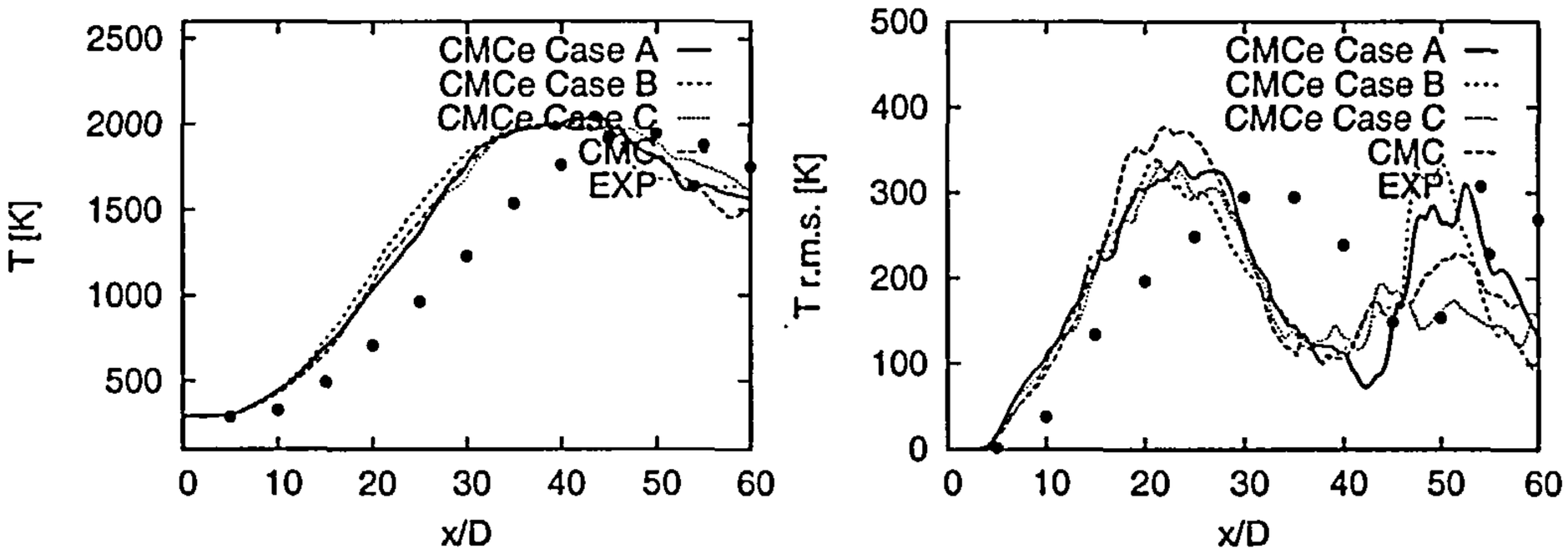


Figure 6.6: Temperature mean and r.m.s. along the centreline

Figure 6.6 shows the mean and r.m.s. temperature along the centreline. The mean temperature is generally overpredicted. This can be attributed in parts to the underprediction of mixture fraction and the overprediction of conditional temperature. Conditional temperature and the extent to which the present model captures local extinction and reignition can be seen in figure 6.9 and a more detailed discussion follows where conditional moments are presented.

Radial profiles of mixture fraction in figure 6.7 show good agreement in the region $x/D < 15$, both for mean and r.m.s.. The jet is predicted somewhat wider than what is measured, but this most probably is an effect of the TVD scheme which is not able to maintain such steep a gradient and diffuses outwards. At $x/D = 7.5$ both shear layers that emanate from the velocity differences between jet and pilot, as well as pilot and surroundings, have merged as indicated by the single maximum of mixture fraction fluctuations. At $x/D = 30$ the underprediction of mixture fraction around the centreline is consistent with the findings from figure 6.5.

Radial profiles of temperature are depicted in figure 6.8. They agree well with experimental findings close to the nozzle at $x/D = 2$, which is not surprising since at that location the jet breakup has not yet occurred and the temperature is likely to be strongly governed by the inflow conditions, that is the pilot temperature. This is also suggested by the lack of discrepancy amongst both standard LES-CMC and all parameter variations of CMCe at this location. At $x/D = 7.5$ and further downstream, turbulence intensifies and predictions of unconditional temperature cannot reproduce the level of extinction seen in the experiment.

One great benefit of CMC is that conditional quantities are directly being solved

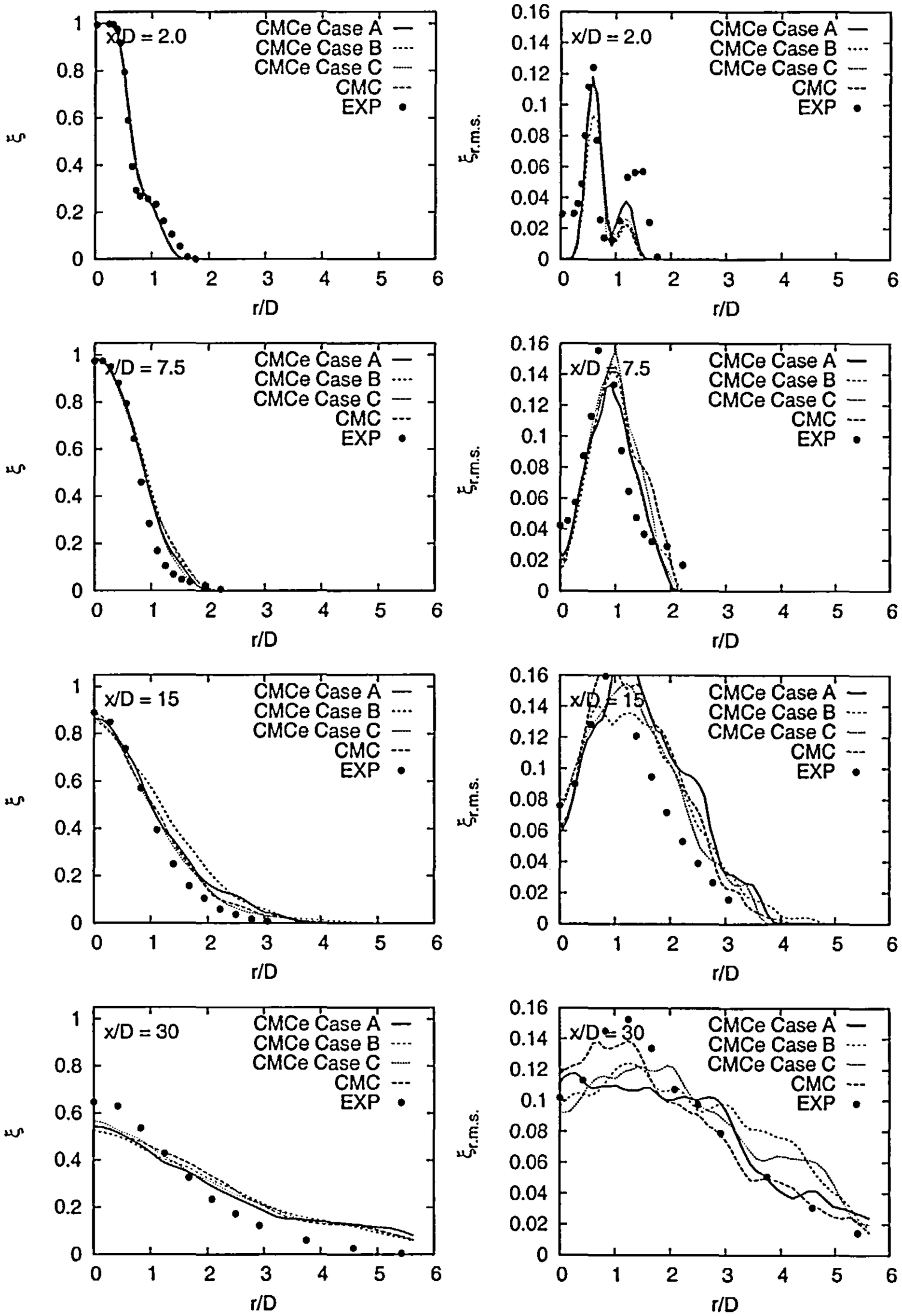


Figure 6.7: Mixture fraction mean and r.m.s. at several downstream locations

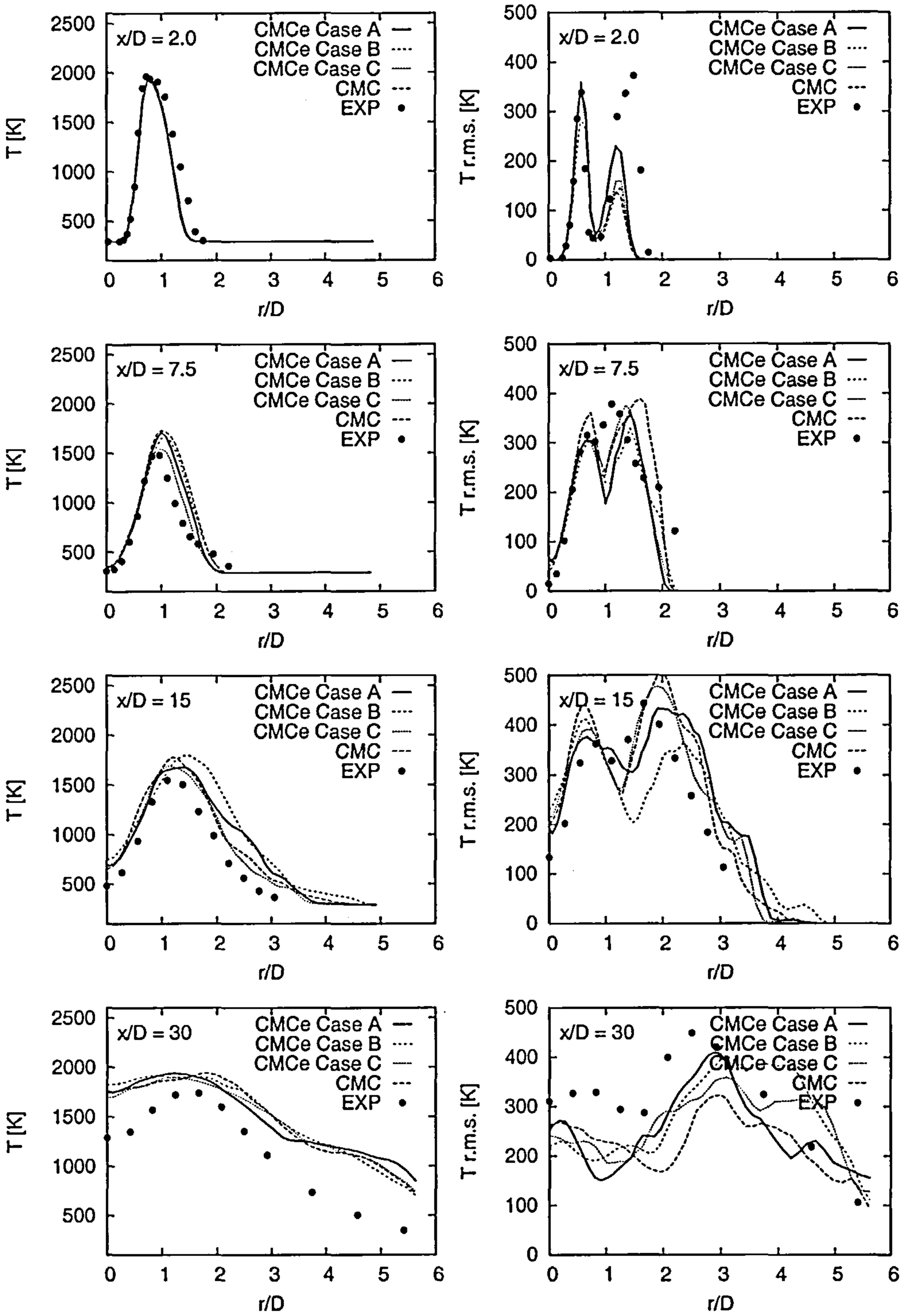


Figure 6.8: Temperature mean and r.m.s. at several downstream location

for. Since a lot of the fluctuations of reactive quantities can be attributed to fluctuations of the mixture fraction, decoupling these offers additional insight in and clarity of the flame structure. Therefore, conditional quantities will be presented and discussed for the remainder of this section.

Figure 6.9 shows conditional temperature predictions as well as the results from the solution of the conditional sensible enthalpy transport equation (5.36). It can be seen that at $x/D = 2$ the conditional temperature is almost of triangular shape, which supports the view that at this location chemistry is still largely determined by the inflow conditions. Some heat release is observed, since the maximum temperature around stoichiometric is higher than the pilot temperature of $\sim 1880K$. No significant difference between the different model predictions can be seen. However, the trend is the one expected. Standard LES-CMC provides the benchmark and predicts the highest temperatures. *Case A* improves upon those, although only moderately. The effect of higher scalar dissipation in *Case B* does not seem to account for the inhibition of combustion compared to a diffusion flame at this location. *Case C* provides a more significant improvement for this location, although the conditional sensible enthalpy variance necessary to reduce the temperature by that amount exceeds the temperature fluctuations observed in the experiment, whereas *Cases A* and *B* are of the correct order.

At $x/D = 7.5$ the magnitude of temperature fluctuations indicates strong extinction and reignition. *Cases A* and *B* capture the level of fluctuations well, since the model and its main free parameter, $\gamma_t$, have been calibrated at that location. *Case C* overpredicts these by around $150K$, which provides significant improvement of the conditional temperature. *Cases A* and *B* improve LES-CMC by around $100K$ which is good, and shows that the main principle behind the consideration that

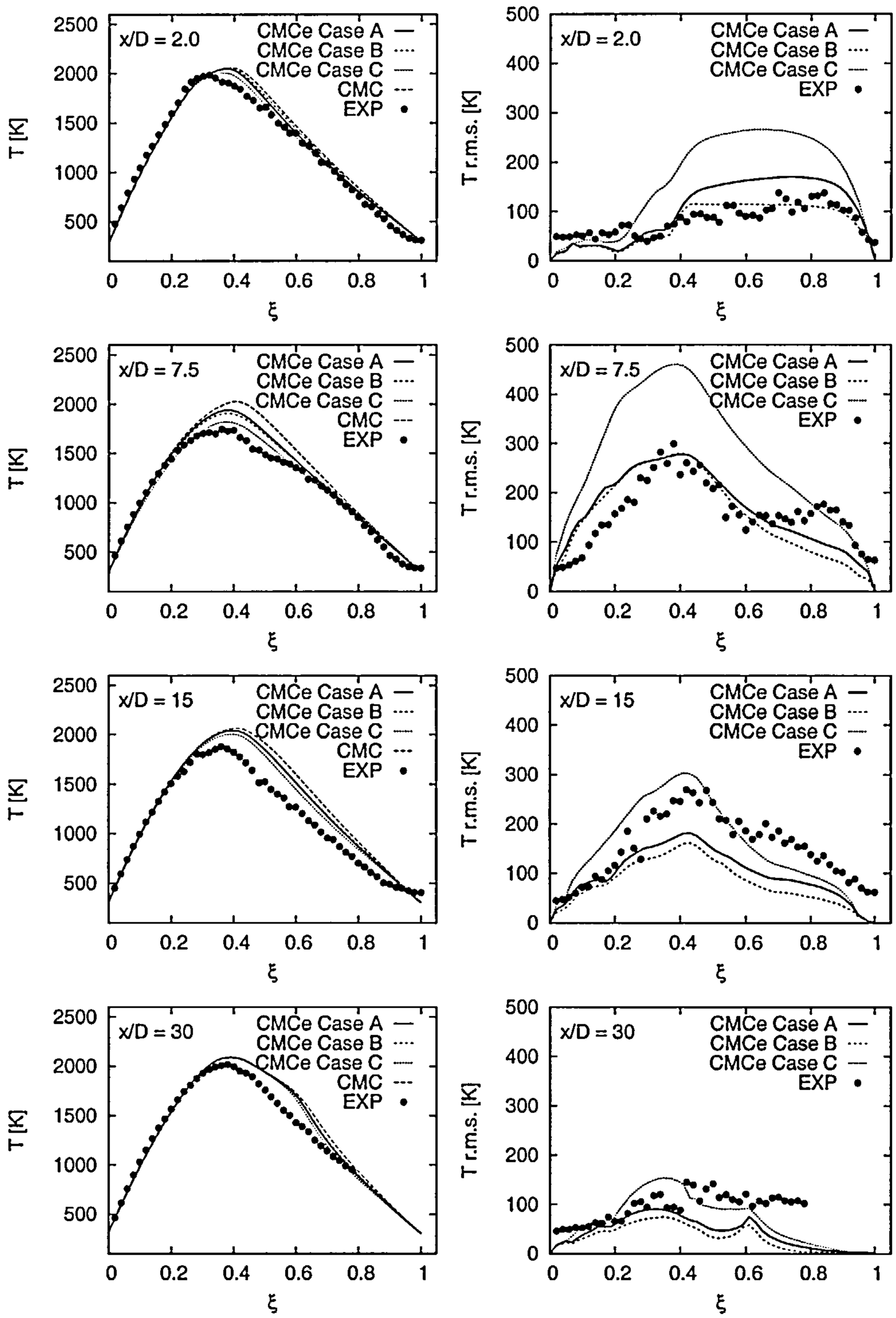


Figure 6.9: Conditional mean temperature and r.m.s. (from conditional variance equation

led to the CMCe methodology is valid. However, since realistic values for the sensible enthalpy variance as input for the CMCe methodology do not bridge the gap between the models predictions and the experimentally observed temperatures, it seems to indicate that other effects than the temperature dependence (expressed as dependence on sensible enthalpy in the present formulation of the model) lead to the strong extinction and reignition phenomena in this flame. Higher values for conditional sensible enthalpy variance, representing an overprediction of conditional temperature fluctuations of about $150K$, lead to very good results for the conditional temperature.

At $x/D = 15$ predictions of conditional temperature fluctuations are too low for *Cases A* and *B* and good for *Case C*. Conditional temperature predictions are practically indistinguishable for *Cases A* and *B*, which is not surprising since the different turbulent Schmidt numbers do not lead to significantly different scalar dissipation rates, as seen in figure 6.14. However, they offer a slight improvement over LES-CMC. *Case C* with its realistic prediction of conditional temperature fluctuations further improves upon the results of *Cases A* and *B*, predominantly in the rich part of the flame. That is another indication that the main idea behind the model is valid, but not sufficient to explain the level of extinction in this flame. Conditional temperatures remain overpredicted by about $150K$.

At $x/D = 30$ conditional temperature fluctuations are relatively small, of the order of $100K$. The trends of the parameter variations of CMCe is consistent with the other locations and *Case C* provides the highest and most realistic results. Despite that, the CMCe method hardly provides improvement of LES-CMC at this location and results resemble a laminar diffusion flame at low strain rate.

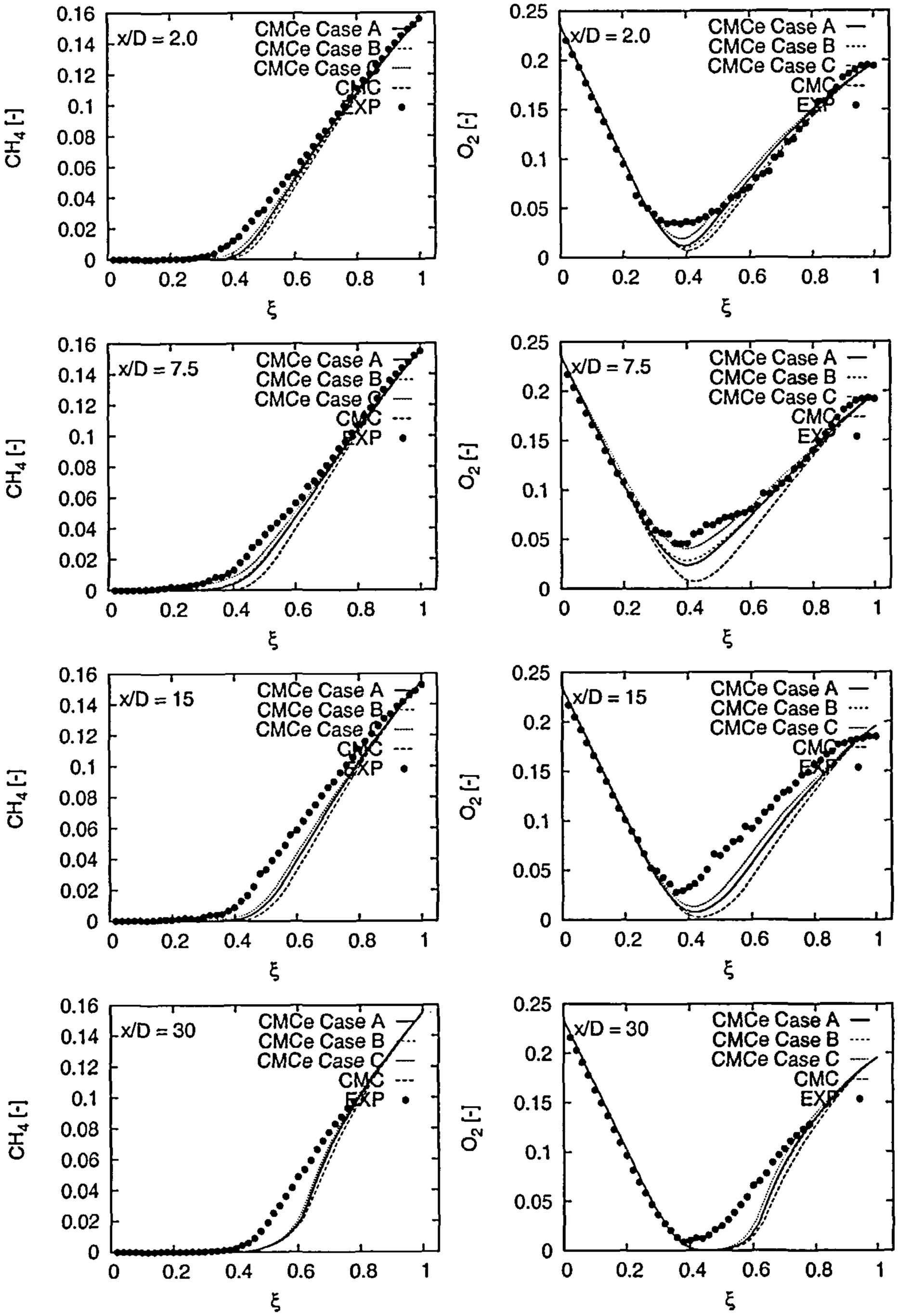


Figure 6.10: Conditional means of methane and oxygen

Results for methane and oxygen are shown in figure 6.10. Conditional concentrations of methane exhibit the trends seen in the predictions of conditional temperatures, with the most pronounced improvements at $x/D = 7.5$. However, even at this location and for the high sensible enthalpy variance case, *Case C*, fuel consumption is still overpredicted, just like at all other downstream locations. The general depletion of oxygen is predicted remarkably well by CMCe for *Case C*, although it has to be kept in mind, that for $x/D = 2$ and $x/D = 7.5$, this goes along with an overprediction of conditional fluctuations of temperature. *Cases A* and *B* improve significantly upon LES-CMC results, but cannot reproduce the experimental findings at any point in the domain.

Similar to the two previously discussed species, conditional means of water and carbon dioxide behave in the same manner. Figure 6.11 shows that the production of water is overpredicted throughout, and differences between LES-CMC and the three cases of CMCe are most pronounced at $x/D = 7.5$, but again, result are not satisfactory. In the case of carbon dioxide, *Case C* yields excellent predictions and *Cases A* and *B* still perform significantly better than LES-CMC.

For the hydroxyl radical, shown in figure 6.12, no model is satisfactory. However, it can be seen that although CMCe does not account for the full level of extinction it is consistently superior to LES-CMC. The same figure shows the results for hydrogen, which is equally overpredicted throughout the domain, but improves upon LES-CMC significantly and consistently.

Carbon monoxide and nitric oxide predictions are given in figure 6.13. At $x/D = 2$ and $x/D = 7.5$ *Case C* gives reasonable predictions for carbon monoxide, whereas all other model perform poorly. At $x/D = 15$ all models overpredict the formation

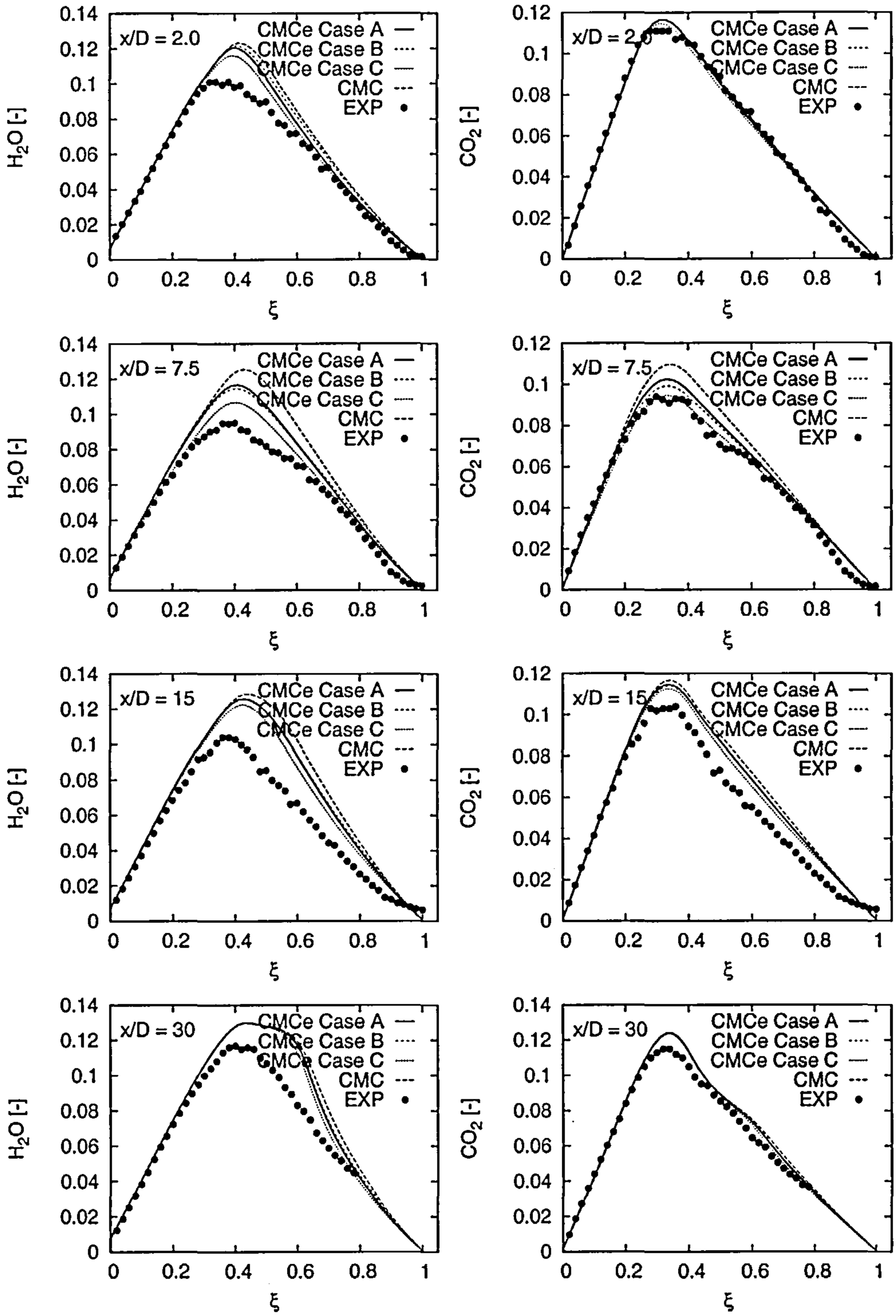


Figure 6.11: Conditional means of water and carbon dioxide

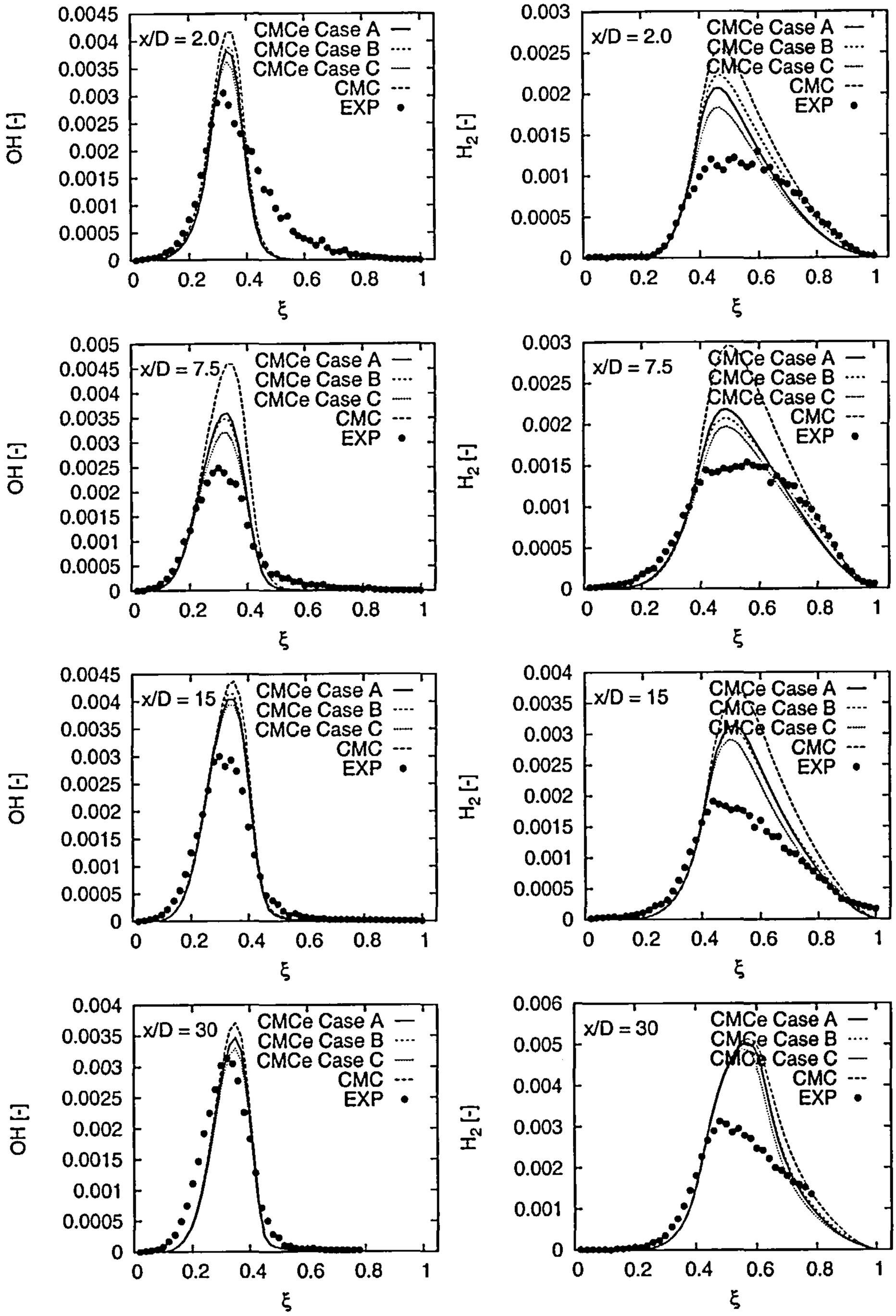


Figure 6.12: Conditional means of hydroxyl and hydrogen

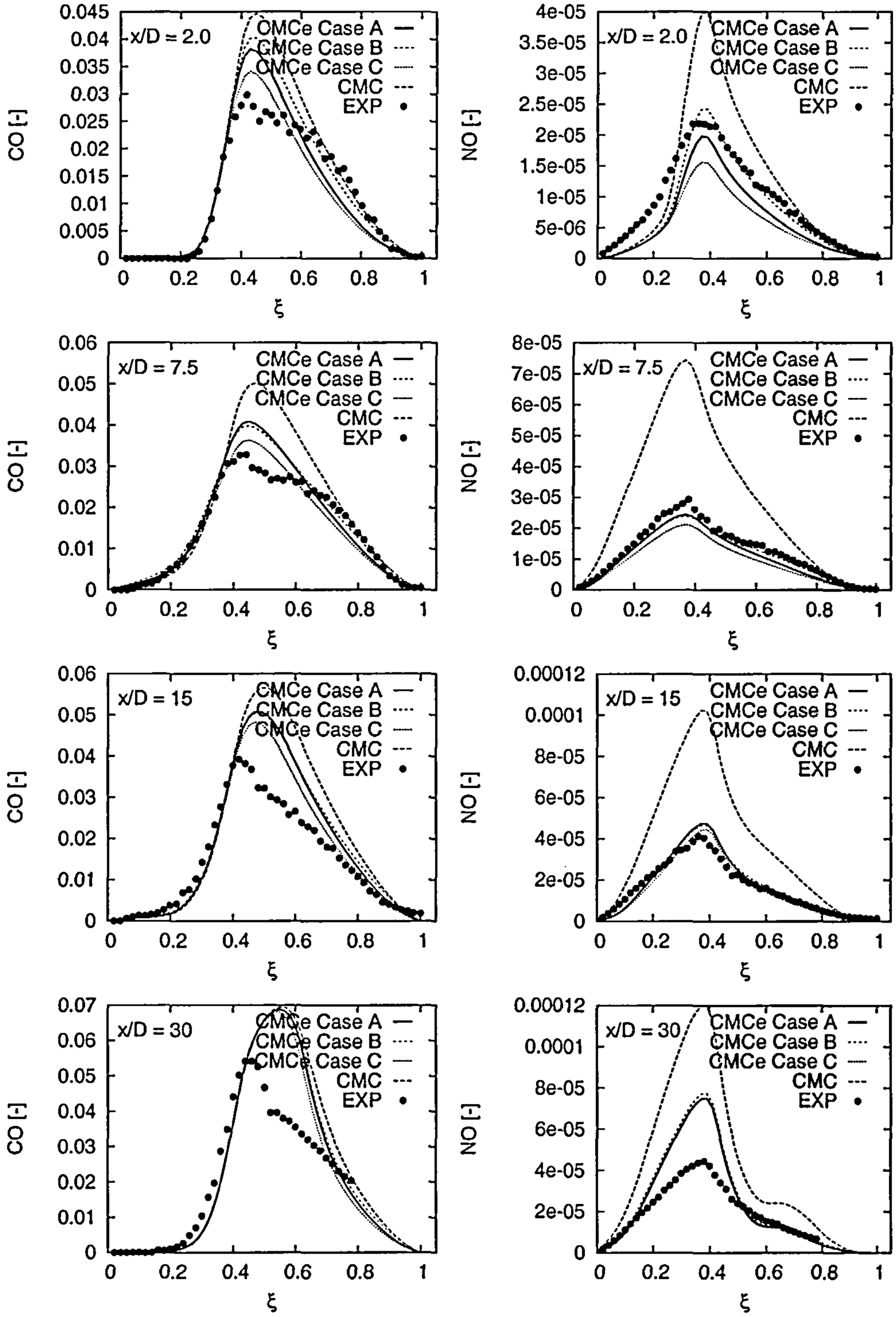


Figure 6.13: Conditional means of carbon monoxide and nitric oxide

of the pollutant, although LES-CMC shows by far the worst results. Further downstream at $x/D = 30$ all models perform equally badly and cannot reproduce the low levels of carbon monoxide at this location. Nitric oxide on the other hand is rather well predicted until $x/D = 15$, although some underprediction is observed for *Case A* and *C*. In contrast to these results, LES-CMC consistently overpredicts NO production by a factor of $2-3$. This is most probably explained by the extreme temperature dependence of nitric oxide producing elementary reactions. For that reason it is not surprising, that taking into account even slight fluctuations of conditional temperature has a great effect on the production rate of this pollutant. At $x/D = 30$, all three cases of CMCe provide significant improvement on the LES-CMC results, but also overpredict the generation of NO.

The scalar dissipation rate, as shown in figure 6.14 is reasonably well predicted by LES-CMC, was well as in *Cases A* and *C*. As intended, *Case B* shows a slightly higher scalar dissipation rate, but conditional temperature and conditional moments of the species indicate this not to have a strong effect. Thus, dissipation is most probably not the mechanism responsible for the extinction in this flame.

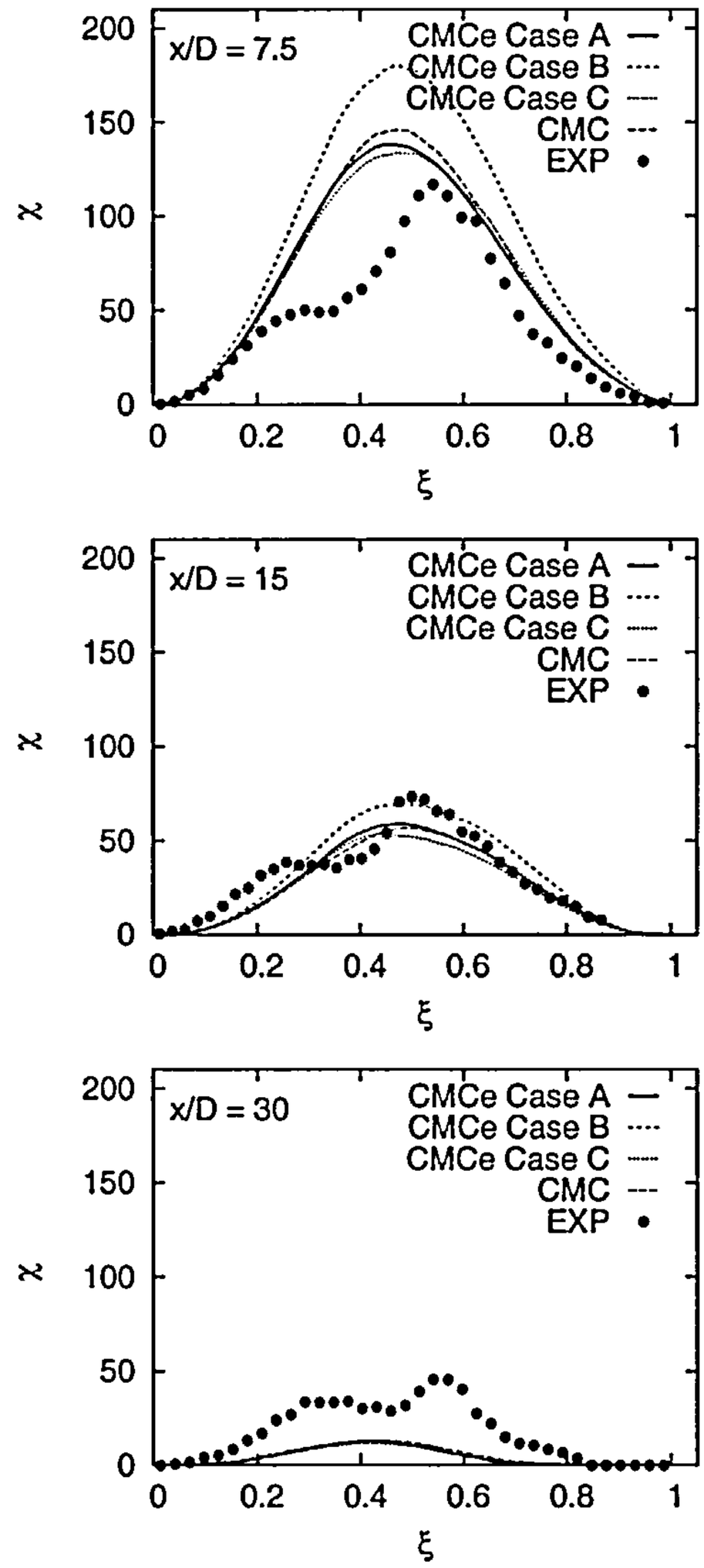


Figure 6.14: Conditional mean scalar dissipation

### 6.3.2 Flame D

For the other turbulent flames of this series no variation of the turbulent Schmidt number was carried out, but the standard value of $Sc_t = 0.4$ has been used as suggested in [65]. However, two calculations using the CMCe methodology were carried out with the two values for $\gamma_t$, to study the influence of varying temperature fluctuations on the performance of the method, given the lower/higher turbulence level in flame D/F.

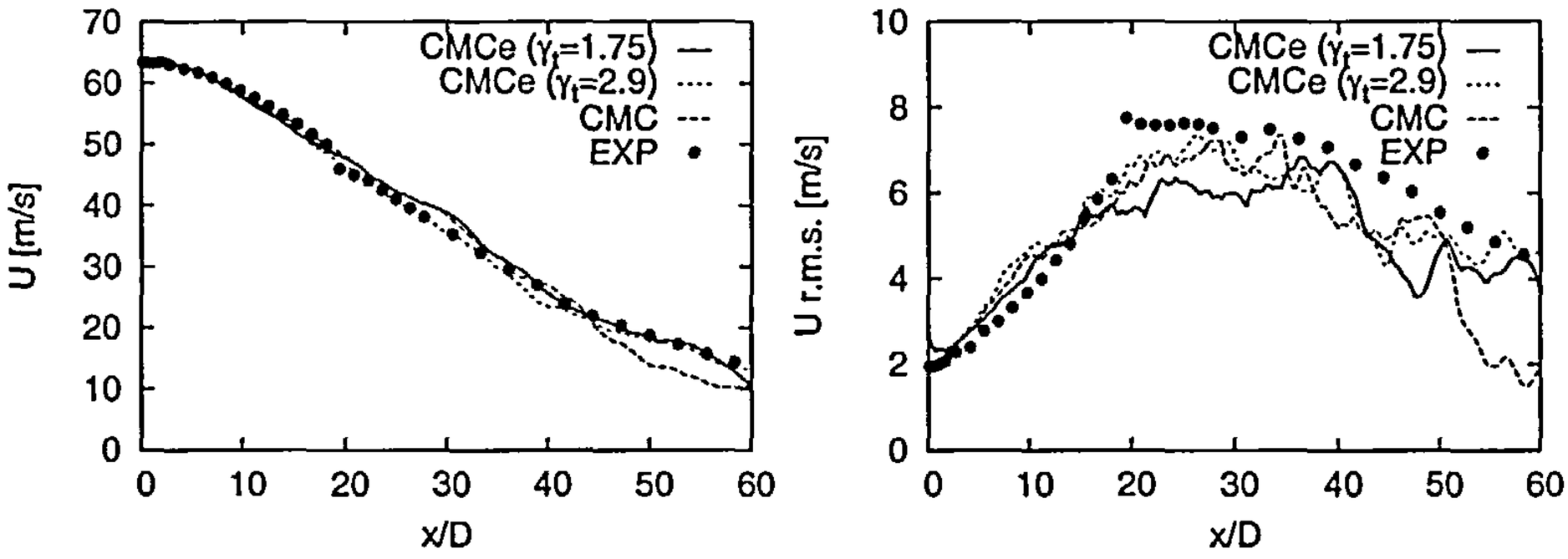


Figure 6.15: Axial velocity mean and r.m.s along the centreline

The mean and r.m.s. axial velocity component is shown in figure 6.15. Excellent agreement with the experiment can be seen for the mean. The r.m.s. is also very well predicted, although the maximum fluctuation levels are somewhat underpredicted for the case of LES-CMC.

The mixture fraction field is also very well predicted, especially in the main area of interest, for $x/D < 30$. Further downstream a slight underprediction is observed, possibly due to excessive numerical dissipation. Fluctuation levels are predicted reasonably well. The discrepancy of experiment and simulation close to the nozzle, is again most likely explained by experimental noise. Far downstream mixture

fraction r.m.s. is slightly underpredicted.

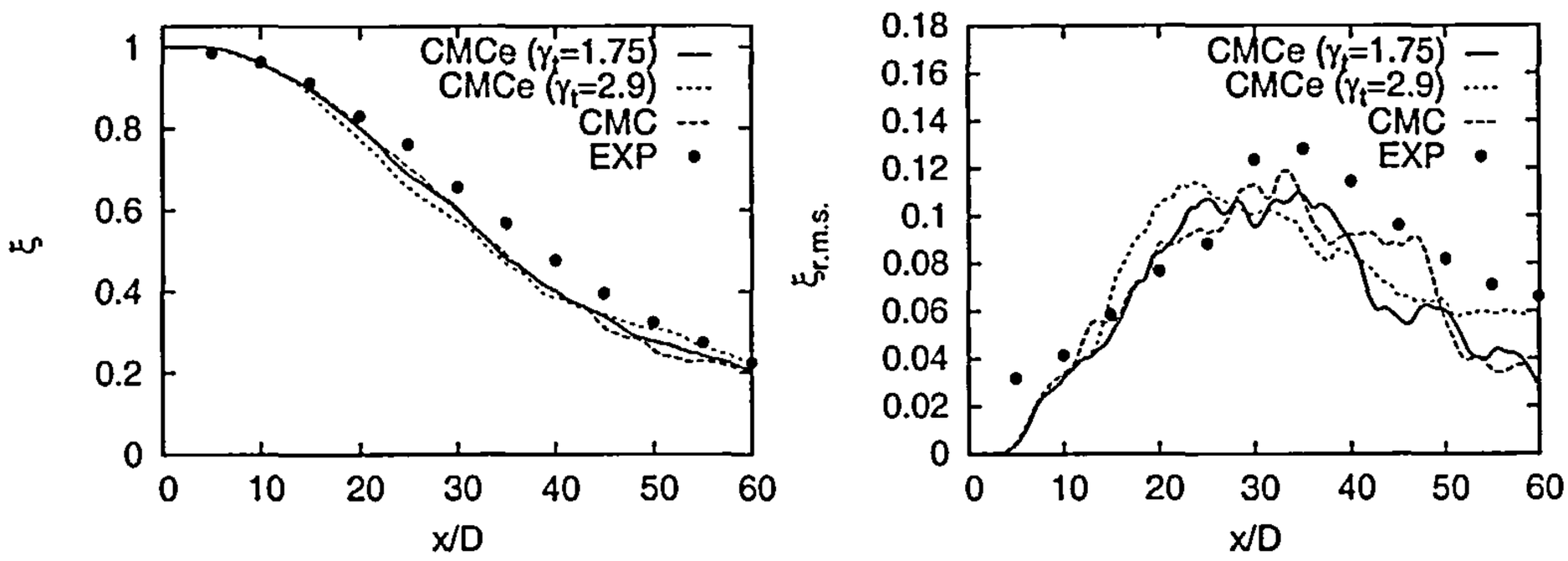


Figure 6.16: Mixture fraction mean and r.m.s. along the centreline

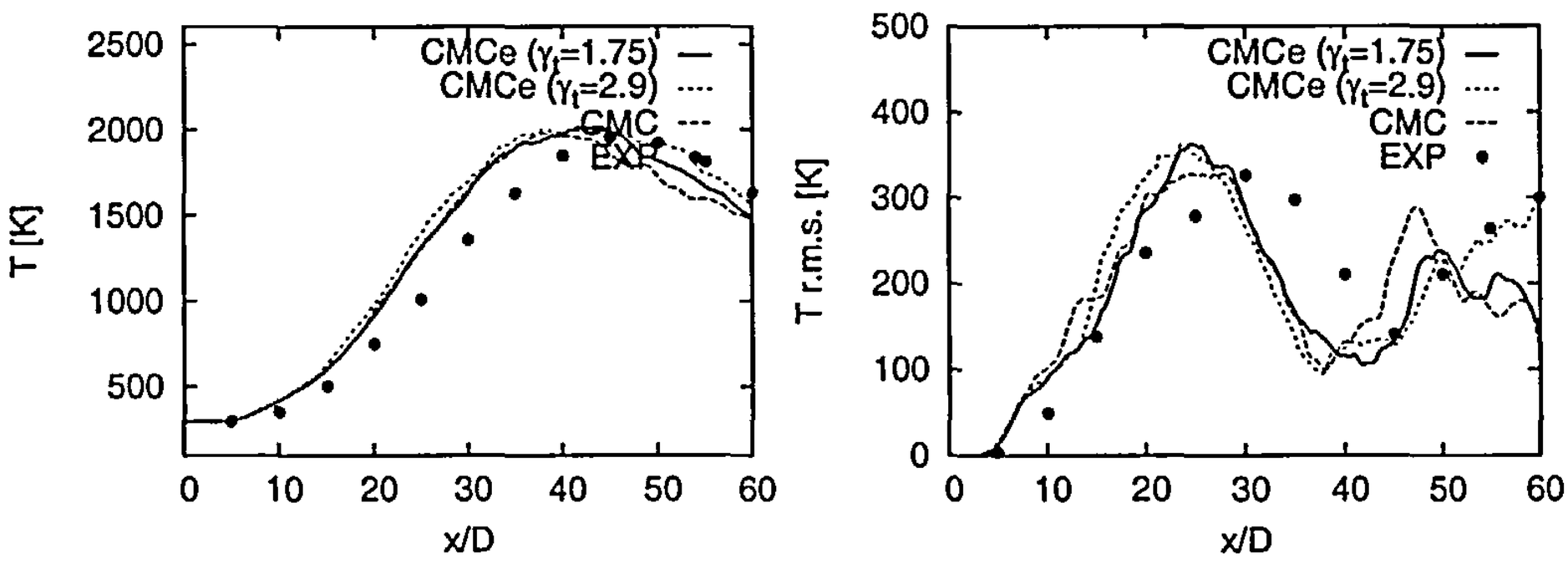


Figure 6.17: Temperature mean and r.m.s. along the centreline

Temperature along the centreline is seen in figure 6.17. It is slightly overpredicted. Temperature fluctuations levels are of similar order as the experimental values. More insightful however, are the conditional temperatures as given by the different models. They will be discussed later in this section.

Figure 6.18 shows radial profiles of the mixture fraction mean and r.m.s. for the relevant downstream locations. Agreement with the measurements is very good, both for the predicted mean and fluctuations. The different models result in only

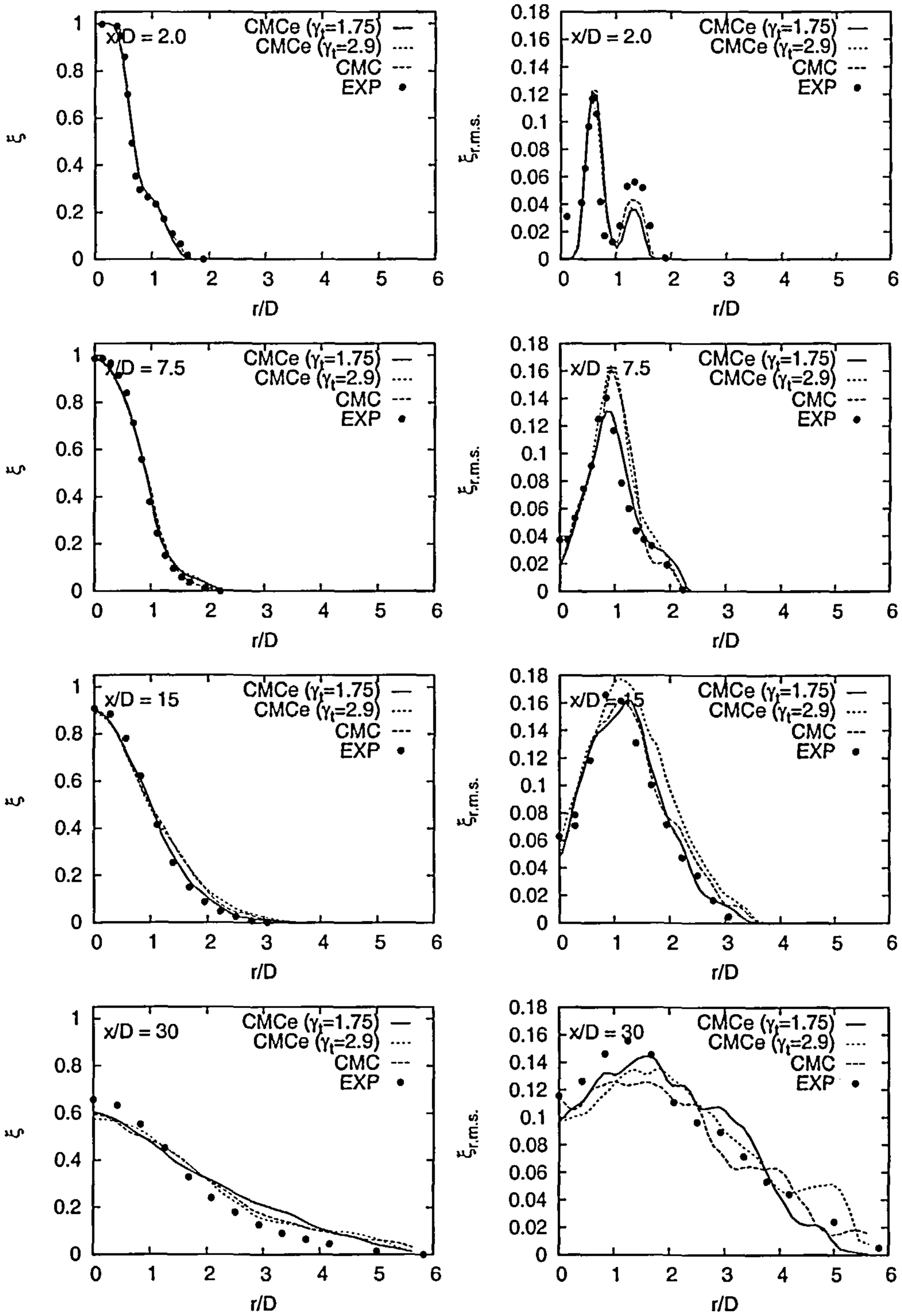


Figure 6.18: Mixture fraction mean and r.m.s. at several downstream location

minor differences in the prediction of the mixture fraction field.

Figure 6.19 gives radial temperature profiles. All models perform well, both for the mean and r.m.s., but again, assessment of their performance is more straightforward if conditional values are viewed.

Since flame D exhibits only little local extinction, and LES-CMC and Eulerian flamelets have proven to work reasonably well for this flame, strong improvements cannot be expected, nor are they needed. Conditional temperatures and conditional fluctuations are shown in figure 6.20. Close to the nozzle it is practically impossible to distinguish between LES-CMC and CMCe, although for the latter extremely good estimates for the temperature fluctuations have been taken into account by the two CMCe cases. At $x/D = 7.5$ CMCe can improve upon the LES-CMC results and the trend is consistent; the high $\gamma_t$ case provides a slight overprediction of conditional temperature fluctuations and lower conditional temperatures, that match the measurements well. Further downstream at $x/D = 15$ all models overpredict the maximum conditional temperature by about $100K$ and only small differences amongst them are seen. At $x/D = 30$ conditional temperature fluctuations are so small that the flame resembles a pure diffusion flame. Hence, LES-CMC and CMCe are fairly close to the experimentally observed conditional temperatures, but deviate in the very rich part of the flame by about $150K$.

Figure 6.21 shows predictions of methane and oxygen, which are reasonable throughout the domain, although the depletion of fuel is overpredicted from $x/D = 15$ onwards. In the case of oxygen, CMCe yields significantly improved predictions over LES-CMC.

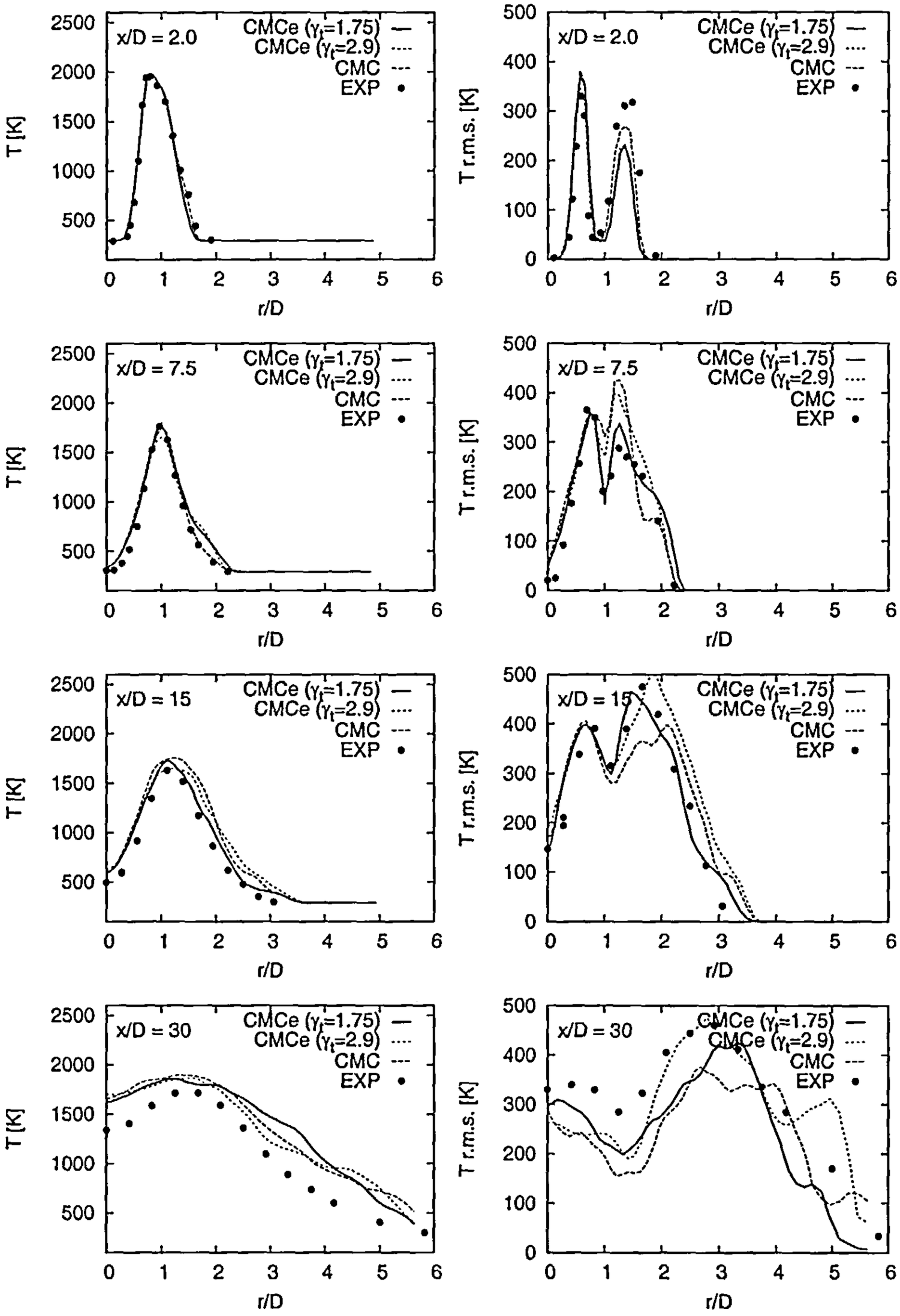


Figure 6.19: Temperature mean and r.m.s. at several downstream location

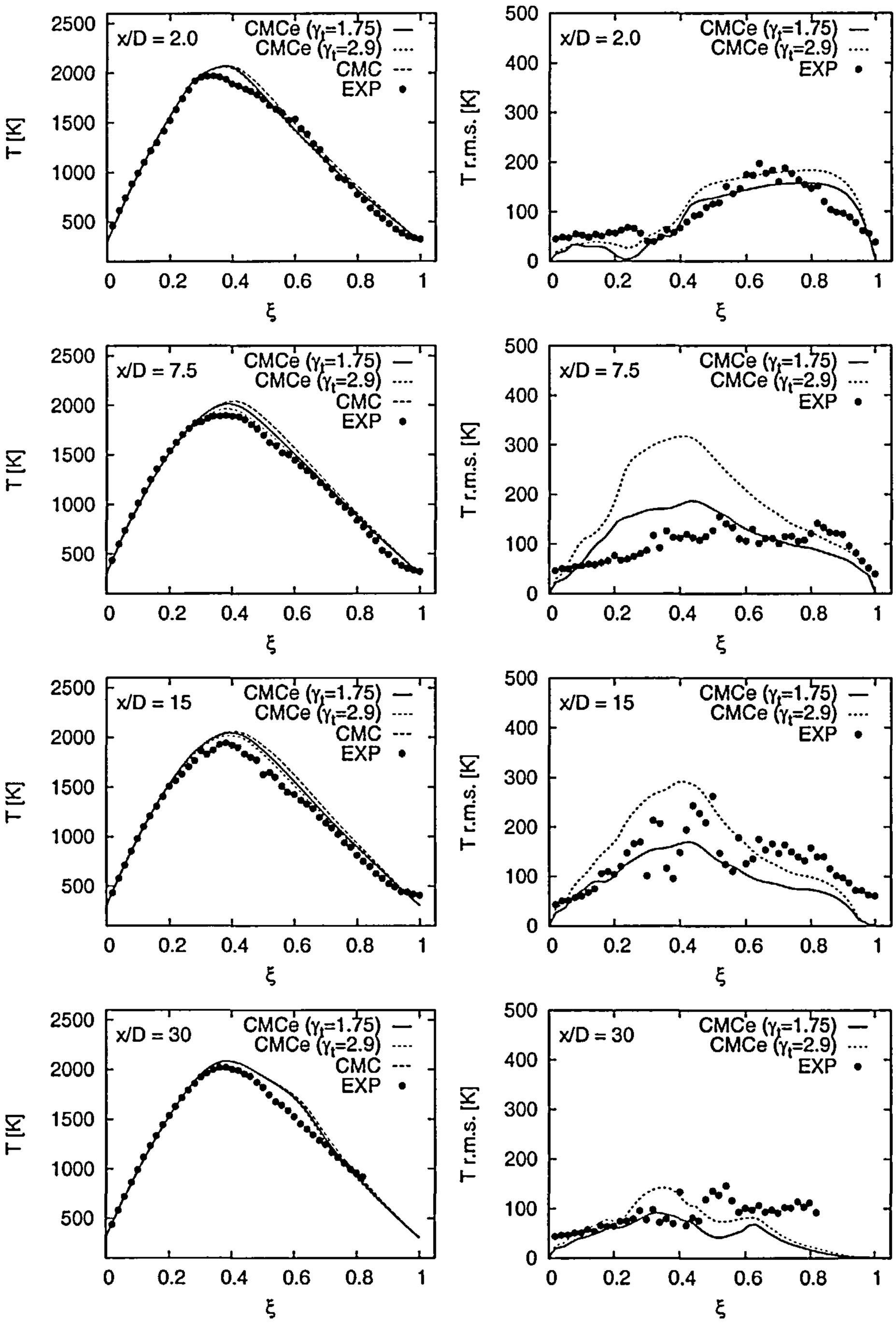


Figure 6.20: Conditional mean temperature and r.m.s. (from conditional variance equation

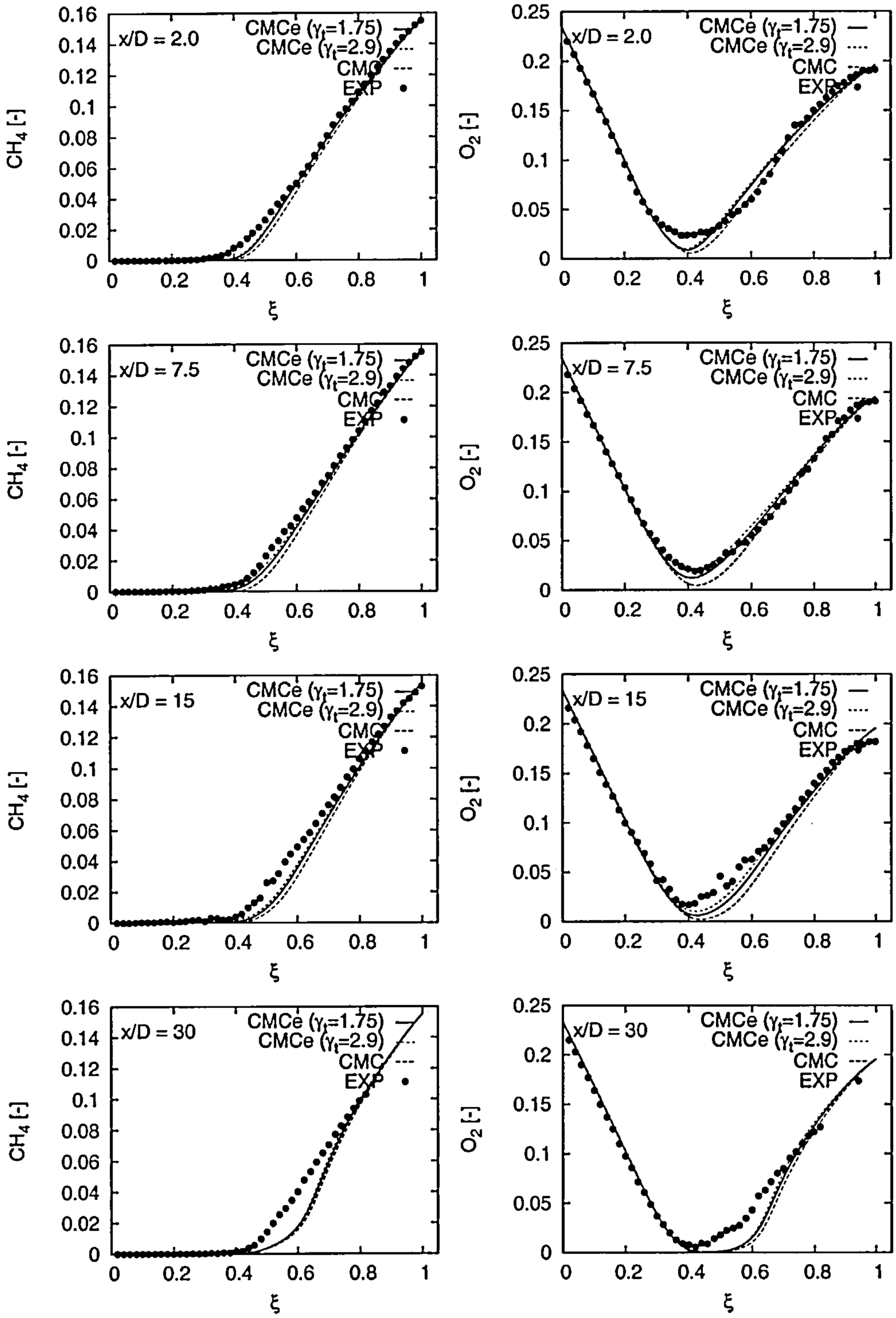


Figure 6.21: Conditional means of methane and oxygen

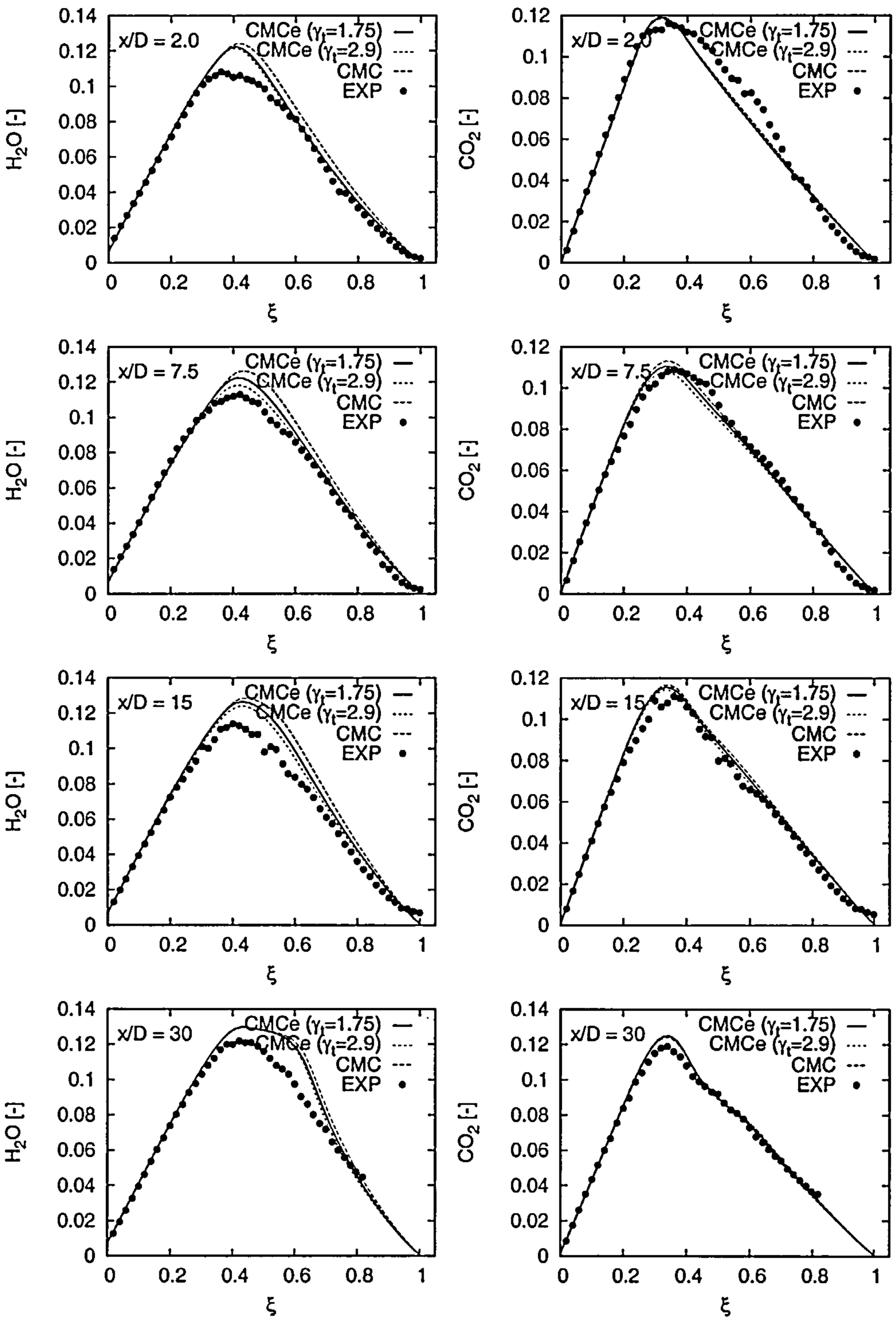


Figure 6.22: Conditional means of water and carbon dioxide

The production of water as seen in figure 6.22 is somewhat overpredicted at every location. Generation of carbon monoxide on the other hand is very well captured by both LES-CMC and CMCe and a strong sensitivity of this pollutant on conditional temperature fluctuations cannot be observed.

The hydroxyl radical in figure 6.23 is generally overpredicted, although CMCe can improve the results of LES-CMC to some extent, but not significantly. At $x/D = 30$ prediction are relatively good for all cases of CMCe, whereas LES-CMC shows a slight overprediction. Hydrogen levels are equally overpredicted, but in this case CMCe offers significant improvement over LES-CMC. However, CMCe still overpredicts the production of OH consistently.

Carbon monoxide is predicted well by CMCe relatively close to the nozzle. Further downstream, from $x/D = 15$ onwards it is overpredicted in the rich part of the flame by all models. As for nitric oxide, LES-CMC predictions are about twice the concentration levels that were measured. CMCe predicts lower levels of NO, but show underproduction of the pollutant close to the nozzle. At $x/D = 15$ results are very good for CMCe and at $x/d = 30$ NO is somewhat overpredicted by CMCe.

For all cases presented, the conditional scalar dissipation rate is very well predicted until $x/D = 15$ as seen in figure 6.25. At $x/D = 30$ however, conditional scalar dissipation is far too low, compared to the experimentally observed values.

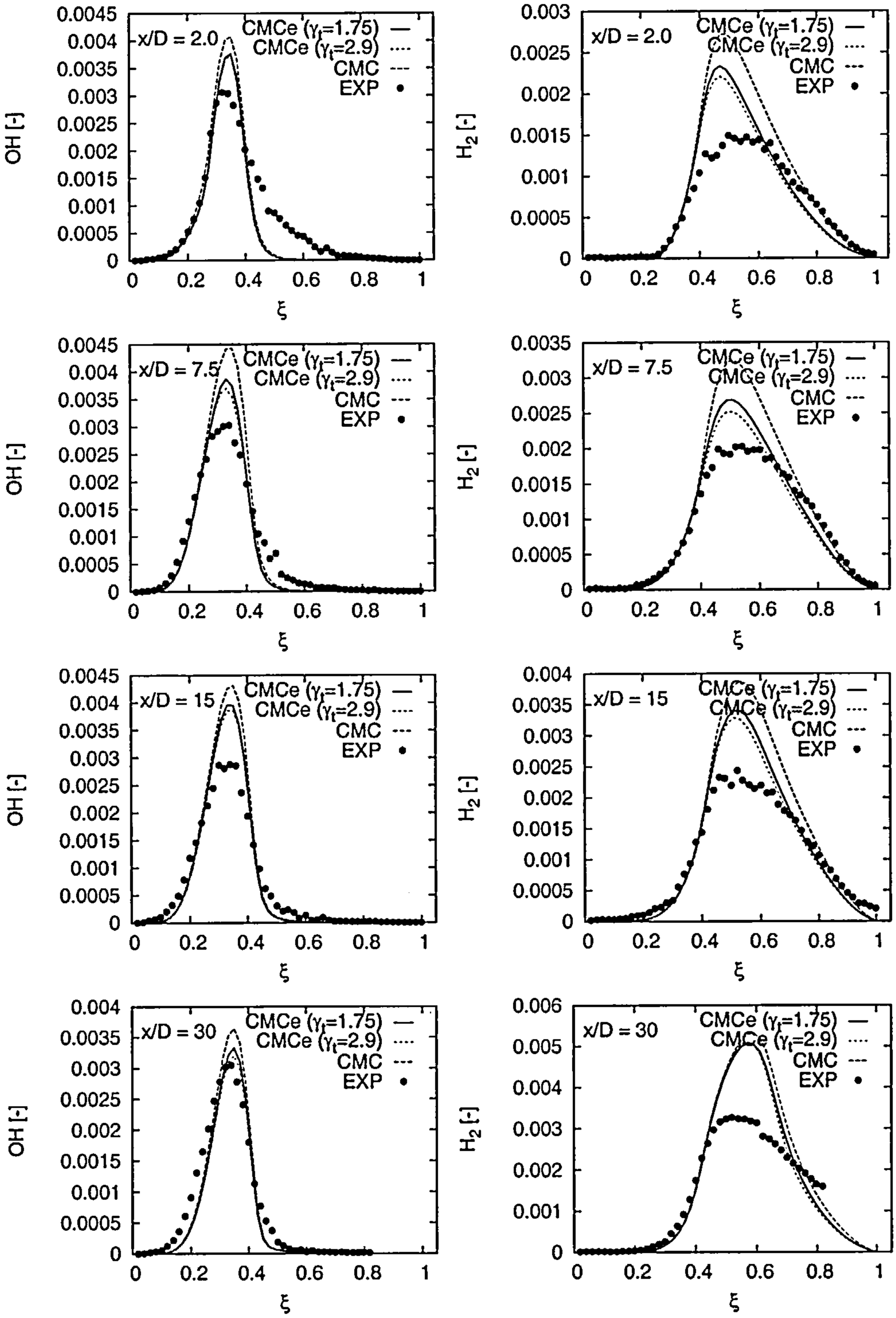


Figure 6.23: Conditional means of hydroxyl and hydrogen

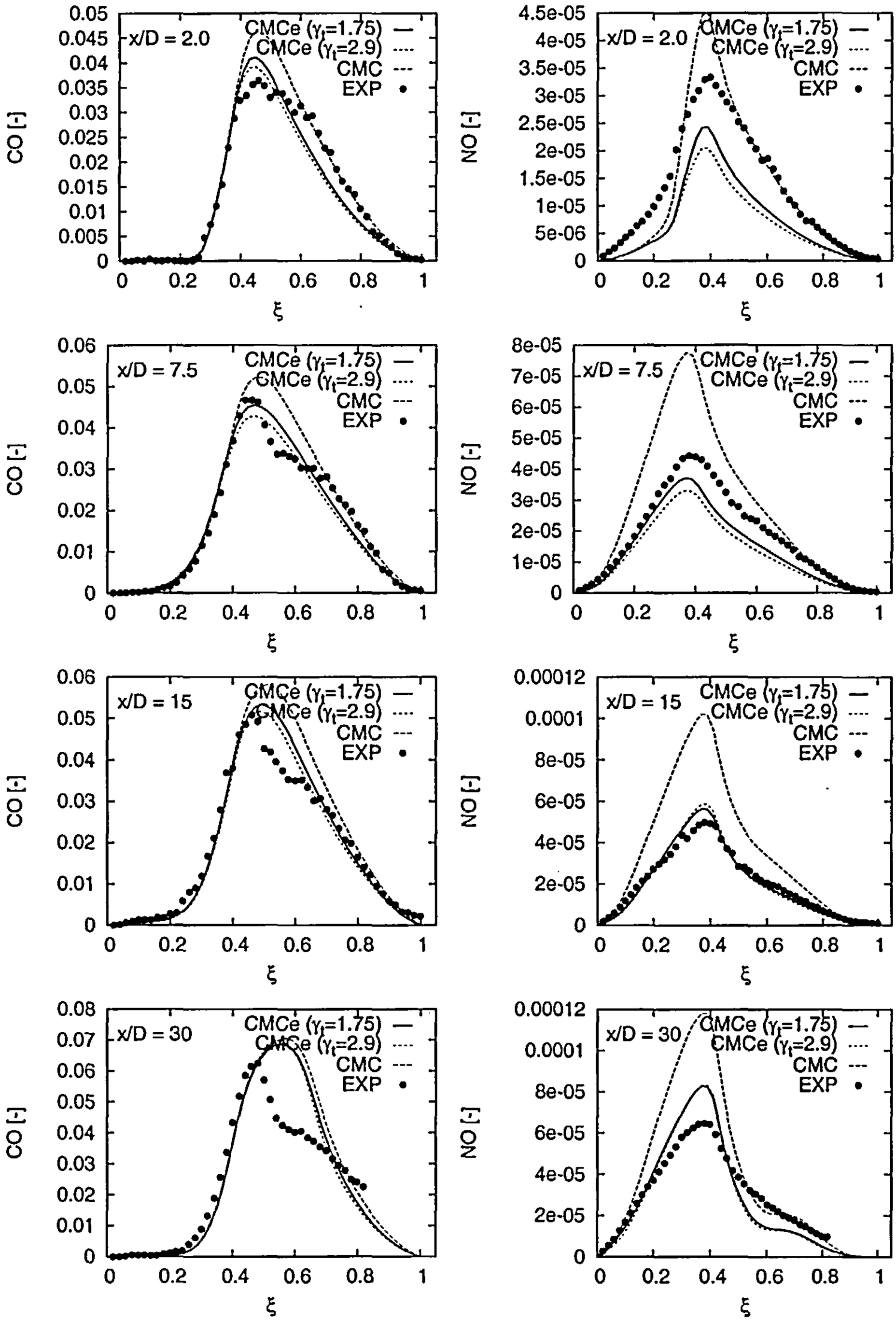


Figure 6.24: Conditional means of carbon monoxide and nitric oxide

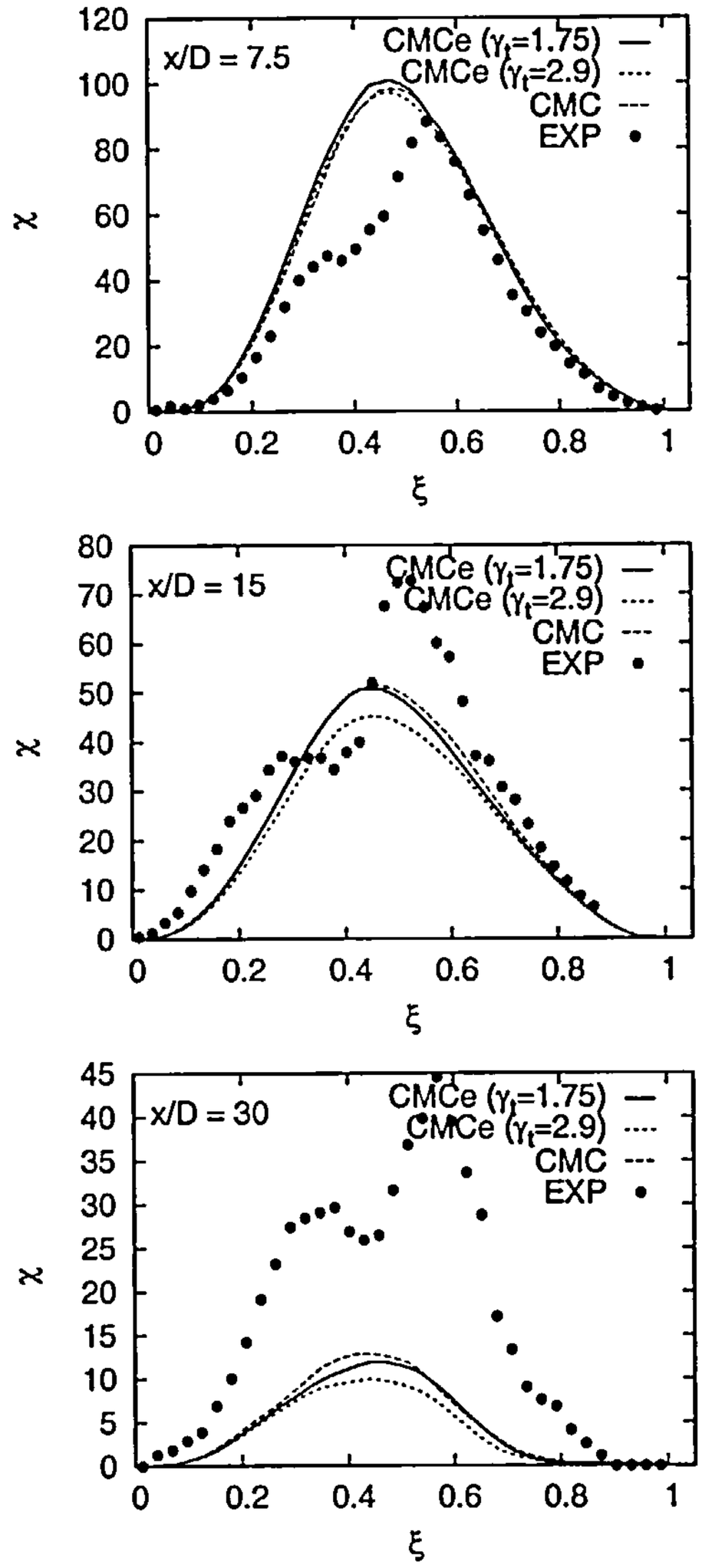


Figure 6.25: Conditional mean scalar dissipation

### 6.3.3 Flame F

Out of this series, flame F is the most difficult flame to model. It is close to global extinction and boundary condition yielding a burning or extinguished flame, lie within the range of experimental uncertainty. For flame F the same calculations were carried out as for flame D. A benchmark is provided by LES-CMC and two calculations invoking the CMCe methodology for one low-($\gamma_t = 1.75$) and one high-$\gamma$ case ($\gamma_t = 2.9$).

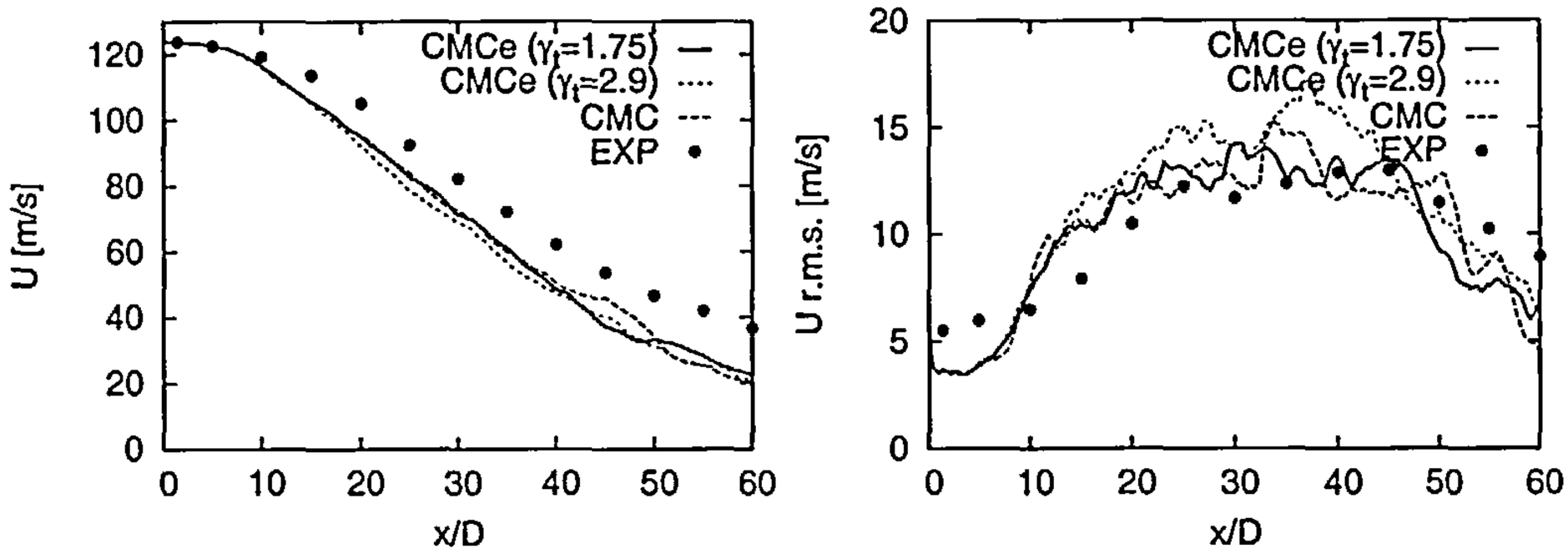


Figure 6.26: Axial velocity mean and r.m.s along the centreline

Figure 6.26 shows results for the axial mean velocity and r.m.s.. From $x/D = 10$ onwards, velocity is consistently slightly underpredicted, whereas the fluctuation levels are quite accurately predicted.

Mixture fraction mean and r.m.s. are well predicted, as seen in figure 6.27 throughout the domain.

Results for the temperature are shown in figure 6.28. It is noticeable that predictions are rather poor; detailed discussion follows, when conditional quantities are presented.

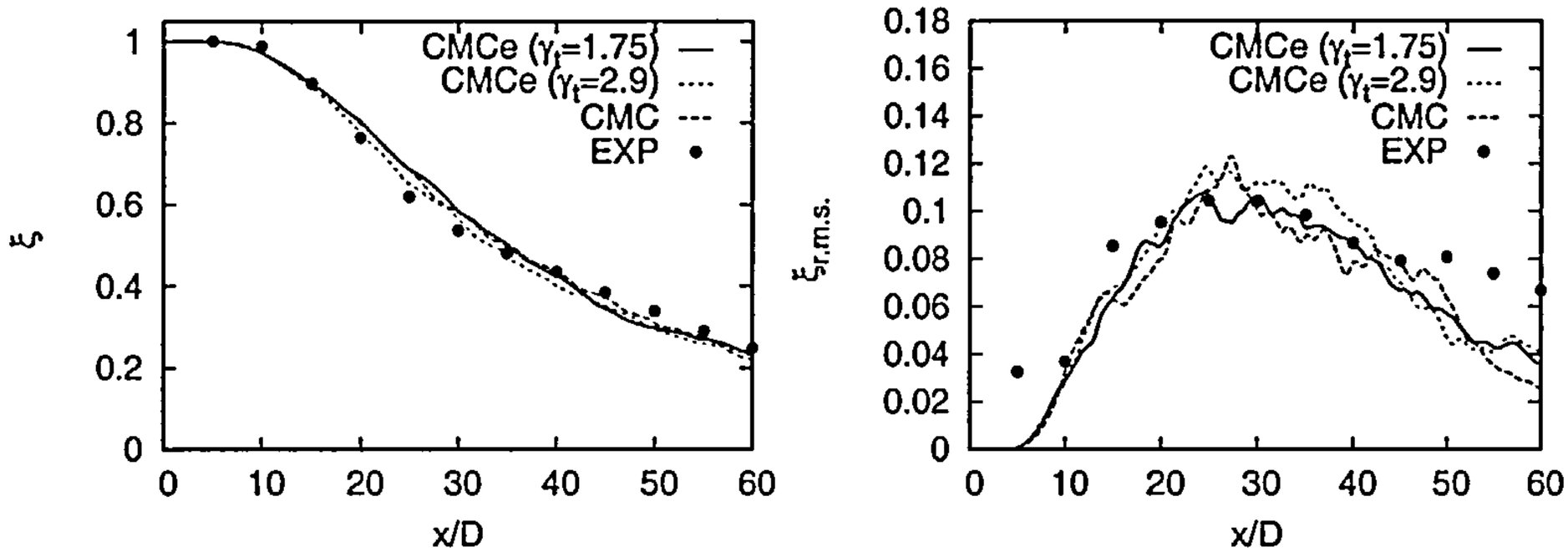


Figure 6.27: Mixture fraction mean and r.m.s. along the centreline

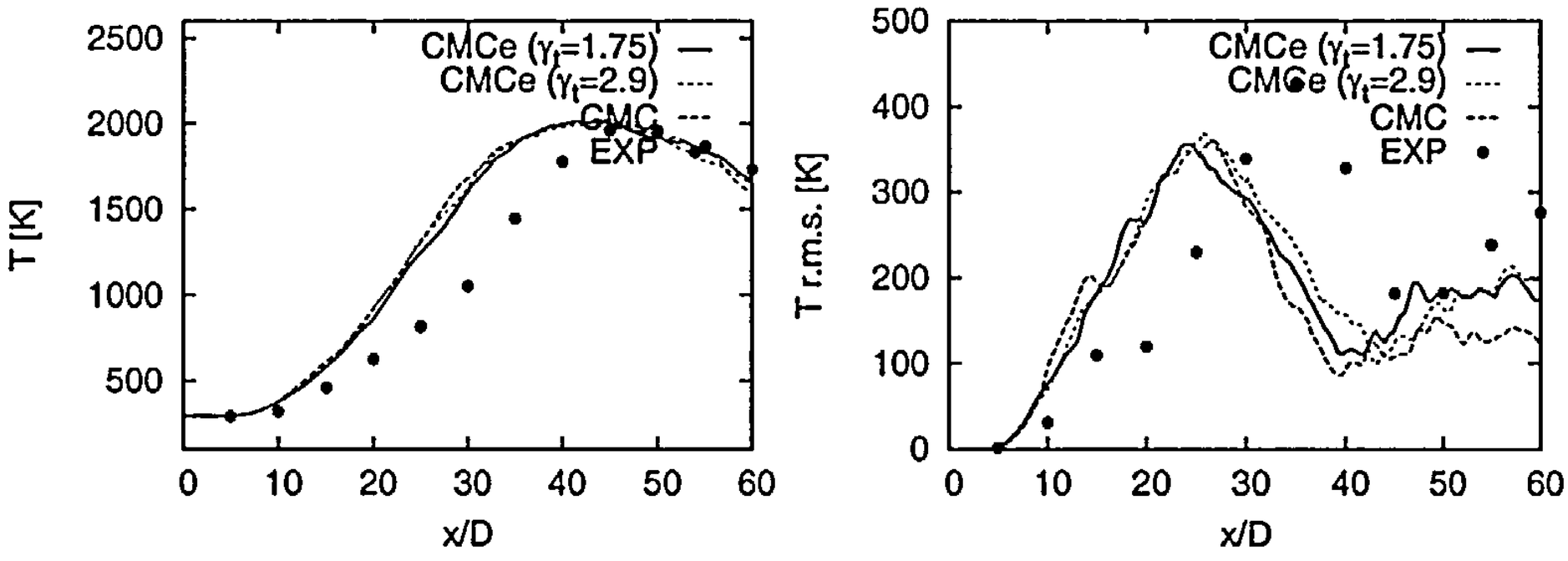


Figure 6.28: Temperature mean and r.m.s. along the centreline

Figure 6.29 gives radial profiles of mixture fraction and mixture fraction fluctuations. Results are very good for both mean and r.m.s. and significant differences between the different models cannot be observed.

Radial temperature and temperature fluctuation profiles are shown in figure 6.30. As observed in the previous flames, at $x/D = 2$ conditions seem dominated by the inflow conditions. Hence, predictions at this location are good. Further downstream however temperatures are severely overpredicted although fluctuation levels are in reasonable agreement with the experimental findings.

Conditional temperatures and modelled conditional temperature fluctuations are

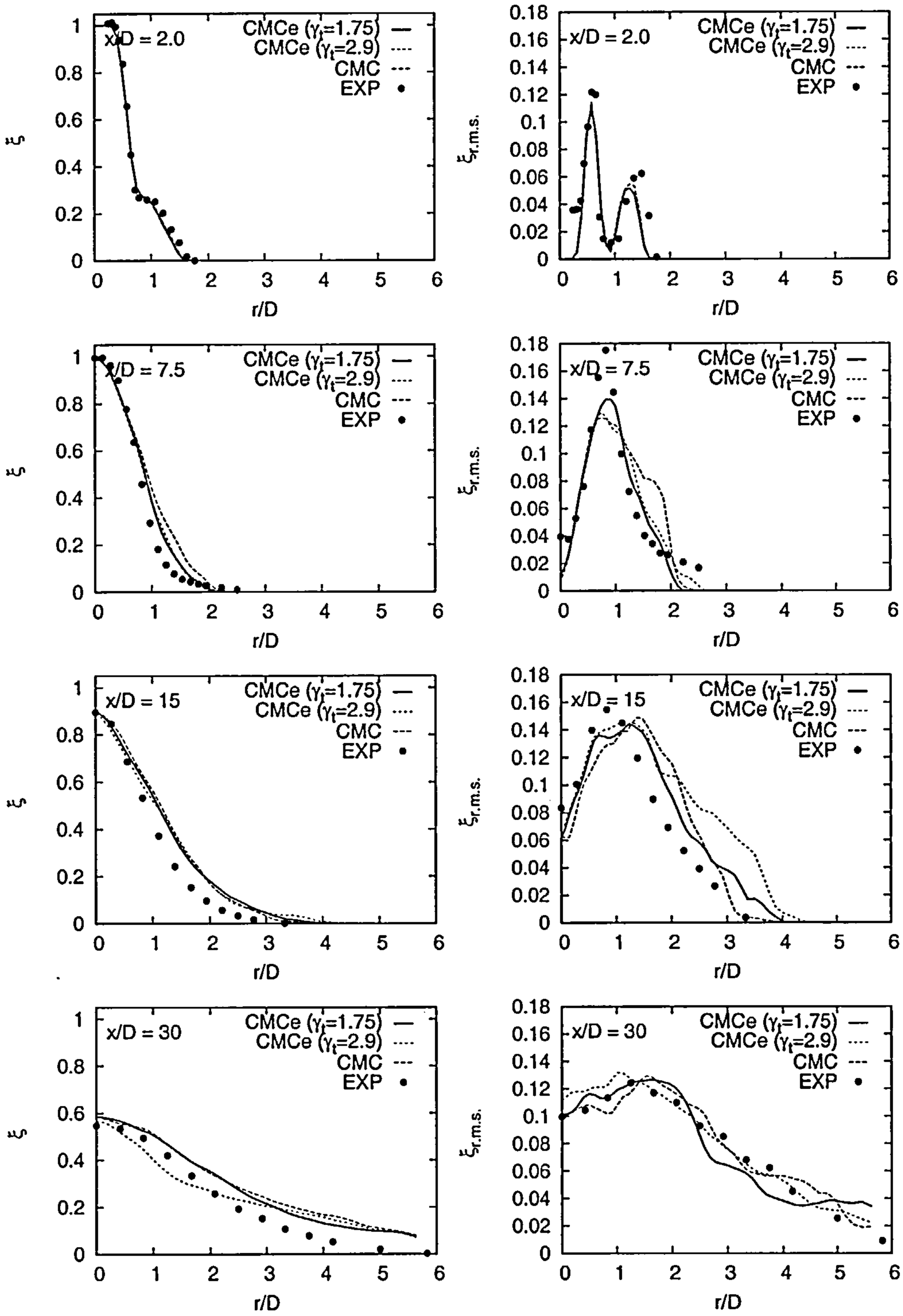


Figure 6.29: Mixture fraction mean and r.m.s. at several downstream location

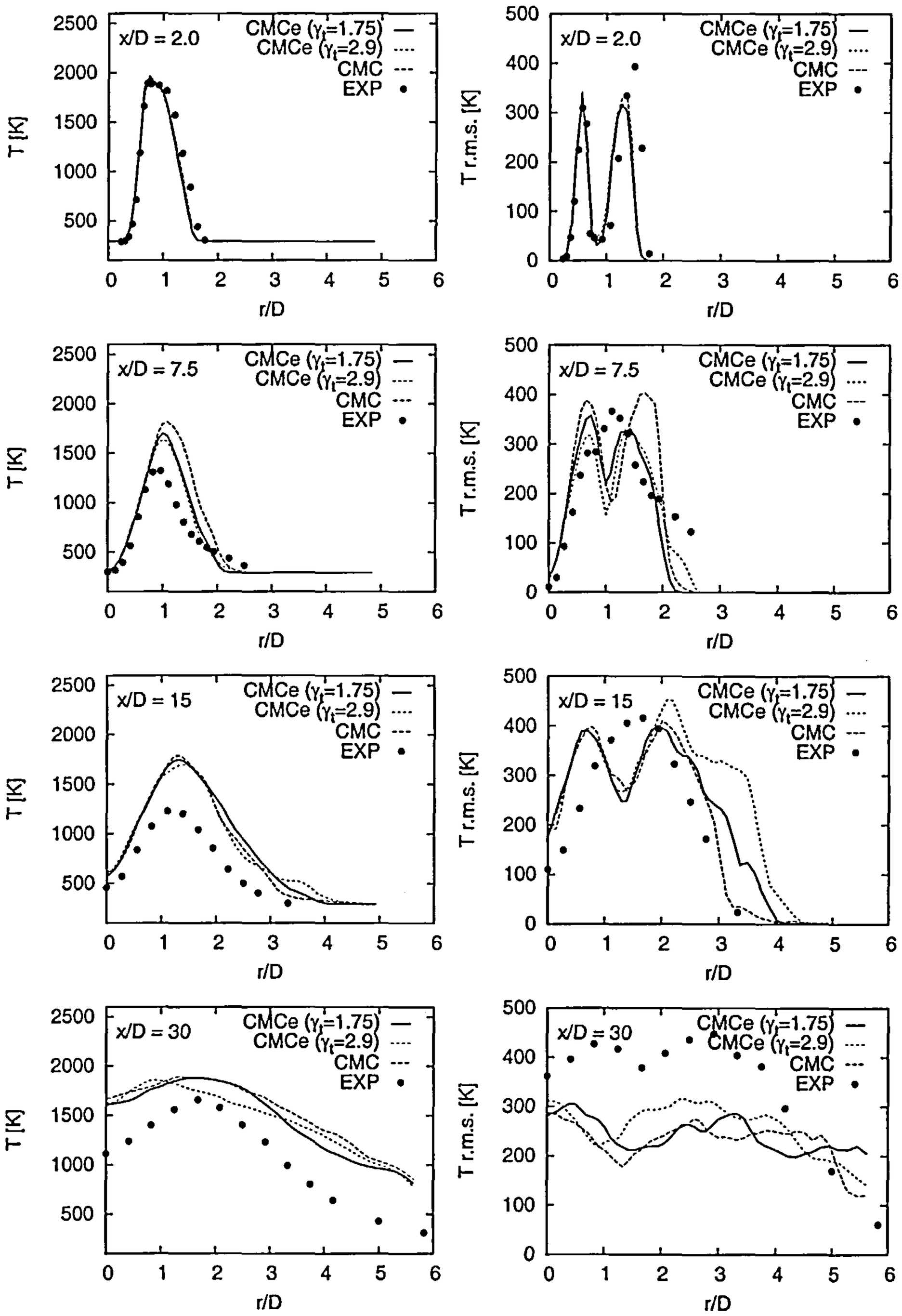


Figure 6.30: Temperature mean and r.m.s. at several downstream location

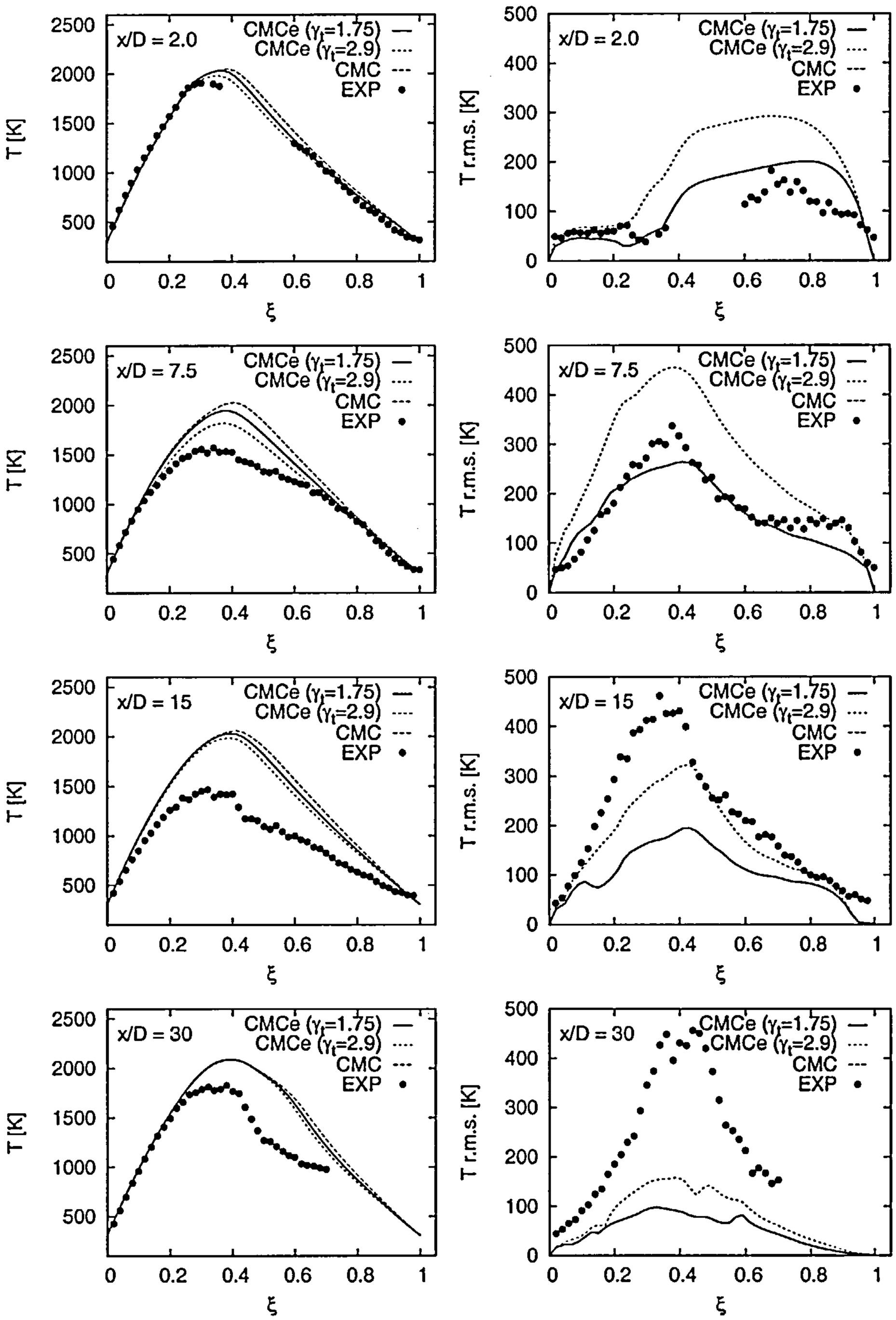


Figure 6.31: Conditional mean temperature and r.m.s. (from conditional variance equation

seen in figure 6.31. At $x/D = 2$ the agreement is good, which is further evidence, that inflow conditions largely determine the thermodynamical state at this location. The shortcomings of the models become apparent at $x/D = 7.5$, where all models largely overpredict conditional temperatures, although for the case of CMCe conditional temperature fluctuations are of the correct order and even overpredicted for the high-$\gamma$ case.

At $x/D = 15$ the range of models fail to capture the extent of extinction, which renders them of no practical use in these extreme combustion scenarios. Conditional temperatures are off by as much as $600K$ here. Even the so far impressive scalability of the conditional sensible variance model to predict conditional temperature fluctuations, as seen for the flames and locations seen so far, breaks down here. Even the high-$\gamma$ model underpredicts the maximum conditional temperature by about $150K$. Similarly, at $x/D = 30$ conditional temperatures are underpredicted by about $300K$ and the still strong temperature fluctuations observed in the experiment are not captured at all. The conditional variance equation predicts them as about $100K$ or $150K$ respectively; about $300K$ less than the measurements.

As expected, given the results for conditional temperatures, methane and oxygen depletion are not well captured by any of the models, as seen in figure 6.32. At $x/D = 2$ results are relatively close to the measurements, but further downstream predictions are poor.

The same can be said for the generation of water and carbon monoxide, as seen in figure 6.33.

This trend carries through and is seen for all remaining species seen in figures

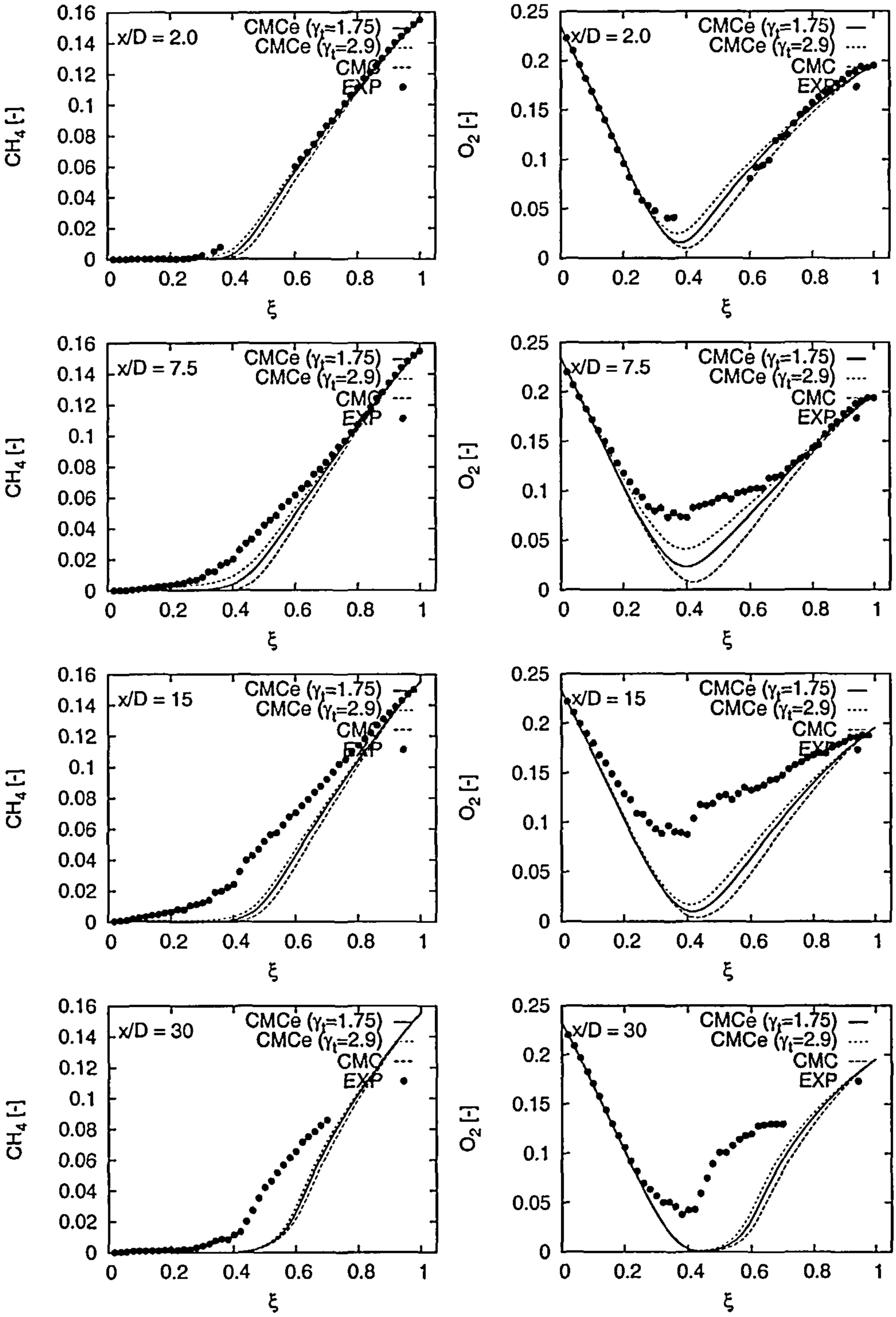


Figure 6.32: Conditional means of methane and oxygen

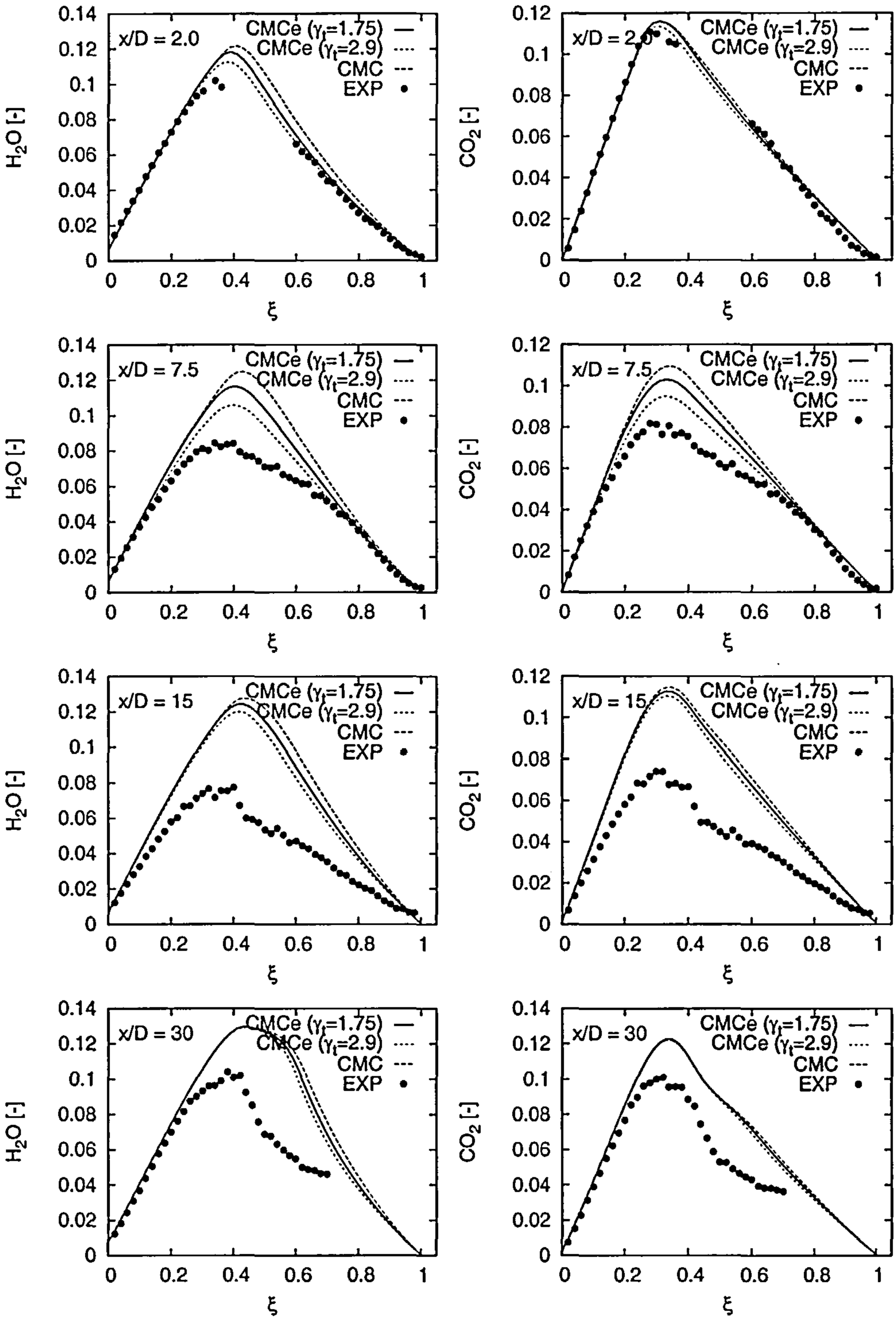


Figure 6.33: Conditional means of water and carbon dioxide

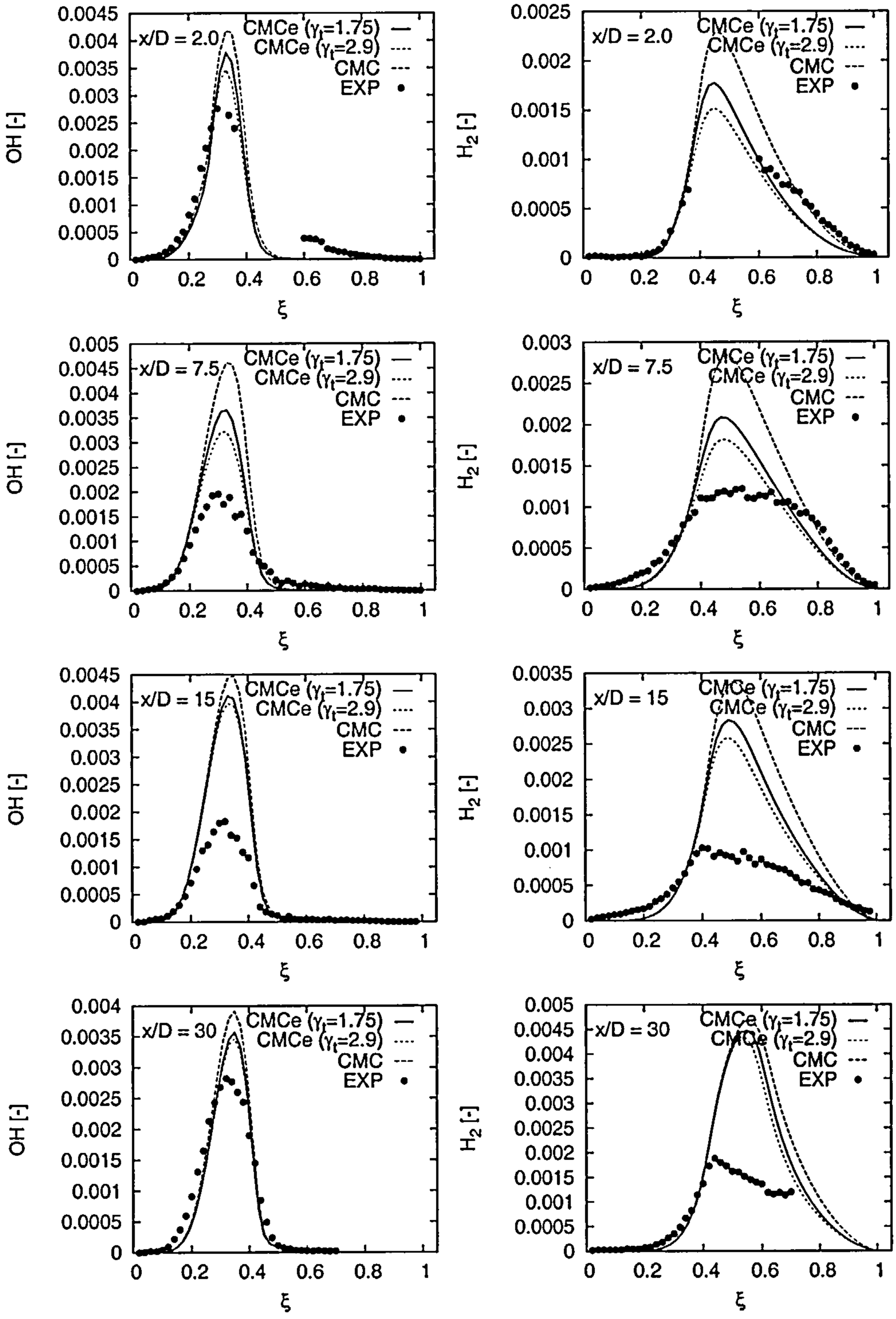


Figure 6.34: Conditional means of hydroxyl and hydrogen

6.34-6.35.

Figure 6.36 gives the predictions of conditional scalar dissipation rate. However, experimental values were not available to assess their agreement with the experiment.

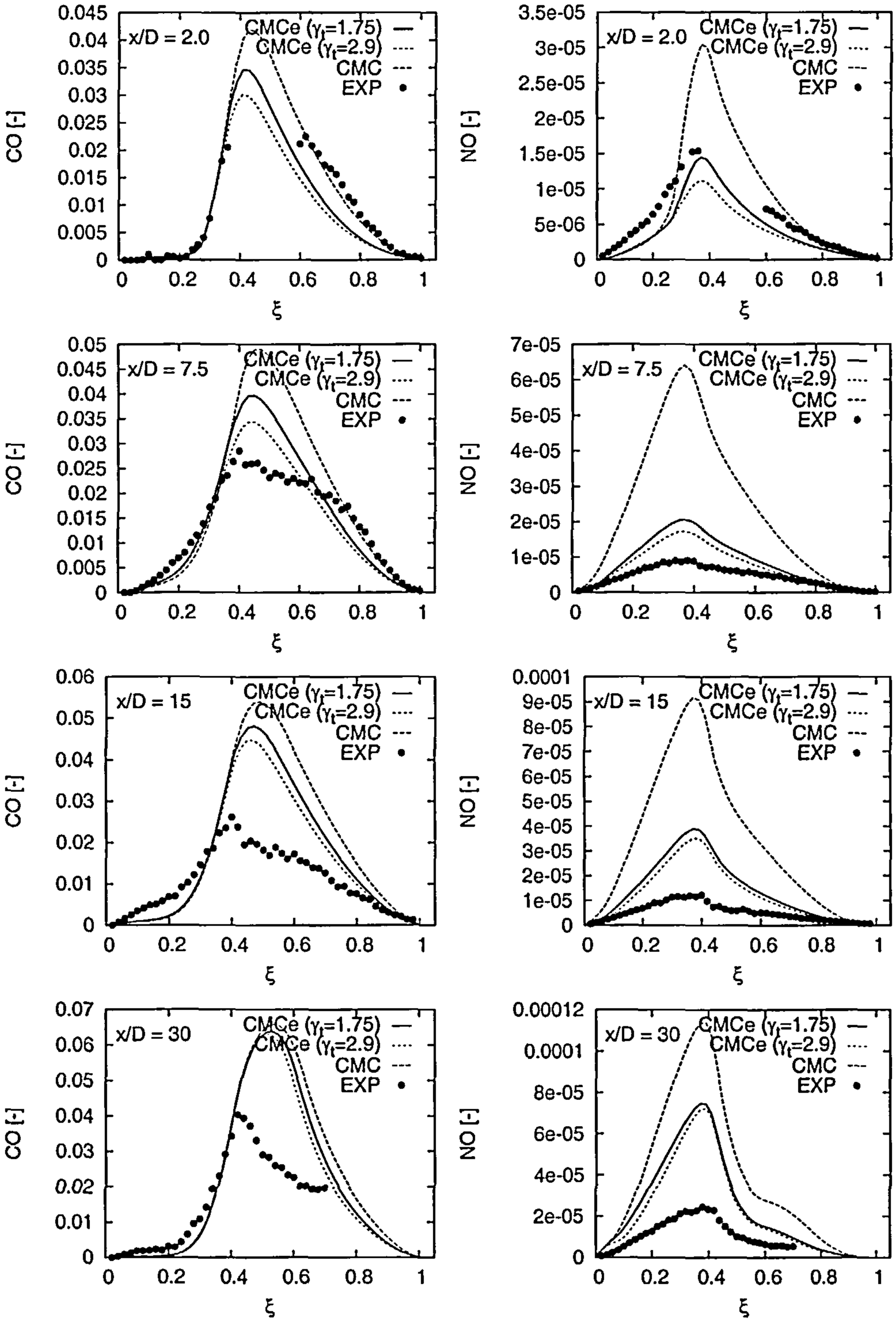


Figure 6.35: Conditional means of carbon monoxide and nitric oxide

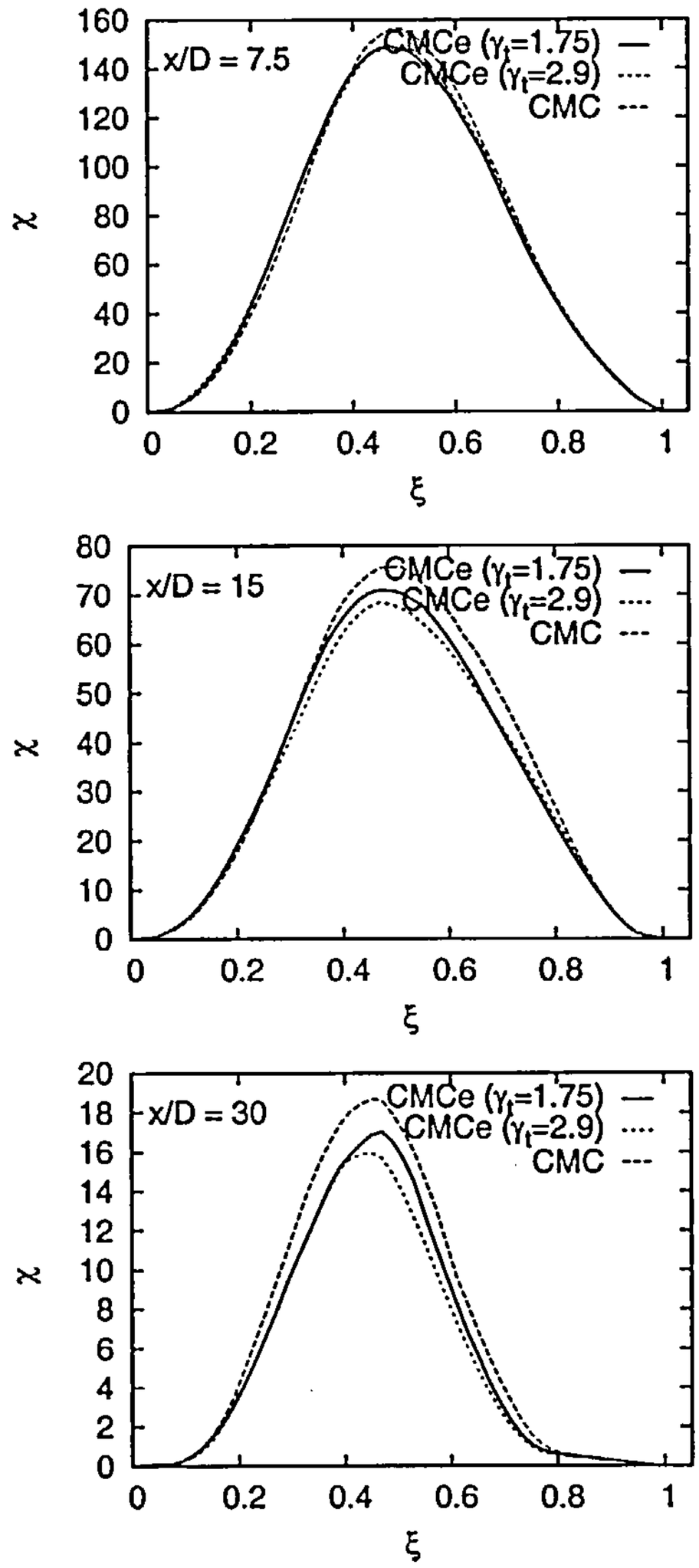


Figure 6.36: Conditional mean scalar dissipation

Chapter 7

# Conclusions and Future Work

The aim of the presented work is to build upon the LES-CMC methodology and extend it to account for the influence of temperature fluctuations on the conditional chemical source term.

The extended conditional moment closure method (CMCe) solves for the conditional sensible enthalpy variance equation to quantify the level of extinction and reignition. The work showed that results from LES-CMC can generally be improved by the presented method. The computation of Sandia flames D, E and F showed varying success, although the general trends observed are encouraging.

Flame E with an intermediate level of extinction and reignition was chosen to assess parameter variations of the CMCe methodology. The influence of the $\gamma_t$ parameter was studied and showed the expected trend. Increasing $\gamma_t$, which results in lower conditional progress variable dissipation, leads to higher predictions of conditional temperature fluctuations. Taking into account higher conditional temperature fluctuations by CMCe leads to lower mean conditional temperatures. However, where predictions of the conditional temperature fluctuations agree well with the experimental findings, the conditional temperature is still consistently

overpredicted to a varying degree.

The variation of the turbulent Schmidt number, leading to higher conditional scalar dissipation rates did not show a significant effect in regions with strong local extinction and reignition. Further downstream the increased turbulent Schmidt number did not raise conditional scalar dissipation rate significantly, possibly because it increases diffusion, which counteracts the effect by decreasing gradients, whereas further upstream turbulence levels seem to be high enough so that mixing is controlled by turbulence and not by diffusion. To investigate and assess the behaviour of the proposed method, Flames D and F were computed to study to performance of CMCe in the case of different turbulence intensities.

Flame D exhibits only moderate local extinction and reignition and conserved scalar approaches have shown to work reasonably well. The proposed extended source term closure provides some improvement over LES-CMC and yields improved predictions of conditional temperatures as well as conditional means of chemical species. Variation of the $\gamma_t$ parameter again proved consistent and a higher value for $\gamma_t$ leads to higher conditional temperature fluctuation levels, which in turn leads to lower conditional mean temperatures, closer to the experimentally observed.

Flame F is the case with the strongest degree of local extinction and reignition. It is close to global extinction and challenging to model. The CMCe method was applied and $\gamma_t$ was varied. Results however, were poor. Even with conditional temperature fluctuations of the correct order the strong levels of extinction observed in the experiments could not be reproduced.

It shall be noted, that although the solution of the conditional sensible enthalpy

variance equation invokes a rather ad hoc model for the conditional reactive scalar dissipation rate, the results and in particular the scalability are impressive. Values of $\gamma_t$ obtained by matching conditional temperature fluctuations in flame E, yield reasonable predictions of the temperature fluctuations for flames D and F. The underprediction of conditional temperature fluctuations further downstream might be alleviated by an improved model for the reactive scalar dissipation rate, incorporating Damköhler number effects as proposed by some researchers [12, 13, 75].

To summarise, the proposed CMCe methodology improves predictions of conditional moments for the three piloted jet flames studied. However, with increasing levels of local extinction and reignition, even realistic estimations of the temperature fluctuations do not yield the low mean temperature that can be observed experimentally. This seems to indicate that other processes that contribute to local extinction are not yet being accounted for.

The solution of the conditional sensible enthalpy variance equation requires modelling of several terms. Previously proposed ad hoc models are employed in the conditional variance transport equation framework used in the present work. This approach proved to perform better than initially considered algebraic models. However, the need to calibrate the $\gamma_t$ coefficient is not entirely satisfactory and provides room for improvement and generalisation.

It seems that treatment of sensible enthalpy as an independent variable should improve the predictive cababilities of any model. Therefore, doubly conditional moment closure should be better suited for cases of high levels of local extinction and reignition. However, the issue of the modelling of reactive scalar dissipation remains. Additionally, it is still a matter of controversy how to treat regions in

phase space, that are characterised by extremely low probabilities. Since boundary conditions for conditional moments can only be imposed at the limits of phase space, the question is how to treat the regions connecting the limits with the region of finite probability.

These issues could be avoided, if one does not solve for the conditional moments, but the product of conditional moments and probability, and focuses on analysis of unconditional quantities rather than conditional ones. In this case the specification of appropriate boundary conditions would be straightforward, since only physically observed values are used; they are the only ones with non-zero probability. Although conditional quantities would not be readily available for evaluation, conditional averaging could easily provide those.

Furthermore, it might be worthwhile considering to solve the joint p.d.f. transport equation of mixture fraction and progress variable in order to overcome the need to presume a functional shape of this p.d.f..

# Bibliography


[1] R.S. Barlow and J. Frank. Piloted $CH_4$/Air Flames C,D,E, and F - Release 2.1. Technical report, Sandia National Laboratories, 2007.

[2] R.W. Bilger. The structure of turbulent nonpremixed flames. *Twenty-second Symposium on Combustion*, pages 475–488, 1988.

[3] R.W. Bilger. Turbulent diffusion flames. *Annual Review of Fluid Mechanics*, 21:101–135, 1989.

[4] R.W. Bilger. Conditional moment closure for turbulent reacting flow. *Physics of Fluids*, A 5(2):436–444, February 1993.

[5] R.B. Bird, W.E. Steward, and E.N. Lightfoot. *Transport Phenomena.* Wiley & Sons, second edition edition, 2007.

[6] N. Branley and W.P. Jones. Large eddy simulation of a turbulent non-premixed flame. *Eleventh Symposium on Turbulent Shear Flows*, 2:21–1,21–6, 1997.

[7] N. Branley and W.P. Jones. Large eddy simulation of a turbulent non-premised flame. *Combustion and Flame*, 127:1914–1934, October 2001.

[8] S.P. Burke and T.E.W. Schumann. Diffusion flames. *First Symposium (International) on Combustion*, pages 2–11, 1928.

[9] J. Carrayrou, R. Mosé, and P. Behra. Operator-splitting procedures for reactive transport and comparison of mass balance errors. *Journal of Contaminant Hydrology*, 68(3-4):239–268, February 2004.

[10] C.M. Cha, G. Kosály, and H. Pitsch. Modeling extinction and reignition in turbulent nonpremixed combustion using a doubly-conditional moment closure approach. *Physics of Fluids*, 13(12):3824–3834, December 2001.

[11] C.M. Cha and H. Pitsch. Higher-order conditional moment closure modelling of local extinction and reignition in turbulent combustion. *Combustion Theory Modelling*, 6:425–437, July 2002.

[12] N. Chakraborty and N. Swaminathan. Influence of the Damköhler number in turbulence-scalar interaction in premixed flames. I. Physical Insight. *Physics of Fluids*, 19(4):045103, 2007.

[13] N. Chakraborty and N. Swaminathan. Influence of the Damköhler number in turbulence-scalar interaction in premixed flames. II. Model Development. *Physics of Fluids*, 19(4):045104, 2007.

[14] S. Chapman and T.G. Cowling. *The Mathematical Theory of Non-Uniform Gases*. Cambridge University Press, 1939.

[15] D. Clayton. *Large Eddy Simulation of of Non-premixed Flow in Complex Geometries*. PhD thesis, Imperial College London, 2006.

[16] P.J. Colucci, F.A. Jaberi, P. Givi, and S.B. Pope. Filtered density function for large eddy simulation of turbulent reacting flows. *Physics of Fluids*, 10(2):499–515, February 1998.

[17] A.W. Cook and J.J. Riley. A subgrid model for equilibrium chemistry in turbulent flows. *Physics of Fluids*, 6(8):2868–2870, August 1994.

[18] C.F. Curtiss and J.O. Hirschfelder. Transport properties of multicomponent gas mixtures. *Journal of Chemical Physics*, 17(6):550–555, June 1949.

[19] L. di Mare, M. Klein, W.P. Jones, and J. Janicka. Synthetic turbulence inflow conditions for large-eddy simulation. *Physics of Fluids*, 18(025107), February 2006.

[20] P. Domingo, L. Vervisch, S. Payet, and R. Hauguel. DNS of a premixed turbulent V flame and LES of a ducted flame using a FSD-PDF subgrid scale closure with FPI-tabulated chemistry. *Combustion and Flame*, 143(4):566–586, December 2005.

[21] R.S. Barlow (Ed.). www.ca.sandia.gov/tnf. Website for the International Workshop on Measurements and Computation of Turbulent Nonpremixed Flames.

[22] M. Fairweather and R.M. Woolley. First- and second-order elliptic conditional moment closure calculations of piloted methane diffusion flames. *Combustion and Flame*, 150(1-2):92–107, 2007.

[23] A. Favre. Statistical equations of turbulent gases. In *Problems of Hydrodynamics and Continuum Mechanics*, pages 231–266, Philadelphia, 1969. Soc. Ind. Appl. Math.

[24] J.H. Ferziger and M. Perić. *Computational Methods for Fluid Dynamics.* Springer, 3., rev. ed. edition, 2002.

[25] B. Fiorina, R. Baron, O. Gicquel, D. Thevenin, S. Carpentier, and N. Darabiha. Modelling non-adiabatic partially premixed flames using flame-prolongation of ILDM. *Combustion Theory Modelling*, 7(3):449–470, 2003.

[26] F. Gao and E.E. O'Brien. A large-eddy simulation scheme for turbulent flows. *Physics of Fluids*, A 5(6):1282–1284, June 1993.

[27] M. Germano. A proposal for a redefinition of the turbulent stresses in the filtered Navier-Stokes equations. *Physics of Fluids*, 29(7):2323–2324, July 1986.

[28] M. Germano. Turbulence: the filtering approach. *Journal of Fluid Mechanics*, 238:325–336, May 1992.

[29] M. Germano, U. Piomelli, P. Moin, and W.H. Cabot. A dynamic subgrid-scale eddy viscosity model. *Physics of Fluids*, A 3(7):1760–1765, July 1991.

[30] S. Ghosal, T.S. Lund, P. Moin, and K. Akselvoll. A dynamic localization model for large-eddy simulation of turbulent flows. *Journal of Fluid Mechanics*, 286:229–255, 1995.

[31] J.O. Hirschfelder, C.F. Curtiss, and R.B. Bird. *Molecular Theory of Gases and Liquids.* Wiley & Sons, 1954.

[32] M. Ihme and H. Pitsch. LES of a non-premixed flame using an extended flamelet/progress variable model. In *Proceedings of the 43rd AIAA Aerospace Sciences Meeting and Exhibit.* AIAA, January 2005.

[33] Clay Mathematics Institute. *www.claymath.org/millenium.*

[34] J. Jiménez, A. Liñán, M.M. Rogers, and F.J. Higuera. *A priori* testing of subgrid models for chemically reacting non-premixed turbulent shear flows. *Journal of Fluid Mechanics*, 349:149–171, 1997.

[35] W.P. Jones and S. Navarro-Martinez. Large eddy simulation of autoignition with a subgrid probability density function method. *Combustion and Flame*, 150:170–187, June 2007.

[36] A. Kempf, R.P. Lindstedt, and J. Janicka. Large-eddy simulation of a bluff body stabilized nonpremixed flame. *Combustion and Flame, in press*, July 2005.

[37] J. Kim and P. Moin. Application of a fractional-step method to incompressible navier-stokes equations. *Journal of Computational Physics*, pages 308–323, 1985.

[38] S.H. Kim. On the conditional variance and covariance equations for second-order conditional moment closure. *Physics of Fluids*, 14(6):2011–2014, 2002.

[39] S.H. Kim, C.H. Choi, and K.Y. Huh. Second-order conditional moment closure modeling of a turbulent $CH_4/H_2/N_2$ jet diffusion flame. *Proceedings of the Combustion Institute*, 30(1):735–742, 2005.

[40] S.H. Kim and K.Y. Huh. Second-order conditional moment closure modeling of turbulent piloted jet diffusion flames. *Combustion and Flame*, 138(4):336–352, 2004.

[41] S.H. Kim, K.Y. Huh, and R.W. Bilger. Second order conditional moment closure modeling of extinction and reignition in turbulent non-premixed hydrocarbon flames. *Proceedings of the Combustion Institute*, 29(2):2131–2137, 2002.

[42] M. Klein, A. Sadiki, and J. Janicka. A digital filter based generation of inflow data for spatially developing direct numerical of large eddy simulation. *Journal of Computational Physics*, 186:652–665, 2003.

[43] A.Y. Klimenko. Multicomponent diffusion of various admixtures in turbulent flows. *Fluid Dynamics*, 25(3):327–334, May 1990.

[44] A.Y. Klimenko and R.W. Bilger. Conditional moment closure for turbulent combustion. *Progress in Energy and Combustion Science*, 25, 1999.

[45] A. Kronenburg. Double conditioning of reactive scalar transport equations in turbulent nonpremixed flames. *Physics of Fluids*, 16(7), July 2004.

[46] A. Kronenburg, R.W. Bilger, and J.H. Kent. Second-order conditional moment closure for turbulent jet diffusion flames. *Proceedings of the Combustion Institute*, 27(1):1097–1104, 1998.

[47] A. Kronenburg and M. Kostka. Modeling extinction and reignition in turbulent flames. *Combustion and Flame*, 143(4):342–356, December 2005.

[48] A. Kronenburg and A.E. Papoutsakis. Conditional moment closure modelling of extinctionand re-ignition in turbulent non-premixed flames. *Proceedings of the Combustion Institute*, 30, 2004.

[49] A. Leonard. Energy cascade in large eddy simulation of turbulent fluid flow. *Advances in Geophysics*, 18A:237–248, 1974.

[50] J.D. Li and R.W. Bilger. Measurements and prediction of the conditional variance in a turbulent reactive-scalar mixing layer. *Physics of Fluids*, A 5:3255–3264, 1993.

[51] D.K. Lilly. A proposed modification of the germano subgrid-scale closure method. *Physics of Fluids*, A 4(3):633–635, March 1992.

[52] E. Mastorakos and R.W. Bilger. Second-order conditional moment closure for the autoignition of turbulent flows. *Physics of Fluids*, 10(6):1246–1248, June 1998.

[53] M. Meyer. *The application of detailed and systematically reduced chemistry to transient laminar flames.* PhD thesis, Imperial College London, 2001.

[54] P. Moin, K. Squires, W. Cabot, and S. Lee. A dynamic subgrid-scale model for compressible turbulence and scalar transport. *Physics of Fluids*, A 3(11):2746–2757, November 1991.

[55] S. Navarro-Martinez, A. Kronenburg, and F. di Mare. Conditional moment closure for large eddy simulation. *Flow, Turbulence and Combustion*, **75**(1-4):245 – 274, December 2005.

[56] N. Peters. Laminar diffusion flamelet models in non-premixed turbulent combustion. *Progress in Energy and Combustion Science*, 10:319–339, 1984.

[57] N. Peters. *Turbulent Combustion*. Cambridge University Press, 2000.

[58] C.D. Pierce and P. Moin. A dynamic model for subgrid-scale variance and dissipation rate of a conserved scalar. *Physics of Fluids*, 10(12):3041–3044, December 1998.

[59] C.D. Pierce and P. Moin. Method for generating equilibrium swirliing inflow conditions. *AIAA Journal*, 36(7):1325–1327, July 1998.

[60] C.D. Pierce and P. Moin. Progress-variable approach for large-eddy simulation of non-premixed turbulent combustion. *Journal of Fluid Mechanics*, 504:73–97, 2004.

[61] U. Piomelli and J. Liu. Large-eddy simulation of rotating channel flows using a localized dynamic model. *Physics of Fluids*, **7**(4):839–848, April 1995.

[62] H. Pitsch. Improved Pollutant Predictions in Large-Eddy Simulations of Turbulent Non-Premixed Combustion by Considering Scalar Dissipation Rate Fluctuations. *Proceedings of the Combustion Institute*, 29:1971–1978, 2002.

[63] H. Pitsch. Large-eddy simulation of turbulent combustion. *Annual Review of Fluid Mechanics*, 38:453–482, 2006.

[64] H. Pitsch and M. Ihme. An unsteady flamelet/progress variable model for LES of nonpremixed turbulent combustion. In *Proceedings of the 43rd AIAA Aerospace Sciences Meeting and Exhibit*. AIAA, January 2005.

[65] H. Pitsch and H. Steiner. Large-eddy simulation of a turbulent piloted methane/air diffusion flame (Sandia flame D). *Physics of Fluids*, 12(10):2541–2554, October 2000.

[66] S.B. Pope. *Turbulent Flows*. Cambridge University Press, 2000.

[67] V. Raman and H. Pitsch. A consistent LES/filtered-density function formulation for the simulation of turbulent flames with detailed chemistry. *Proceedings of the Combustion Institute*, 31:1711–1719, 2007.

[68] V. Raman, H. Pitsch, and R.O. Fox. Eulerian transported probability density function sub-filter model for large eddy simulations of turbulent combustion. *Combustion Theory Modelling*, 10(3):439–458, June 2006.

[69] J. Smagorinsky. General circulation experiments with the primitive equations. *Monthly Weather Review*, 91(3):99–164, March 1963.

[70] H. Steiner and W.K. Bushe. Large eddy simulation of a turbulent reacting jet with conditional source-term estimation. *Physics of Fluids*, **13**(3):754–769, March 2001.

[71] G. Strang. On the construction and comparison of difference schemes. *SIAM Journal on Numerical Analysis*, 5(3):506–517, September 1968.

[72] N. Swaminathan and R.W. Bilger. Conditional variance equation and its analysis. *Proceedings of the Combustion Institute*, 27(1):1191–1198, 1998.

[73] N. Swaminathan and R.W. Bilger. Study of the conditional covariance and variance equations for second order conditional moment closure. *Physics of Fluids*, 11(9):2679–2695, September 1999.

[74] N. Swaminathan and K.N.C. Bray. Effect of dilatation on scalar dissipation in turbulent premixed flames. *Combustion and Flame*, 143:549–565, October 2005.

[75] N. Swaminathan and R.W. Grout. Interaction of turbulence and scalar fields in premixed flames. *Physics of Fluids*, 18:045102, 2006.

[76] Q. Tang, J. Xu, and S.B. Pope. Probability density function calculations of local extinction and no production in piloted-jet turbulent methane/air flames. *Proceedings of the Combustion Institute*, 28:133–139, 2000.

[77] L. Valiño. A field monte carlo formulation for calculating the probability density function of a single scalar in a turbulent flow. *Flow, Turbulence and Combustion*, 60:157–172, 1998.

[78] L. Vervisch, R. Hauguel, P. Domingo, and M. Rullaud. Three facets of turbulent combustion modelling: DNS of premixed V-Flame, LES of lifted nonpremixed flame and RANS of jet-flame. *Journal of Turbulence*, 5(4), January 2004.

[79] C.R. Wilke. A viscosity equation for gas mixtures. *Journal of Chemical Physics*, 18(4):517–519, April 1950.

[80] F.A. Williams. *Combustion Theory.* Benjamin Cummings, 1985.

[81] J. Xu and S.B. Pope. Pdf calculations of turbulent nonpremixed flames with local extinction. *Combustion and Flame*, 123(3):281–307, November 2000.

[82] N.N. Yanenko. *The Method of Fractional Steps.* Springer, 1971.

Appendix **A**

# The Relation between density weighted and non-density weighted p.d.f.

Given the definitions of a conditional filtering procedure, equation (4.8), the common definition of Favre or density weighted filtering of a quantity $\phi$, as introduced by Favre [23]:

$$\bar{\rho}\,\widetilde{\phi} = \overline{\rho\,\phi}, \tag{A.1}$$

where the tilde denotes Favre filtering and the overbar denotes non-density weighted filtering, it is shown that the following relation must hold to ensure consistency between the two forms of the p.d.f. and to ensure the normalization condition for both; a fundamental, mathematical characteristic of any p.d.f..

$$\frac{1}{\bar{\rho}} = \int \frac{1}{\overline{\rho \mid \eta}}\,\widetilde{P}(\eta)d\eta. \tag{A.2}$$

The definition of the conditional filter, applied to the density yields:

$$\overline{\rho \mid \eta}\,P(\eta, \mathbf{x}, t) = \int \rho\,\psi[\eta - \phi(\mathbf{x}', t)]\,G(\mathbf{x} - \mathbf{x}')d\mathbf{x}'. \tag{A.3}$$

Considering the r.h.s. of equation (A.1), the following relation must hold:

$$\overline{\rho\,P} = \int \rho\,\psi[\eta - \phi(\mathbf{x}', t)]\,G(\mathbf{x} - \mathbf{x}')d\mathbf{x}'. \tag{A.4}$$

Since the r.h.s. of equations (A.3) and (A.4) are identical, equating these yields:

$$\overline{\rho\, P} = \overline{\rho \mid \eta}\, P(\eta). \tag{A.5}$$

Substituting the definition of Favre filtering, equation (A.5) leads to:

$$\bar{\rho}\, \widetilde{P}(\eta) = \overline{\rho \mid \eta}\, P(\eta), \tag{A.6}$$

which can be rearranged to

$$P(\eta) = \frac{\bar{\rho}\, \widetilde{P}(\eta)}{\overline{\rho \mid \eta}}. \tag{A.7}$$

Invoking the normalization condition yields:

$$\int P(\eta) d\eta \stackrel{!}{=} 1 = \int \frac{\bar{\rho}}{\overline{\rho \mid \eta}} \widetilde{P}(\eta)\, d\eta. \tag{A.8}$$

Since the unconditional density $\bar{\rho}$ is not a function of $\eta$ it can be moved outside of the integral.

$$1 = \bar{\rho} \int \frac{1}{\overline{\rho \mid \eta}}\, \widetilde{P}(\eta)\, d\eta \tag{A.9}$$

$$\Leftrightarrow \frac{1}{\bar{\rho}} = \int \frac{1}{\overline{\rho \mid \eta}}\, \widetilde{P}(\eta)\, d\eta.$$

Appendix B

# Chemical mechanism

For reference, the parameters of the chemical mechanism proposed by Meyer [53], which was used for the presented work, is given below.

Tabulated are the constants in the expression $k = BT^n\ e^{-\frac{E}{RT}}$ for the individual reaction rate constant.

Table B.1: Chemical mechanism used, for details see Meyer [53].

| No | Reaction | | | B | n | E [kJ/mole] |
|---|---|---|---|---|---|---|
| 1 | $H + O_2$ | $\rightleftharpoons$ | $OH + O$ | 2.000E+11 | 0.00 | 70.30 |
| 2 | $O + H_2$ | $\rightleftharpoons$ | $OH + H$ | 5.120E+01 | 2.67 | 26.30 |
| 3 | $OH + H_2$ | $\rightleftharpoons$ | $H_2O + H$ | 1.000E+05 | 1.60 | 13.80 |
| 4 | $OH + OH$ | $\rightleftharpoons$ | $H_2O + O$ | 3.570E+01 | 2.40 | -8.84 |
| 5 | $O_2 + H + M$ | $\rightleftharpoons$ | $HO_2 + M$ | 2.300E+12 | -0.80 | 0.00 |
| 6 | $HO_2 + H$ | $\rightleftharpoons$ | $OH + OH$ | 1.680E+11 | 0.00 | 3.66 |
| 7 | $HO_2 + H$ | $\rightleftharpoons$ | $H_2 + O_2$ | 4.270E+10 | 0.00 | 5.90 |
| 8 | $HO_2 + OH$ | $\rightleftharpoons$ | $H_2O + O_2$ | 2.890E+10 | 0.00 | -2.08 |
| 9 | $HO_2 + H$ | $\rightleftharpoons$ | $H_2O + O$ | 3.000E+10 | 0.00 | 7.20 |
| 10 | $HO_2 + O$ | $\rightleftharpoons$ | $OH + O_2$ | 3.190E+10 | 0.00 | 0.00 |
| 11 | $H + H + M$ | $\rightleftharpoons$ | $H_2 + M$ | 6.530E+11 | -1.00 | 0.00 |
| 12 | $H + H + M$ | $\rightleftharpoons$ | $H_2 + M$ | 9.200E+10 | -0.60 | 0.00 |
| 13 | $H + H + M$ | $\rightleftharpoons$ | $H_2 + M$ | 6.000E+13 | -1.25 | 0.00 |

Table B.1: continued

| No | Reaction | | | B | n | E [kJ/mole] |
|---|---|---|---|---|---|---|
| 14 | $H + H + M$ | $\rightleftharpoons$ | $H_2 + M$ | 5.490E+14 | -2.00 | 0.00 |
| 15 | $H + OH + M$ | $\rightleftharpoons$ | $H_2O + M$ | 2.200E+16 | -2.00 | 0.00 |
| 16 | $O + O + M$ | $\rightleftharpoons$ | $O_2 + M$ | 1.000E+11 | -1.00 | 0.00 |
| 17 | $CO + OH$ | $\rightleftharpoons$ | $CO_2 + H$ | 4.400E+03 | 1.50 | -3.10 |
| 18 | $CO + HO_2$ | $\rightleftharpoons$ | $CO_2 + OH$ | 1.500E+11 | 0.00 | 98.93 |
| 19 | $CO + O + M$ | $\rightleftharpoons$ | $CO_2 + M$ | 5.300E+07 | 0.00 | -19.01 |
| 20 | $CO + O_2$ | $\rightleftharpoons$ | $CO_2 + O$ | 2.500E+09 | 0.00 | 200.00 |
| 21 | $CH + O_2$ | $\rightleftharpoons$ | $CHO + O$ | 7.500E+10 | 0.00 | 0.00 |
| 22 | $CH + CO_2$ | $\rightleftharpoons$ | $CHO + CO$ | 3.400E+09 | 0.00 | 2.90 |
| 23 | $CH + O$ | $\rightleftharpoons$ | $CO + H$ | 4.000E+10 | 0.00 | 0.00 |
| 24 | $CH + OH$ | $\rightleftharpoons$ | $CHO + H$ | 3.000E+10 | 0.00 | 0.00 |
| 25 | $CH + H_2O$ | $\rightleftharpoons$ | $CH_2OH$ | 5.730E+09 | 0.00 | -3.16 |
| 26 | $CH + CH_2O$ | $\rightleftharpoons$ | $C_2H_2O + H$ | 9.460E+10 | 0.00 | -2.16 |
| 27 | $CH + CH_2(T)$ | $\rightleftharpoons$ | $C_2H_2 + H$ | 4.000E+10 | 0.00 | 0.00 |
| 28 | $CH + CH_3$ | $\rightleftharpoons$ | $C_2H_3 + H$ | 3.000E+10 | 0.00 | 0.00 |
| 29 | $CH + CH_4$ | $\rightleftharpoons$ | $C_2H_4 + H$ | 6.000E+10 | 0.00 | 0.00 |
| 30 | $CHO + H$ | $\rightleftharpoons$ | $CO + H_2$ | 9.000E+10 | 0.00 | 0.00 |
| 31 | $CHO + O$ | $\rightleftharpoons$ | $CO + OH$ | 3.000E+10 | 0.00 | 0.00 |
| 32 | $CHO + O$ | $\rightleftharpoons$ | $CO_2 + H$ | 3.000E+10 | 0.00 | 0.00 |
| 33 | $CHO + OH$ | $\rightleftharpoons$ | $CO + H_2O$ | 1.000E+11 | 0.00 | 0.00 |
| 34 | $CHO + O_2$ | $\rightleftharpoons$ | $CO + HO_2$ | 4.520E+14 | -1.85 | 1.47 |
| 35 | $CHO + M$ | $\rightleftharpoons$ | $CO + H + M$ | 1.860E+14 | -1.00 | 71.10 |
| 36 | $CH_2(S) + H_2$ | $\rightleftharpoons$ | $CH_3 + H$ | 7.230E+10 | 0.00 | 0.00 |
| 37 | $CH_2(S) + H$ | $\rightleftharpoons$ | $CH + H_2$ | 7.000E+10 | 0.00 | 0.00 |
| 38 | $CH_2(S) + O$ | $\rightleftharpoons$ | $CO + H + H$ | 1.500E+10 | 0.00 | 0.00 |
| 39 | $CH_2(S) + O$ | $\rightleftharpoons$ | $CO + H_2$ | 1.500E+10 | 0.00 | 0.00 |
| 40 | $CH_2(S) + OH$ | $\rightleftharpoons$ | $CH_2O + H$ | 3.000E+10 | 0.00 | 0.00 |
| 41 | $CH_2(S) + O_2$ | $\rightleftharpoons$ | $CO + OH + H$ | 3.000E+10 | 0.00 | 0.00 |
| 42 | $CH_2(S) + CO_2$ | $\rightleftharpoons$ | $CH_2O + CO$ | 3.000E+09 | 0.00 | 0.00 |
| 43 | $CH_2(S) + CH_3$ | $\rightleftharpoons$ | $C_2H_4 + H$ | 1.800E+10 | 0.00 | 0.00 |
| 44 | $CH_2(S) + CH_4$ | $\rightleftharpoons$ | $CH_3 + CH_3$ | 4.270E+10 | 0.00 | 0.00 |

Table B.1: continued

| No | Reaction | | | B | n | E [kJ/mole] |
|---|---|---|---|---|---|---|
| 45 | $CH_2(S) + M$ | $\rightleftharpoons$ | $CH_2(T) + M$ | 1.000E+10 | 0.00 | 0.00 |
| 46 | $CH_2(T) + H_2$ | $\rightleftharpoons$ | $CH_3 + H$ | 3.000E+06 | 0.00 | 0.00 |
| 47 | $CH_2(T) + H$ | $\rightleftharpoons$ | $CH + H_2$ | 1.100E+11 | 0.00 | 0.00 |
| 48 | $CH_2(T) + O$ | $\rightleftharpoons$ | $CO + H + H$ | 4.880E+10 | 0.00 | 0.00 |
| 49 | $CH_2(T) + O$ | $\rightleftharpoons$ | $CO + H_2$ | 3.250E+10 | 0.00 | 0.00 |
| 50 | $CH_2(T) + OH$ | $\rightleftharpoons$ | $CH + H_2O$ | 1.130E+04 | 2.00 | 12.56 |
| 51 | $CH_2(T) + OH$ | $\rightleftharpoons$ | $CH_2O + H$ | 2.500E+10 | 0.00 | 0.00 |
| 52 | $CH_2(T) + O_2$ | $\rightleftharpoons$ | $CO + H + OH$ | 1.642E+18 | -3.30 | 12.00 |
| 53 | $CH_2(T) + O_2$ | $\rightleftharpoons$ | $CO_2 + H + H$ | 3.285E+18 | -3.30 | 12.00 |
| 54 | $CH_2(T) + O_2$ | $\rightleftharpoons$ | $CH_2O + O$ | 3.285E+18 | -3.30 | 12.00 |
| 55 | $CH_2(T) + O_2$ | $\rightleftharpoons$ | $CO_2 + H_2$ | 2.630E+18 | -3.30 | 12.00 |
| 56 | $CH_2(T) + O_2$ | $\rightleftharpoons$ | $CO + H_2O$ | 2.240E+19 | -3.30 | 12.00 |
| 57 | $CH_2(T) + CO_2$ | $\rightleftharpoons$ | $CH_2O + CO$ | 1.100E+08 | 0.00 | 4.19 |
| 58 | $CH_2(T) + CH_2(T)$ | $\rightleftharpoons$ | $C_2H_2 + H + H$ | 1.200E+11 | 0.00 | 3.32 |
| 59 | $CH_2(T) + CH_3$ | $\rightleftharpoons$ | $C_2H_4 + H$ | 4.000E+10 | 0.00 | 0.00 |
| 60 | $CH_2O + H$ | $\rightleftharpoons$ | $CHO + H_2$ | 2.180E+05 | 1.77 | 12.55 |
| 61 | $CH_2O + O$ | $\rightleftharpoons$ | $CHO + OH$ | 4.150E+08 | 0.57 | 11.56 |
| 62 | $CH_2O + OH$ | $\rightleftharpoons$ | $CHO + H_2O$ | 1.130E+06 | 1.18 | -1.87 |
| 63 | $CH_2O + O_2$ | $\rightleftharpoons$ | $CHO + HO_2$ | 6.000E+10 | 0.00 | 170.00 |
| 64 | $CH_2O + CH_3$ | $\rightleftharpoons$ | $CHO + CH_4$ | 4.090E+09 | 0.00 | 37.00 |
| 65 | $CH_3 + CH_3$ | $\rightleftharpoons$ | $C_2H_5 + H$ | 5.000E+09 | 0.10 | 44.36 |
| 66 | $CH_3 + CH_3$ | $\rightleftharpoons$ | $C_2H_6$ | 3.600E+10 | 0.00 | 0.00 |
| 67 | $CH_3 + O$ | $\rightleftharpoons$ | $CH_2O + H$ | 8.430E+10 | 0.00 | 0.00 |
| 68 | $CH_3 + OH$ | $\rightleftharpoons$ | $CH_2OH + H$ | 1.500E+11 | 0.00 | 34.46 |
| 69 | $CH_3 + OH$ | $\rightleftharpoons$ | $CH_2(S) + H_2O$ | 4.000E+10 | 0.00 | 10.47 |
| 70 | $CH_3 + OH$ | $\rightleftharpoons$ | $CH_2O + H_2$ | 1.024E+09 | 0.00 | 0.00 |
| 71 | $CH_3 + OH$ | $\rightleftharpoons$ | $CH_3O + H$ | 5.740E+09 | -0.23 | 58.28 |
| 72 | $CH_3 + O_2$ | $\rightleftharpoons$ | $CH_3O + O$ | 1.320E+11 | 0.00 | 131.36 |
| 73 | $CH_3 + O_2$ | $\rightleftharpoons$ | $CH_2O + OH$ | 3.300E+08 | 0.00 | 37.40 |
| 74 | $CH_3 + HO_2$ | $\rightleftharpoons$ | $CH_3O + OH$ | 1.800E+10 | 0.00 | 0.00 |
| 75 | $CH_3 + CHO$ | $\rightleftharpoons$ | $CH_4 + CO$ | 1.200E+11 | 0.00 | 0.00 |

Table B.1: continued

| No | Reaction | | | B | n | E [kJ/mole] |
|---|---|---|---|---|---|---|
| 76 | $CH_3O + M$ | $\rightleftharpoons$ | $CH_2OH + M$ | 3.010E+08 | 0.00 | 17.04 |
| 77 | $CH_3O + H$ | $\rightleftharpoons$ | $CH_2O + H_2$ | 2.000E+10 | 0.00 | 0.00 |
| 78 | $CH_3O + O$ | $\rightleftharpoons$ | $CH_2O + OH$ | 6.000E+09 | 0.00 | 0.00 |
| 79 | $CH_3O + OH$ | $\rightleftharpoons$ | $CH_2O + H_2O$ | 1.800E+10 | 0.00 | 0.00 |
| 80 | $CH_3O + O_2$ | $\rightleftharpoons$ | $CH_2O + HO_2$ | 6.600E+07 | 0.00 | 10.88 |
| 81 | $CH_3O + M$ | $\rightleftharpoons$ | $CH_2O + H + M$ | 5.450E+10 | 0.00 | 56.50 |
| 82 | $CH_2OH + H$ | $\rightleftharpoons$ | $CH_2O + H_2$ | 3.000E+10 | 0.00 | 0.00 |
| 83 | $CH_2OH + O$ | $\rightleftharpoons$ | $CH_2O + OH$ | 4.220E+10 | 0.00 | 0.00 |
| 84 | $CH_2OH + OH$ | $\rightleftharpoons$ | $CH_2O + H_2O$ | 2.400E+10 | 0.00 | 0.00 |
| 85 | $CH_2OH + O_2$ | $\rightleftharpoons$ | $CH_2O + HO_2$ | 1.000E+11 | 0.00 | 21.00 |
| 86 | $CH_2OH + M$ | $\rightleftharpoons$ | $CH_2O + H + M$ | 1.220E+25 | -4.00 | 133.42 |
| 87 | $CH_3 + H$ | $\rightleftharpoons$ | $CH_4$ | 2.100E+11 | 0.00 | 0.00 |
| 88 | $CH_4 + H$ | $\rightleftharpoons$ | $CH_3 + H_2$ | 3.860E+03 | 2.11 | 32.42 |
| 89 | $CH_4 + O$ | $\rightleftharpoons$ | $CH_3 + OH$ | 9.033E+05 | 1.56 | 35.50 |
| 90 | $CH_4 + OH$ | $\rightleftharpoons$ | $CH_3 + H_2O$ | 1.560E+04 | 1.83 | 11.60 |
| 91 | $C_2H + H_2$ | $\rightleftharpoons$ | $C_2H_2 + H$ | 5.670E+07 | 0.90 | 8.34 |
| 92 | $C_2H + O$ | $\rightleftharpoons$ | $CO + CH$ | 1.000E+10 | 0.00 | 0.00 |
| 93 | $C_2H + OH$ | $\rightleftharpoons$ | $C_2HO + H$ | 2.000E+10 | 0.00 | 0.00 |
| 94 | $C_2H + O_2$ | $\rightleftharpoons$ | $CO + CO + H$ | 9.040E+09 | 0.00 | -1.91 |
| 95 | $C_2H + H_2O$ | $\rightleftharpoons$ | $C_2H_2O + H$ | 1.140E+10 | 0.00 | 1.66 |
| 96 | $C_2HO + H$ | $\rightleftharpoons$ | $CH_2(S) + CO$ | 1.000E+11 | 0.00 | 0.00 |
| 97 | $C_2HO + O$ | $\rightleftharpoons$ | $CO + CO + H$ | 9.635E+10 | 0.00 | 0.00 |
| 98 | $C_2HO + O_2$ | $\rightleftharpoons$ | $CO + CO + OH$ | 1.000E+10 | 0.00 | 0.00 |
| 99 | $C_2HO + O_2$ | $\rightleftharpoons$ | $CO_2 + CO + H$ | 1.000E+10 | 0.00 | 0.00 |
| 100 | $C_2H_2 + O$ | $\rightleftharpoons$ | $CH_2(T) + CO$ | 2.893E+03 | 2.09 | 6.54 |
| 101 | $C_2H_2 + O$ | $\rightleftharpoons$ | $C_2HO + H$ | 4.340E+03 | 2.09 | 6.54 |
| 102 | $C_2H_2 + OH$ | $\rightleftharpoons$ | $C_2H + H_2O$ | 3.370E+04 | 2.00 | 58.58 |
| 103 | $C_2H_2 + OH$ | $\rightleftharpoons$ | $C_2H_2O + H$ | 3.750E+03 | 1.70 | 4.18 |
| 104 | $C_2H_2 + O_2$ | $\rightleftharpoons$ | $C_2HO + OH$ | 2.000E+05 | 1.50 | 126.00 |
| 105 | $CH_2(T) + CO$ | $\rightleftharpoons$ | $C_2H_2O$ | 0.000E+00 | 0.00 | 0.00 |
| 106 | $C_2H_2O + H$ | $\rightleftharpoons$ | $CH_3 + CO$ | 1.110E+04 | 2.00 | 8.37 |

Table B.1: continued

| No | Reaction | | | B | n | E [kJ/mole] |
|---|---|---|---|---|---|---|
| 107 | $C_2H_2O + H$ | $\rightleftharpoons$ | $C_2HO + H_2$ | 1.800E+11 | 0.00 | 35.98 |
| 108 | $C_2H_2O + O$ | $\rightleftharpoons$ | $CO_2 + CH_2(T)$ | 2.000E+10 | 0.00 | 9.60 |
| 109 | $C_2H_2O + O$ | $\rightleftharpoons$ | $C_2HO + OH$ | 2.000E+04 | 2.00 | 41.69 |
| 110 | $C_2H_2O + OH$ | $\rightleftharpoons$ | $CH_2OH + CO$ | 1.020E+10 | 0.00 | 0.00 |
| 111 | $C_2H_2O + OH$ | $\rightleftharpoons$ | $C_2HO + H_2O$ | 1.000E+04 | 2.00 | 12.56 |
| 112 | $C_2H_3$ | $\rightleftharpoons$ | $C_2H_2 + H$ | 2.000E+14 | 0.00 | 166.28 |
| 113 | $C_2H_3 + H$ | $\rightleftharpoons$ | $C_2H_2 + H_2$ | 3.000E+10 | 0.00 | 0.00 |
| 114 | $C_2H_3 + O$ | $\rightleftharpoons$ | $C_2H_2O + H$ | 3.000E+10 | 0.00 | 0.00 |
| 115 | $C_2H_3 + OH$ | $\rightleftharpoons$ | $C_2H_2 + H_2O$ | 2.000E+10 | 0.00 | 0.00 |
| 116 | $C_2H_3 + O_2$ | $\rightleftharpoons$ | $CHO + CH_2O$ | 3.360E+09 | 0.00 | -1.00 |
| 117 | $C_2H_3 + O_2$ | $\rightleftharpoons$ | $C_2H_2 + HO_2$ | 1.500E+08 | 0.00 | -1.00 |
| 118 | $C_2H_4 + H$ | $\rightleftharpoons$ | $C_2H_3 + H_2$ | 1.325E+03 | 2.53 | 51.21 |
| 119 | $C_2H_4 + O$ | $\rightleftharpoons$ | $CH_3 + CHO$ | 1.320E+05 | 1.55 | 1.79 |
| 120 | $C_2H_4 + OH$ | $\rightleftharpoons$ | $C_2H_3 + H_2O$ | 1.570E+01 | 2.75 | 17.46 |
| 121 | $C_2H_5 + O_2$ | $\rightleftharpoons$ | $C_2H_4 + HO_2$ | 1.020E+07 | 0.00 | -9.14 |
| 122 | $C_2H_5 + O$ | $\rightleftharpoons$ | $CH_3 + CH_2O$ | 6.600E+10 | 0.00 | 0.00 |
| 123 | $C_2H_4 + H$ | $\rightleftharpoons$ | $C_2H_5$ | 3.974E+06 | 1.28 | 5.40 |
| 124 | $C_2H_6$ | $\rightleftharpoons$ | $C_2H_5 + H$ | 8.850E+20 | -1.23 | 427.70 |
| 125 | $C_2H_6 + H$ | $\rightleftharpoons$ | $C_2H_5 + H_2$ | 1.445E+06 | 1.50 | 31.00 |
| 126 | $C_2H_6 + O$ | $\rightleftharpoons$ | $C_2H_5 + OH$ | 1.000E+06 | 1.50 | 24.30 |
| 127 | $C_2H_6 + OH$ | $\rightleftharpoons$ | $C_2H_5 + H_2O$ | 7.226E+03 | 2.00 | 3.62 |
| 128 | $CH_2(T) + M$ | $\rightleftharpoons$ | $C1 + H_2 + M$ | 1.148E+11 | 0.00 | 233.70 |
| 129 | $CH + M$ | $\rightleftharpoons$ | $C1 + H + M$ | 1.000E+11 | 0.00 | 267.95 |
| 130 | $CH + H$ | $\rightleftharpoons$ | $C1 + H_2$ | 3.000E+10 | 0.00 | 0.00 |
| 131 | $CH + OH$ | $\rightleftharpoons$ | $C1 + H_2O$ | 4.000E+04 | 2.00 | 12.55 |
| 132 | $C1 + OH$ | $\rightleftharpoons$ | $CO + H$ | 5.000E+10 | 0.00 | 0.00 |
| 133 | $C1 + O_2$ | $\rightleftharpoons$ | $CO + O$ | 1.200E+11 | 0.00 | 16.71 |
| 134 | $C1 + CO_2$ | $\rightleftharpoons$ | $CO + CO$ | 0.000E+00 | 0.00 | 0.00 |
| 135 | $C1 + CH_3$ | $\rightleftharpoons$ | $C_2H_2 + H$ | 5.000E+10 | 0.00 | 0.00 |
| 136 | $C1 + CH_2(T)$ | $\rightleftharpoons$ | $C_2H + H$ | 5.000E+10 | 0.00 | 0.00 |
| 137 | $C_2H + C_2H$ | $\rightleftharpoons$ | $C_2H_2 + C_2$ | 1.810E+09 | 0.00 | 0.00 |

Table B.1: continued

| No | Reaction | | | B | n | E [kJ/mole] |
|---|---|---|---|---|---|---|
| 138 | $C_2H + H$ | $\rightleftharpoons$ | $C_2 + H_2$ | 3.610E+10 | 0.00 | 118.25 |
| 139 | $C1 + C1 + M$ | $\rightleftharpoons$ | $C_2 + M$ | 1.800E+15 | -1.60 | 0.00 |
| 140 | $C_2 + O$ | $\rightleftharpoons$ | $CO + C1$ | 3.610E+11 | 0.00 | 0.00 |
| 141 | $C_2 + O_2$ | $\rightleftharpoons$ | $CO + CO$ | 8.970E+09 | 0.00 | 4.10 |
| 142 | $NH_3 + M$ | $\rightleftharpoons$ | $NH_2 + H + M$ | 1.400E+13 | 0.06 | 379.07 |
| 143 | $NH_3 + H$ | $\rightleftharpoons$ | $NH_2 + H_2$ | 6.360E+02 | 2.39 | 42.56 |
| 144 | $NH_3 + OH$ | $\rightleftharpoons$ | $NH_2 + H_2O$ | 2.040E+03 | 2.04 | 2.37 |
| 145 | $NH_3 + O$ | $\rightleftharpoons$ | $NH_2 + OH$ | 2.100E+10 | 0.00 | 37.66 |
| 146 | $NH_2 + H$ | $\rightleftharpoons$ | $NH + H_2$ | 5.670E+08 | 0.59 | 15.26 |
| 147 | $NH_2 + OH$ | $\rightleftharpoons$ | $NH + H_2O$ | 9.000E+04 | 1.50 | -1.91 |
| 148 | $NH_2 + O$ | $\rightleftharpoons$ | $NH + OH$ | 7.000E+09 | 0.00 | 0.00 |
| 149 | $NH_2 + O$ | $\rightleftharpoons$ | $HNO + H$ | 9.900E+11 | -0.50 | 0.00 |
| 150 | $NH_2 + O$ | $\rightleftharpoons$ | $NO + H_2$ | 5.000E+09 | 0.00 | 0.00 |
| 151 | $NH_2 + N$ | $\rightleftharpoons$ | $N_2 + H + H$ | 7.200E+10 | 0.00 | 0.00 |
| 152 | $NH_2 + NO$ | $\rightleftharpoons$ | $N_2 + H_2O$ | 3.000E+17 | -2.60 | 3.87 |
| 153 | $NH_2 + NO$ | $\rightleftharpoons$ | $NNH + OH$ | 1.395E+09 | 0.00 | 0.00 |
| 154 | $NH_2 + NO$ | $\rightleftharpoons$ | $N_2O + H_2$ | 5.000E+10 | 0.00 | 102.43 |
| 155 | $NH_2 + O_2$ | $\rightleftharpoons$ | $HNO + OH$ | 1.510E+09 | -0.39 | 151.04 |
| 156 | $NH_2 + O_2$ | $\rightleftharpoons$ | $NH + HO_2$ | 1.000E+11 | 0.00 | 209.19 |
| 157 | $NH_2 + HO_2$ | $\rightleftharpoons$ | $NH_3 + O_2$ | 4.520E+10 | 0.00 | 0.00 |
| 158 | $NH_2 + NH$ | $\rightleftharpoons$ | $N_2H_2 + H$ | 1.000E+12 | -0.50 | 0.00 |
| 159 | $NH_2 + NH_2$ | $\rightleftharpoons$ | $N_2H_2 + H_2$ | 4.000E+10 | 0.00 | 49.55 |
| 160 | $NH_2 + NH_2$ | $\rightleftharpoons$ | $NH + NH_3$ | 5.000E+10 | 0.00 | 41.57 |
| 161 | $NH + H$ | $\rightleftharpoons$ | $N + H_2$ | 1.000E+10 | 0.00 | 0.00 |
| 162 | $NH + O$ | $\rightleftharpoons$ | $NO + H$ | 7.000E+10 | 0.00 | 0.00 |
| 163 | $NH + O$ | $\rightleftharpoons$ | $N + OH$ | 7.000E+09 | 0.00 | 0.00 |
| 164 | $NH + OH$ | $\rightleftharpoons$ | $N + H_2O$ | 2.000E+06 | 1.20 | 0.03 |
| 165 | $NH + OH$ | $\rightleftharpoons$ | $HNO + H$ | 4.000E+10 | 0.00 | 0.00 |
| 166 | $NH + O_2$ | $\rightleftharpoons$ | $NO + OH$ | 1.000E+10 | -0.20 | 20.04 |
| 167 | $NH + O_2$ | $\rightleftharpoons$ | $HNO + O$ | 4.610E+02 | 2.00 | 27.20 |
| 168 | $NH + N$ | $\rightleftharpoons$ | $N_2 + H$ | 3.000E+10 | 0.00 | 0.00 |

Table B.1: continued

| No | Reaction | | | B | n | E [kJ/mole] |
|---|---|---|---|---|---|---|
| 169 | $NH + NO$ | $\rightleftharpoons$ | $N_2O + H$ | 2.940E+11 | -0.40 | 0.00 |
| 170 | $NH + NO$ | $\rightleftharpoons$ | $N_2 + OH$ | 2.160E+10 | -0.23 | 0.00 |
| 171 | $NH + NO$ | $\rightleftharpoons$ | $NNH + O$ | 5.600E+09 | 0.21 | 45.48 |
| 172 | $NH + NH$ | $\rightleftharpoons$ | $N_2 + H + H$ | 2.540E+10 | 0.00 | 0.00 |
| 173 | $N + O_2$ | $\rightleftharpoons$ | $NO + O$ | 6.400E+06 | 1.00 | 26.28 |
| 174 | $N + OH$ | $\rightleftharpoons$ | $NO + H$ | 3.800E+10 | 0.00 | 0.00 |
| 175 | $N + NO$ | $\rightleftharpoons$ | $N_2 + O$ | 3.300E+09 | 0.30 | 0.00 |
| 176 | $N_2H_2 + M$ | $\rightleftharpoons$ | $NNH + H + M$ | 1.170E+14 | 0.00 | 209.20 |
| 177 | $N_2H_2 + H$ | $\rightleftharpoons$ | $NNH + H_2$ | 5.000E+10 | 0.00 | 4.18 |
| 178 | $N_2H_2 + NO$ | $\rightleftharpoons$ | $NH_2 + N_2O$ | 3.000E+09 | 0.00 | 0.00 |
| 179 | $NNH + M$ | $\rightleftharpoons$ | $N_2 + H + M$ | 1.700E+09 | 0.00 | 59.86 |
| 180 | $NNH + OH$ | $\rightleftharpoons$ | $N_2 + H_2O$ | 5.000E+10 | 0.00 | 0.00 |
| 181 | $NNH + NO$ | $\rightleftharpoons$ | $N_2 + HNO$ | 9.100E+08 | 0.00 | 0.00 |
| 182 | $NNH + NH$ | $\rightleftharpoons$ | $N_2 + NH_2$ | 5.000E+10 | 0.00 | 0.00 |
| 183 | $NNH + O$ | $\rightleftharpoons$ | $N_2 + OH$ | 1.000E+10 | 0.00 | 20.92 |
| 184 | $N_2O + H$ | $\rightleftharpoons$ | $N_2 + OH$ | 2.230E+11 | 0.00 | 70.08 |
| 185 | $N_2O + H$ | $\rightleftharpoons$ | $NNH + O$ | 2.400E+16 | -1.26 | 197.04 |
| 186 | $N_2O + O$ | $\rightleftharpoons$ | $NO + NO$ | 2.900E+10 | 0.00 | 96.92 |
| 187 | $N_2O + O$ | $\rightleftharpoons$ | $N_2 + O_2$ | 1.400E+09 | 0.00 | 45.22 |
| 188 | $N_2O$ | $\rightleftharpoons$ | $N_2 + O$ | 1.300E+11 | 0.00 | 249.42 |
| 189 | $N_2O + OH$ | $\rightleftharpoons$ | $N_2 + HO_2$ | 1.300E-05 | 4.72 | 152.97 |
| 190 | $HNO + M$ | $\rightleftharpoons$ | $H + NO + M$ | 2.360E+13 | 0.00 | 203.81 |
| 191 | $HNO + H$ | $\rightleftharpoons$ | $H_2 + NO$ | 4.500E+08 | 0.72 | 2.74 |
| 192 | $HNO + OH$ | $\rightleftharpoons$ | $H_2O + NO$ | 1.300E+04 | 1.88 | -4.00 |
| 193 | $HNO + O$ | $\rightleftharpoons$ | $OH + NO$ | 3.600E+10 | 0.00 | 0.00 |
| 194 | $HNO + HNO$ | $\rightleftharpoons$ | $H_2O + N_2O$ | 3.900E+09 | 0.00 | 209.20 |
| 195 | $HNO + NH_2$ | $\rightleftharpoons$ | $NH_3 + NO$ | 2.000E+10 | 0.00 | 4.18 |
| 196 | $HNO + NO$ | $\rightleftharpoons$ | $N_2O + OH$ | 2.000E+09 | 0.00 | 108.78 |
| 197 | $HNO + O_2$ | $\rightleftharpoons$ | $NO + HO_2$ | 3.160E+09 | 0.00 | 12.55 |
| 198 | $HNO + NO_2$ | $\rightleftharpoons$ | $HNO_2 + NO$ | 6.022E+08 | 0.00 | 8.31 |
| 199 | $NO + HO_2$ | $\rightleftharpoons$ | $NO_2 + OH$ | 2.110E+09 | 0.00 | -2.00 |

Table B.1: continued

| No | Reaction | | | B | n | E [kJ/mole] |
|---|---|---|---|---|---|---|
| 200 | $NO_2$ | $\rightleftharpoons$ | $NO + O$ | 7.600E+18 | -1.27 | 306.64 |
| 201 | $NO_2 + H$ | $\rightleftharpoons$ | $NO + OH$ | 3.500E+11 | 0.00 | 6.28 |
| 202 | $NO_2 + O$ | $\rightleftharpoons$ | $NO + O_2$ | 3.900E+09 | 0.00 | -1.00 |
| 203 | $NO_2 + NO_2$ | $\rightleftharpoons$ | $NO + NO + O_2$ | 1.626E+09 | 0.00 | 109.30 |
| 204 | $NO_2 + HO_2$ | $\rightleftharpoons$ | $HNO_2 + O_2$ | 4.640E+08 | 0.00 | -2.01 |
| 205 | $NO_2 + NO$ | $\rightleftharpoons$ | $N_2O + O_2$ | 1.000E+09 | 0.00 | 252.00 |
| 206 | $HNO_2$ | $\rightleftharpoons$ | $OH + NO$ | 0.000E+00 | 0.00 | 0.00 |
| 207 | $HNO_2 + H$ | $\rightleftharpoons$ | $H_2 + NO_2$ | 1.200E+10 | 0.00 | 24.94 |
| 208 | $HNO_2 + OH$ | $\rightleftharpoons$ | $H_2O + NO_2$ | 1.260E+07 | 1.00 | 0.56 |
| 209 | $HNO_2 + O$ | $\rightleftharpoons$ | $OH + NO_2$ | 1.200E+10 | 0.00 | 30.76 |
| 210 | $NO + C1$ | $\rightleftharpoons$ | $N + CO$ | 2.800E+10 | 0.00 | 0.00 |
| 211 | $NO + C1$ | $\rightleftharpoons$ | $CN + O$ | 2.000E+10 | 0.00 | 0.00 |
| 212 | $NO + CH$ | $\rightleftharpoons$ | $HCN + O$ | 4.800E+10 | 0.00 | 0.00 |
| 213 | $NO + CH$ | $\rightleftharpoons$ | $CO + NH$ | 5.000E+09 | 0.00 | 0.00 |
| 214 | $NO + CH_2(T)$ | $\rightleftharpoons$ | $HCNO + H$ | 2.500E+09 | 0.00 | 25.00 |
| 215 | $NO + CH_2(S)$ | $\rightleftharpoons$ | $HCNO + H$ | 6.600E+09 | 0.00 | 0.00 |
| 216 | $NO + CH_3$ | $\rightleftharpoons$ | $HCN + H_2O$ | 1.200E+11 | 0.00 | 121.30 |
| 217 | $NO + CHO$ | $\rightleftharpoons$ | $HNO + CO$ | 7.226E+09 | 0.00 | 0.00 |
| 218 | $NO + CH_2O$ | $\rightleftharpoons$ | $HNO + CHO$ | 1.023E+10 | 0.00 | 170.77 |
| 219 | $NO + CH_3O$ | $\rightleftharpoons$ | $CH_2O + HNO$ | 1.300E+11 | -0.70 | 0.00 |
| 220 | $NO + C_2HO$ | $\rightleftharpoons$ | $HCN + CO_2$ | 1.800E+10 | 0.00 | 2.91 |
| 221 | $NO + C_2HO$ | $\rightleftharpoons$ | $HCNO + CO$ | 4.200E+10 | 0.00 | 2.91 |
| 222 | $NO_2 + CH$ | $\rightleftharpoons$ | $CHO + NO$ | 1.010E+11 | 0.00 | 0.00 |
| 223 | $NO_2 + CH_3$ | $\rightleftharpoons$ | $CH_3O + NO$ | 1.300E+10 | 0.00 | 0.00 |
| 224 | $NO_2 + CH_4$ | $\rightleftharpoons$ | $CH_3 + HNO_2$ | 1.200E+10 | 0.00 | 125.52 |
| 225 | $NO_2 + CHO$ | $\rightleftharpoons$ | $HNO_2 + CO$ | 1.700E+10 | 0.00 | 0.00 |
| 226 | $NO_2 + CO$ | $\rightleftharpoons$ | $NO + CO_2$ | 9.033E+10 | 0.00 | 141.34 |
| 227 | $N_2O + C1$ | $\rightleftharpoons$ | $CN + NO$ | 1.000E+10 | 0.00 | 0.00 |
| 228 | $N_2O + CO$ | $\rightleftharpoons$ | $N_2 + CO_2$ | 3.200E+08 | 0.00 | 85.00 |
| 229 | $N_2 + CH$ | $\rightleftharpoons$ | $HCN + N$ | 3.680E+04 | 1.42 | 86.70 |
| 230 | $N_2 + CH_2(T)$ | $\rightleftharpoons$ | $HCN + NH$ | 1.000E+09 | 0.00 | 309.00 |

Table B.1: continued

| No | Reaction | | | B | n | E [kJ/mole] |
|---|---|---|---|---|---|---|
| 231 | $N + CH$ | $\rightleftharpoons$ | $CN + H$ | 1.300E+10 | 0.00 | 0.00 |
| 232 | $N + CH_2(T)$ | $\rightleftharpoons$ | $HCN + H$ | 5.000E+10 | 0.00 | 0.00 |
| 233 | $N + CH_3$ | $\rightleftharpoons$ | $HCN + H_2$ | 7.000E+09 | 0.00 | 0.00 |
| 234 | $N + CH_4$ | $\rightleftharpoons$ | $NH + CH_3$ | 1.000E+10 | 0.00 | 100.42 |
| 235 | $NH + CH$ | $\rightleftharpoons$ | $HCN + H$ | 5.000E+10 | 0.00 | 0.00 |
| 236 | $NH + CH_2(T)$ | $\rightleftharpoons$ | $H_2CN + H$ | 3.000E+10 | 0.00 | 0.00 |
| 237 | $HCN + O$ | $\rightleftharpoons$ | $CN + OH$ | 4.200E+07 | 0.40 | 86.50 |
| 238 | $HCN + O$ | $\rightleftharpoons$ | $NH + CO$ | 5.400E+05 | 1.21 | 31.34 |
| 239 | $HCN + O$ | $\rightleftharpoons$ | $NCO + H$ | 2.000E+05 | 1.47 | 31.76 |
| 240 | $HCN + OH$ | $\rightleftharpoons$ | $CN + H_2O$ | 3.900E+03 | 1.83 | 43.06 |
| 241 | $HCN + OH$ | $\rightleftharpoons$ | $HNCO + H$ | 4.800E+08 | 0.00 | 46.02 |
| 242 | $HCN + OH$ | $\rightleftharpoons$ | $HOCN + H$ | 9.200E+09 | 0.00 | 62.76 |
| 243 | $HCN + OH$ | $\rightleftharpoons$ | $NH_2 + CO$ | 7.830E-07 | 4.00 | 16.74 |
| 244 | $CN + O$ | $\rightleftharpoons$ | $CO + N$ | 7.700E+10 | 0.00 | 0.00 |
| 245 | $CN + H_2$ | $\rightleftharpoons$ | $HCN + H$ | 3.000E+02 | 2.45 | 9.36 |
| 246 | $CN + OH$ | $\rightleftharpoons$ | $NCO + H$ | 6.000E+10 | 0.00 | 0.00 |
| 247 | $CN + O_2$ | $\rightleftharpoons$ | $NCO + O$ | 6.620E+09 | 0.00 | -1.70 |
| 248 | $CN + NO_2$ | $\rightleftharpoons$ | $NCO + NO$ | 3.000E+10 | 0.00 | 0.00 |
| 249 | $CN + N_2O$ | $\rightleftharpoons$ | $NCO + N_2$ | 1.000E+10 | 0.00 | 0.00 |
| 250 | $CN + CH_4$ | $\rightleftharpoons$ | $HCN + CH_3$ | 2.170E+10 | 0.00 | 5.12 |
| 251 | $CN + N$ | $\rightleftharpoons$ | $C1 + N_2$ | 1.040E+12 | -0.50 | 0.00 |
| 252 | $CN + NO$ | $\rightleftharpoons$ | $N_2 + CO$ | 1.080E+11 | 0.00 | 33.59 |
| 253 | $CN + NO$ | $\rightleftharpoons$ | $N + NCO$ | 9.640E+10 | 0.00 | 176.26 |
| 254 | $NCO + M$ | $\rightleftharpoons$ | $N + CO + M$ | 1.020E+12 | 0.00 | 195.39 |
| 255 | $NCO + H$ | $\rightleftharpoons$ | $NH + CO$ | 5.000E+10 | 0.00 | 0.00 |
| 256 | $NCO + O$ | $\rightleftharpoons$ | $NO + CO$ | 5.600E+10 | 0.00 | 0.00 |
| 257 | $NCO + OH$ | $\rightleftharpoons$ | $NO + CHO$ | 5.000E+09 | 0.00 | 62.80 |
| 258 | $NCO + NO$ | $\rightleftharpoons$ | $N_2O + CO$ | 6.200E+14 | -1.73 | 3.19 |
| 259 | $NCO + NO$ | $\rightleftharpoons$ | $N_2 + CO_2$ | 7.800E+14 | -1.73 | 3.19 |
| 260 | $NCO + N$ | $\rightleftharpoons$ | $N_2 + CO$ | 2.000E+10 | 0.00 | 0.00 |
| 261 | $NCO + HNO$ | $\rightleftharpoons$ | $HNCO + NO$ | 1.800E+10 | 0.00 | 0.00 |

Table B.1: continued

| No | Reaction | B | n | E [kJ/mole] |
|---|---|---|---|---|
| 262 | $NCO + NCO \rightleftharpoons N_2 + CO + CO$ | 1.800E+10 | 0.00 | 0.00 |
| 263 | $NCO + O_2 \rightleftharpoons NO + CO_2$ | 2.000E+09 | 0.00 | 83.74 |
| 264 | $HNCO + M \rightleftharpoons NCO + H + M$ | 5.000E+12 | 0.00 | 498.84 |
| 265 | $HNCO + H \rightleftharpoons NCO + H_2$ | 5.500E+11 | 0.00 | 113.90 |
| 266 | $HNCO + H \rightleftharpoons NH_2 + CO$ | 2.089E+11 | 0.00 | 70.67 |
| 267 | $HNCO + O \rightleftharpoons NCO + OH$ | 2.230E+03 | 2.11 | 47.80 |
| 268 | $HNCO + O \rightleftharpoons NH + CO_2$ | 9.600E+04 | 1.41 | 35.67 |
| 269 | $HNCO + O \rightleftharpoons HNO + CO$ | 1.500E+05 | 1.57 | 184.27 |
| 270 | $HNCO + OH \rightleftharpoons NCO + H_2O$ | 3.450E+04 | 1.50 | 15.04 |
| 271 | $HNCO + OH \rightleftharpoons NH_2 + CO_2$ | 3.630E+03 | 1.50 | 15.04 |
| 272 | $HNCO + CN \rightleftharpoons HCN + NCO$ | 1.500E+10 | 0.00 | 0.00 |
| 273 | $HNCO + NH \rightleftharpoons NH_2 + NCO$ | 2.000E+10 | 0.00 | 49.87 |
| 274 | $HOCN + H \rightleftharpoons NH_2 + CO$ | 1.200E+05 | 0.61 | 8.69 |
| 275 | $HOCN + H \rightleftharpoons NCO + H_2$ | 2.400E+05 | 1.50 | 27.69 |
| 276 | $HOCN + O \rightleftharpoons NCO + OH$ | 1.700E+05 | 1.50 | 17.29 |
| 277 | $HOCN + OH \rightleftharpoons NCO + H_2O$ | 1.200E+03 | 2.00 | -1.04 |
| 278 | $N + CH_3 \rightleftharpoons H_2CN + H$ | 7.100E+10 | 0.00 | 0.00 |
| 279 | $NO + CH_3 \rightleftharpoons H_2CN + OH$ | 5.200E+09 | 0.00 | 101.43 |
| 280 | $NH + CH_3 \rightleftharpoons H_2CN + H_2$ | 7.100E+10 | 0.00 | 0.00 |
| 281 | $H_2CN + H \rightleftharpoons HCN + H_2$ | 1.000E+11 | 0.00 | 0.00 |
| 282 | $H_2CN + OH \rightleftharpoons HCN + H_2O$ | 1.000E+11 | 0.00 | 0.00 |
| 283 | $H_2CN + M \rightleftharpoons HCN + H + M$ | 3.000E+11 | 0.00 | 92.05 |
| 284 | $H_2CN + N \rightleftharpoons CH_2(T) + N_2$ | 2.000E+10 | 0.00 | 0.00 |
| 285 | $NO + CH \rightleftharpoons NCO + H$ | 1.800E+10 | 0.00 | 0.00 |
| 286 | $NO + CH \rightleftharpoons CHO + N$ | 2.600E+10 | 0.00 | 0.00 |
| 287 | $NO + CH_2(T) \rightleftharpoons HCN + OH$ | 5.012E+08 | 0.00 | 12.00 |
| 288 | $NO + CH_2(S) \rightleftharpoons HCN + OH$ | 3.300E+09 | 0.00 | 0.00 |
| 289 | $NO + C_2H \rightleftharpoons HCN + CO$ | 6.000E+10 | 0.00 | 2.39 |
| 290 | $HOCN + M \rightleftharpoons HNCO + M$ | 3.100E+05 | 0.84 | 8.02 |
| 291 | $HCNO + M \rightleftharpoons HNCO + M$ | 2.100E+12 | -0.69 | 11.93 |
| 292 | $HCNO + M \rightleftharpoons HOCN + M$ | 1.400E+08 | -0.19 | 10.39 |

Table B.1: continued

| No | Reaction | | | B | n | E [kJ/mole] |
|---|---|---|---|---|---|---|
| 293 | $HCNO + H$ | $\rightleftharpoons$ | $HCN + OH$ | 2.700E+08 | 0.18 | 8.85 |
| 294 | $HCNO + H$ | $\rightleftharpoons$ | $NH_2 + CO$ | 1.700E+11 | -0.75 | 12.10 |
| 295 | $HCNO + O$ | $\rightleftharpoons$ | $CHO + NO$ | 7.000E+10 | 0.00 | 0.00 |
| 296 | $HCNO + OH$ | $\rightleftharpoons$ | $CH_2O + NO$ | 4.000E+10 | 0.00 | 0.00 |
| 297 | $C_2H_2 + O_2$ | $\rightleftharpoons$ | $C_2H + HO_2$ | 1.200E+10 | 0.00 | 311.70 |
| 298 | $HCN + M$ | $\rightleftharpoons$ | $HNC + M$ | 1.600E+23 | -3.23 | 207.43 |
| 299 | $HNC + O$ | $\rightleftharpoons$ | $NH + CO$ | 4.600E+09 | 0.00 | 9.14 |
| 300 | $HNC + OH$ | $\rightleftharpoons$ | $HNCO + H$ | 2.800E+10 | 0.00 | 15.46 |

Table B.1: Chemical mechanism used, for details see Meyer [53](End).